Wiley Interdisciplinary Reviews: Computational Molecular Science

WILEY

WIREs COMPUTATIONAL MOLECULAR SCIENCE

UPDATE OPEN ACCESS

Dissipative Particle Dynamics Modeling in Polymer Science and Engineering

Sousa Javan Nikkhah | Matthias Vandichel

School of Chemical Sciences and Chemical Engineering, Bernal Institute, University of Limerick, Limerick, Ireland

Correspondence: Sousa Javan Nikkhah (sousa.javannikkhah@ul.ie)

Received: 1 February 2025 | **Revised:** 16 March 2025 | **Accepted:** 18 March 2025

Associate Editor: Modesto Orozco | **Editor-in-Chief:** Peter R. Schreiner

Funding: This work was supported by European Union's Horizon 2020 research and innovation programme under the Marie Skłodowska-Curie grant agreement 847402 (ID: MF20210297) and Research Ireland under the Frontiers for the Future Program (23/FFP-A/12221).

Keywords: coarse-graining | dissipative particle dynamics | mesoscale modeling | polymer rheology and interfaces | polymer self-assembly | polymer solutions | polymeric composites, membranes and blends | polymerization reactions | zwitterionic and charged polymeric systems

ABSTRACT

Polymeric materials are intricate systems with unique properties across different length and time scales, presenting challenges in understanding the hierarchical features that govern their behavior. Advancing innovative polymeric systems requires a deep comprehension of these complexities. Dissipative particle dynamics (DPD), a mesoscale simulation technique, has proven instrumental in elucidating polymer behavior. Unlike molecular dynamics, which tracks individual molecules, DPD employs a coarse-graining approach, to describe molecular systems as particles interacting via soft potentials. Thanks to its computational efficiency, DPD has enabled researchers to numerically study several complex fluid applications in detail. Moreover, with the ever-increasing high-performance computing resources, it has become possible to tackle larger molecular systems beyond the nanoscale, typically micrometer-sized systems. An in-depth analysis of the theoretical foundations of DPD is presented, focusing on its methodology, mathematical formulations, and computational implementation. This review then explores various applications of DPD simulations for polymeric systems, demonstrating DPD's ability to accurately capture phenomena such as polymer self-assembly, polymer behavior in solutions and blends, charged polymers, polymer interfaces, polymer rheology, polymeric membranes, polymerization reactions, and polymeric composites. Overall, this review examines the adoption of DPD as a predictive modeling tool for polymeric materials, focusing on its key features and its integration with methods such as atomistic molecular dynamics to determine the interaction parameters. Building on these advancements, future directions for DPD include its potential applications in other systems like biological membranes, macromolecules, and shape-memory materials.

1 | Introduction

Molecular modeling simulations are gradually becoming a universal tool in many fields of science and engineering, including computational methods with varying degrees of accuracy to describe molecular model systems at different time and length scales (Scheme 1). These methods, or a combination thereof, allow the description of polymer materials and provide an enhanced understanding of their properties. Within the field of molecular modeling there are empirical 'top-down' models typically based on experimental data, and first-principles-based 'bottom-up' models starting from a finite molecular model system and a Hamiltonian describing the interaction between particles, which could be

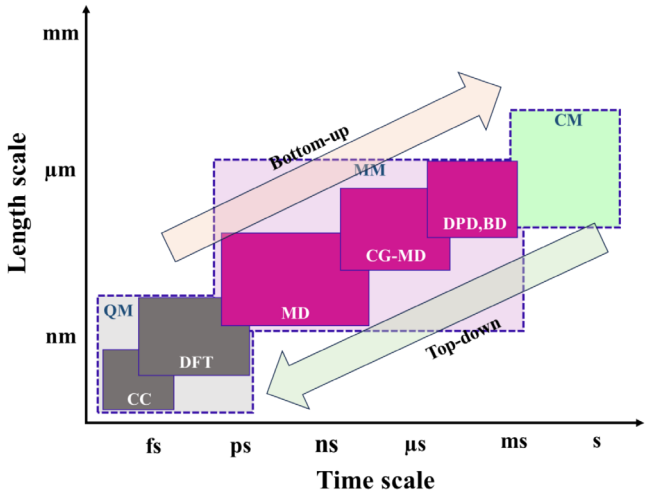

SCHEME 1 | Overview of molecular modeling methods to tackle different length and time scales.

electrons (electronic structure methods), atoms (atomistic force field methods), or groups of atoms (coarse-grained methods). Beyond these methods, there are continuum methods attempting at an overall description of macroscale processes by solving partial differential equations of discrete flow elements (e.g., finite element computational fluid dynamics).

Nowadays, diverse model systems and methodologies can be developed and employed to comprehend various aspects of the polymer processes, including polymer behavior in suspension, solvent, or melt, flow characteristics, mechanical properties, interface formation in composites, rheological properties, and more. Traditional methods for predicting the flow and deformation of polymers have generally worked well in a variety of processing conditions. But when it comes to larger systems, these models, which are based on empirical mathematics, often have trouble accurately predicting the behavior of complex fluids like molten polymers [1, 2]. Atomistic molecular dynamics (MD) simulations are ideal for sampling the potential energy surface of molecular systems and have been useful in various applications, such as polymer rheology [3–8], nevertheless, these simulations result in huge computational costs even for simple systems [9, 10]. Employing mesoscale particle-based methods to investigate polymers' static and dynamic properties is a practical approach to reduce the computational cost and yet provide a deep insight into different phenomena at the molecular level [11–13].

At the mesoscale, molecules are replaced by "*beads*" through a process known as coarse-graining (CG) [14]. In the CG process, molecules are divided based on their chemical features, and the individual atoms within each segment are merged together to form a single bead. This reduces the number of *degrees of freedom*, enabling more efficient computational modeling of macromolecule systems [15, 16]. Each bead in a CG model represents a group of molecules or atoms. While the size of a bead is relatively large compared to the individual atoms on the atomistic scale, it is still considered small on the macroscale. This allows for the modeling of macromolecule systems at a more manageable scale, while retaining the essential features of the system [16–18]. Within each bead, the atomistic details of the constituent molecules or atoms are combined. This simplification allows for more efficient simulations and enables the study of larger time and length scales than would be possible with atomistic modeling [15, 19, 20].

Atomistic modeling, while useful for understanding the behavior of individual molecules and small systems, is limited in its ability to simulate many physical phenomena. This is because atomistic simulations are restricted to shorter time and length scales due to the high computational cost of modeling large and complex systems with a high number of degrees of freedom. Coarse-grained models are commonly employed to simulate larger systems over extended time scales,[21, 22], which allows for fundamental studies of the physics and chemistry of macromolecule systems that can be investigated via a coarse-grained model at a reasonable computational time. Therefore, coarse-grained modeling is a valuable tool for studying large and complex systems over longer time scales [23]. It allows for the study of larger and more complex systems than can be modeled with atomistic simulations, while still capturing some of the molecular-level details that are lost in continuum modeling. Coarse-grained models thus offer a valuable intermediate approach for studying the behavior of complex materials and biological systems [23, 24].

In coarse-grained modeling, effective potentials are used to help us analyze physical systems by simplifying things without losing important details. They represent the way particles interact, but in a way that captures the key behaviors of the system. These potentials help us predict the system's behavior and understand its underlying physics by maintaining key properties like thermodynamics [14, 25, 26]. However, the process of creating them can take time, as it often involves going through several stages to fine-tune the accuracy [11, 27–30].

Among all coarse-graining methods, coarse-grained molecular dynamics (CG-MD) [31] and dissipative particle dynamics (DPD) [9] are the two widely used coarse-graining methods. In contrast to CG-MD [32], DPD is generalized to apply simplified soft potentials [9], making the study of polymeric systems easier [11, 26, 33]. This review paper begins by introducing the history and theory behind the DPD method and then goes on to explore its applications in polymer science and engineering.

1.1 | Theoretical Background

To understand the history of the DPD method, it is necessary to answer the question of why it was proposed in the first place. In the past, MD simulations of flow phenomena in simple fluids had been reported, but the computational costs associated with MD simulations made it challenging to use them as a tool for studying complex fluids in three dimensions. To address this issue, researchers explored particle-based simulations of fluids, such as lattice-gas automata (LGA) [34–37].

Let us first introduce the LGA method; the LGA method is a type of coarse-grained approach for particle-based simulations of fluids that constrains the motion of particles on a regular lattice. This is similar to the way Navier–Stokes equations are used to study actual molecular fluids and predict their hydrodynamic behavior [9, 34, 38, 39]. This coarse-grained approach,

computationally more efficient than atomistic MD, can simulate complex fluid systems such as colloidal suspensions [40] and polymer solutions [41]. Although the LGA method significantly increases computational efficiency, it brings about two fundamental problems: statistical noise and lack of Galilean invariance [9, 42]. Therefore, Hoogerbrugge and Koelman [9] proposed the DPD method, a new particle-based method, which was aimed at overcoming the limitations of the LGA method as well as enabling mesoscopic simulations of complex fluids. DPD is a hybrid simulation method that combines the advantages of LGA's larger time scale simulations and MD's mesh-free algorithm [43]. Being able to cover the larger length and longer time scales, DPD modeling has successfully been applied to describe larger fluid systems; for example, polymer and DNA suspensions [44–46], red blood cells in blood flow [47, 48], and platelet aggregation [49], which are beyond the ability of MD [50]. The DPD method combines the time-stepping of the LGA method with MD to develop a faster and isotropic stochastic particle model for isothermal fluid systems than MD.

In DPD, the system is described by updating all N particle positions $\boldsymbol{r_i}$ and momenta $\boldsymbol{p_i}$ ($i=1, ..., N$) in individual time steps $\boldsymbol{\delta t}$ (based on LGA). In each step, the momenta are simultaneously updated via the following simple rule [9].

$$\boldsymbol{p}_i'(t+\delta t) = \boldsymbol{p}_i(t) + \sum_j \Omega_{ij}\boldsymbol{e}_{ij}(t) \tag{1}$$

Here, $\boldsymbol{e}_{ij}(t) = \left(\boldsymbol{r}_i - \boldsymbol{r}_j\right) / \left|\boldsymbol{r}_i - \boldsymbol{r}_j\right|$ represents the unit vector pointing from particle j to particle i, while the scalar variable Ω_{ij} denotes the momentum transferred from particle j to particle i. The positions of the particles are updated in accordance with

$$\boldsymbol{r}_i'(t+\delta t) = \boldsymbol{r}_i(t) + \frac{\delta t}{m_i}\boldsymbol{p}_i'(t+\delta t) \tag{2}$$

where m_i is the mass of particle i. For being a valid model, it is needed that the above system satisfies the laws of conservation. The conservation of linear and angular momentum is ensured when these momentum transfers are symmetric with respect to the particle labels: Ω_{ij}=Ω_{ji}. Furthermore, it should be noted that Ω_{ij} depends only on scalar quantities, that is, relative positions and velocities. Therefore, the model is completely isotropic and Galilean invariant [51]. For systems of particles with equal mass, Ω_{ij} can be written as follows

$$\Omega_{ij} = W\left(\left|\boldsymbol{r}_i - \boldsymbol{r}_j\right|\right).\left\{\Pi_{ij} - \omega\left(\boldsymbol{p}_i - \boldsymbol{p}_j\right)\bullet\boldsymbol{e}_{ij}\right\} \tag{3}$$

Here, ω is a positive number, and $W(r)$ is a dimensionless, positive weighting function that becomes zero when $r > r_C$, with r_C the cut off beyond which the weight function vanishes, and particle interactions are no longer considered. In addition, for every pair of particles, a random number Π_{ij} is sampled from a distribution, with mean $<\Pi_{ij}> = \Pi_0$ and variance $<\left(\Pi_{ij}-\Pi_0\right)^2> = \delta\Pi^2$. The terms between curly brackets {} in the equation act as a thermostat together, such that in too hot systems, the second term $\omega\left(\boldsymbol{p}_i - \boldsymbol{p}_j\right)\bullet\boldsymbol{e}_{ij}$ will control and cool the systems. However, in too cold systems, the stochastic term Π_{ij} will act as a controller to reach higher temperatures, resulting in more particle collisions, and higher kinetic energy [9, 52].

In DPD simulations, particles interact with each other based on simplified force laws and move according to Newton's equations of motion [38]. Unlike Self-Consistent Field (SCF) theory, DPD allows for the investigation of both the equilibrium thermodynamic properties and dynamic properties of structures [53, 54]. DPD, besides being capable of investigating several classic problems, including hydrodynamic interactions [38], can also be applied to study the static and dynamic properties of polymers [55–57], amphiphiles [58–60], microphase separation [61–63], surfactant behavior [21, 64], self-assembly of block copolymers [65, 66] representing excluded volume interactions and hydrodynamics [67], collapse transitions going from good to poor/bad solvents [68, 69], rheological properties [70], and aggregation in heavy crude oil [71].

1.2 | DPD Simulation Method

The original DPD method was suggested by Hoogerbrugge and Koelman [9] in 1992 and was revised by Español and Warren [72] in 1995. Subsequently, Groot and Warren [18, 61] established a relationship between DPD and the Flory-Huggins solution theory through a simple functional form, which led to the extensive use of DPD in studying complex systems at the mesoscale [73–78].

In the DPD method, a linear polymer is represented as a series of connected beads using bond potentials such as harmonic springs or finite-extensible non-linear elastic (FENE) potentials. The statistical distribution of the polymer is accounted for by assigning each bead as a segment with a Gaussian chain model [26, 79–81]. To construct DPD chain models, it is necessary to map macroscopic or microscopic properties of real polymers onto groups of atoms, such as monomers and Kuhn segments, which will be represented by spherical DPD beads [11]. This can be accomplished by employing different structural and conformational parameters, including polymer molecular weight, characteristic ratio, mean squared end-to-end distance, persistence length, and statistical Kuhn segment length, to represent the Gaussian chain model for realistic polymer blocks [82].

$$C_n = \frac{<R^2>_0}{Nl^2}, L_p = \left(1/l_i\right)\sum_{j\neq i} <l_i.l_j>, a_k = \frac{<R^2>}{R_{max}} \tag{4}$$

where C_n, L_p and a_k are characteristic ratio, persistence length, and statistical Kuhn segment length, respectively. $<R^2>_0$, N and l_i represent the mean square end-to-end distance of a freely rotating chain, the number of statistical skeletal units in the polymer chain, and the root-mean-square length of a skeletal unit, respectively. The number of beads in a polymer chain is defined by combining these statistical parameters with the following expression [83].

$$C_{SGD} = \frac{M_p}{M_m(SSL)} \tag{5}$$

where C_{SGD} is bead numbers (statistical segments) with Gaussian distribution, M_p is the molar mass of the polymer, M_m is the molar mass of a repeat unit, and SSL stands statistical segment level, which depends on C_n, L_p, a_k, and so on [82].

A DPD simulation consists of a system of interacting particles, with their time-dependent behavior determined by Newton's equations of motion.

$$\frac{d\mathbf{r}_i}{dt} = \mathbf{v}_i, \quad \mathrm{m}_i . \frac{d\mathbf{v}_i}{dt} = \mathbf{f}_i \tag{6}$$

Choosing an appropriate integration algorithm and time-step for the DPD equations of motion is crucial for ensuring simulation accuracy. In the past, simple first-order algorithms were commonly used for DPD simulations [84, 85]. Besides these, also more accurate approaches for DPD simulations were developed by implementing a second-order semi-implicit scheme instead of the initial simple first-order algorithms [86, 87]. For simplicity, if the masses of all particles (m_i) are set to 1, the force acting on a particle directly corresponds to its acceleration. Three fundamental forces govern the interactions between all particles: a conservative force $\mathbf{F}^{\mathrm{C}}$, a dissipative force $\mathbf{F}^{\mathrm{D}}$, and a random force $\mathbf{F}^{\mathrm{R}}$, each of which is pairwise additive.

$$\mathbf{f}_{\mathrm{i}} = \sum_{j \neq i} \left(\mathbf{F}_{ij}^{\mathrm{C}} + \mathbf{F}_{ij}^{\mathrm{D}} + \mathbf{F}_{ij}^{\mathrm{R}} \right) \tag{7}$$

The forces acting on a particle in DPD simulations are a result of its interactions with neighboring particles within a cutoff radius of r_c. These interactions are isotropic and pairwise and gradually decrease to zero when the distance between the particles exceeds r_c. Additionally, other conservative forces like electrostatic interactions and spring forces connecting beads in chains can be included based on the simulation requirements [18].

Moreover, it is essential to set length, time, and mass scales to observe and thus interpret properly single or multiscale phenomena. To facilitate that, reduced DPD units are utilized during DPD simulation (see Table 1). More specifically, r_c and k_BT are taken as the unit of length and the unit of energy, respectively [18]. Hoogerbrugge and Koelman chose to work in reduced units such that $k_BT = 1$ and $r_c = 1$, via the introduction of a reference temperature and cut-off radius. Based on these factors, the unit of time, τ, can be determined as follows [18, 75].

$$\tau = r_c \sqrt{m / (k_B T)} \tag{8}$$

The conservative force is a soft repulsion potential that acts in the direction of the line between centers of i and j particles and is given as follows [18, 38],

$$\mathbf{F}_{ij}^{\mathrm{C}} = \left\{ \begin{array}{ll} a_{ij}(1 - r_{ij})\hat{\mathbf{r}}_{ij} & (r_{ij} < r_c) \\ 0 & (r_{ij} \geq r_c) \end{array} \right\} \tag{9}$$

where a_{ij} is a maximum repulsion between bead i and bead j. Furthermore, $\boldsymbol{r}_{ij} = \boldsymbol{r}_i - \boldsymbol{r}_j$, $r_{ij} = |\boldsymbol{r}_{ij}|$, and $\hat{\mathbf{r}}_{ij} = \boldsymbol{r}_{ij} / \left| \boldsymbol{r}_{ij} \right|$. The conservative force constant a_{ij} is a vital parameter because it inherits all the chemical and physical characteristics of the system [23]. The dissipative forces act to reduce the relative velocity between pairs of beads by performing an equal and opposite drag force on each pair, which is given by [18],

$$\mathbf{F}_{ij}^{\mathrm{D}} = -\gamma w^{\mathrm{D}}(r_{ij}) (\hat{\mathbf{r}}_{ij} . \mathbf{v}_{ij}) \hat{\mathbf{r}}_{ij} \tag{10}$$

The remaining random force is expressed as:

$$\mathbf{F}_{ij}^{\mathrm{R}} = \sigma w^{\mathrm{R}}(r_{ij}) \zeta_{ij} \Delta t^{-1/2} \hat{\mathbf{r}}_{ij} \tag{11}$$

where w^{D} and w^{R} are r-dependent weight functions vanishing for $r > r_c$, $\mathbf{v}_{ij} = \mathbf{v}_i - \mathbf{v}_j$, and ζ_{ij} is a random number from a Gaussian distribution with unit variance. The equations of motion are solved with a time step Δt. γ is the friction coefficient, and σ is the amplitude of the noise [18]. The movement of each bead leads to energy dissipation and resists the relative motion of other beads, with the friction coefficient ranging from 2 to 32 [23]. The random force in the model originates from the molecular random motions and their associated fluctuation amplitude σ [23]. In the majority of the works reported in the literature, the values of 3.0 and 4.5 for σ and γ parameters have been applied, respectively [23, 88–91]. The combination of both forces between two interacting particles, which also performs along the line of centers, satisfies Newton's third law, which results in a thermostat that conserves the system's total momentum [92, 93]. Español and Warren [72] indicated that to obey the fluctuation-dissipation theorem, it could be possible to choose one of the two weight functions appearing in Equations (10) and (11) arbitrarily, and the other can be fixed based on this choice

TABLE 1 | Summary of units and variables used in DPD simulations.

Quantity	Real unit conversion	DPD reduced unit
Mass M	DPD bead weight, m	M/m
Length L	Cut-off radius $\left(r_c = \left(\rho V_{bead}\right)^{1/3}\right)$	L/r_c
Energy E	$E^* = k_BT$	$E / \left(k_BT\right)$
Time unit t	$\tau = \left(m{r_c}^2/(k_BT)\right)^{1/2}$	t/τ
Time step Δt	$\tau = \left(m{r_c}^2/(k_BT)\right)^{1/2}$	$\Delta t/\tau$
Force constant a_{ii}	$\left(k_BT\right)/r_c$	$a_{ii} / \left(\left(k_BT\right)/r_c\right)$
Force constant $a_{ij} = a_{ji}$	$\left(k_BT\right)/r_c$	$a_{ij} / \left(\left(k_BT\right)/r_c\right)$
Number density n	${r_c}^3$	$n / {r_c}^3$

Note: The reference quantities that are used for unit reduction.

according to Equation (12). Accordingly, the amplitudes and k_BT are related as follows [18].

$$w^D(r) = \left[w^R(r)\right]^2, \qquad \sigma^2 = 2\gamma k_B T \tag{12}$$

As a simple choice, the same function as in the conservative force is usually taken for $w^R(r)$.

$$w^D(r) = \left[w^R(r)\right]^2 = \begin{Bmatrix} (1-r)^2 & (r<1) \\ 0 & (r\geq 1) \end{Bmatrix} \tag{13}$$

It is highly probable to conduct a simulation where the equilibrium distribution aligns with the Gibbs-Boltzmann distribution within a canonical ensemble. To ensure this, the relationship between the dissipative and noise weight functions, as outlined in Equation (13), must be satisfied [18].

DPD method is a suitable method for studying complex macromolecule systems for three main reasons:

1. Non-bonding interactions are described through a soft repulsive potential [18, 94] rather than the Lennard-Jones potential used in MD simulations. This allows for a larger time step, making it more efficient.
2. Pairwise dissipative and random potentials act as a thermostat, conserving momentum and preserving hydrodynamic modes [18, 94]. As a result, the simulated fluid obeys the Navier–Stokes equations [95]. This differs from other thermostats, where the dissipative force is proportional to the particle's velocity relative to a stationary background, resulting in the loss of momentum conservation and the disruption of hydrodynamic modes [96, 97].
3. Unlike other approaches, such as dynamic density functional theory, which is entirely diffusive (characterized by random and dispersed particle motion), or Monte Carlo methods, which drive the system toward an ordered thermodynamic equilibrium, DPD stands out as inherently superior due to its characterization as momentum-conserving Brownian dynamics with soft interactions [38, 98].

As previously stated, the DPD method is limited to isothermal systems and cannot be used to model temperature-varying or non-isothermal systems because the system's energy is not conserved [99]. Nevertheless, it is possible to use isothermal DPD equations to simulate heat transport in non-isothermal fluid systems by incorporating internal energy as an additional property in the DPD model. This approach improves the conservation of energy within the simulation [99, 100]. This method is known in the literature as eDPD [101], in which each particle is associated with its internal energy, along with other properties such as position and momentum. Consequently, heat transfer can be simulated through the exchange of internal energy between particles. The eDPD method has been effectively employed to study heat conduction in nanocomposites [101], heat transfer in natural convection [102], and heat transfer in nanoparticle suspensions [103], and heat flow [104].

1.3 | DPD Repulsive Parameter

The DPD method has the potential to provide insights into phenomena that are difficult to observe through macroscopic experiments [105]. However, the accuracy and realism of mesoscopic structure modeling rely heavily on proper parametrization. To ensure successful modeling, it is essential to capture the chemical interactions within the system accurately [15].

The forces experienced by particles in DPD modeling are similar to those experienced by atoms in MD simulations, including electrostatic, van der Waals, and hydrogen bonding interactions. These forces are described using interparticle interaction parameters, a_{ii} and a_{ij}, which represent repulsive interactions when particles are at close distance. However, at the mesoscale, fluid properties are better represented by interactions between molecular clusters rather than detailed atomistic models.

$$k^{-1} = \frac{1}{nk_BTk_T} = \frac{1}{k_BT}\left(\frac{\partial p'}{\partial n}\right)_T \tag{14}$$

p' is the number density of molecules, and k_T is the isothermal compressibility. The dimensionless compressibility of water is represented by the value $k^{-1} = 15.9835$ at room temperature (300 K). To define an equation of state for this model, pressure is determined from the simulation as a function of density. Based on the virial theorem and simulations, Groot and Warren [18] obtained an empirical relationship, which provides a reasonable approximation for the pressure and is applicable for high densities ($\rho > 2$):

$$p' = \rho k_B T + \alpha a \rho^2 \qquad (\alpha = 0.101 \pm 0.001) \tag{15}$$

Therefore, at high densities, the dimensionless compressibility in Equation (14) can be then expressed based on the repulsive parameter by $k^{-1} = 1 + \frac{2\alpha a\rho}{k_BT} \approx 1 + \frac{0.2a\rho}{k_BT}$. To guarantee that the equation of state is satisfied during DPD simulations, especially since soft potentials are used, it is necessary to have a particle number density ρ greater than 3. Therefore, according to $\rho = 3$ $\left(\rho r_c^3 = 3\right)$ and matching the compressibility of water, $k_{water}^{-1} \approx 16$, Groot and Warren obtained the "universal" like-like interaction parameter of $a = 25k_BT$ [15, 18].

1.3.1 | Mapping on to Flory-Huggins Theory

Groot and Warren proposed that the parameters for pairwise interactions can be determined by mapping them to the Flory-Huggins χ-parameters [106]. In this manner, the method can be viewed as a continuous extension of Flory-Huggins lattice theory. Consequently, for a two-component system of chains, the free energy density (G_V) can be expressed as:

$$\frac{G_V}{k_BT} = \frac{\rho_A}{N_A}\ln\rho_A + \frac{\rho_B}{N_B}\ln\rho_B - \frac{\rho_A}{N_A} - \frac{\rho_B}{N_B} + \frac{\alpha\left(a_{AA}\rho_A^2 + 2a_{AB}\rho_A\rho_B + a_{BB}\rho_B^2\right)}{k_BT} \tag{16}$$

N_A and N_B are the number of segments per molecule, A and B. Thus, by the assumption of $a_{AA} = a_{BB} = a$ and $\rho_A + \rho_B =$ constant (ρ_A and ρ_B are particle number densities of components A and B, respectively), the following relation is obtained.

$$\chi = \frac{2\alpha\left(a_{AB} - a_{AA}\right)\left(\rho_A + \rho_B\right)}{k_B T} \tag{17}$$

They suggested a good linear relation between χ and $\Delta a = a_{AB} - a$ for two densities.

$$\chi = (0.286 \pm 0.002)\Delta a \qquad (\rho = 3) \tag{18}$$

$$\chi = (0.689 \pm 0.002)\Delta a \qquad (\rho = 5) \tag{19}$$

As mentioned before, the repulsion parameter for particles of the same type is defined as $a_{ii} = a_{jj} = 75\, k_B T/\rho$ and for unlike particles i and j, the cross-term repulsion parameters are chosen as

$$a_{ij} = \frac{75\, k_B T}{\rho} + \Delta a \qquad (i \neq j) \tag{20}$$

As a result, the interactions between non-bonding polymer beads are computed by adding two components: a neutral interaction term (a_{ii}) and pairwise interaction terms that are proportional to χ_{ij}, which represents the level of dislike between the bead types, as described by the following equation [18, 23, 107].

$$a_{ij} = a_{ii} + 3.27\chi_{ij} \tag{21}$$

The above equation has been widely successful in describing numerous polymeric systems and their applications [23, 108–111]. On the other hand, the Groot-Warren model was primarily developed for systems containing water, where the value of a_{ii} is derived from the compressibility of water with the assumption that $a_{ii} = a_{jj}$ for mixtures of two (i and j) or more types of beads. This assumption necessitates that all bead types have the same molecular volume and density (i.e., water density). However, during the process of coarse-graining, it can be challenging to control the number of atoms per bead when identifying the chemical functional groups, which can result in notable variations in bead volume [15, 23].

To fix this problem in 2007, Travis et al. [112] proposed a specific relationship between Scatchard–Hildebrand's regular solution theory and DPD interaction parameters a_{ii}. They established a connection between a_{ii} and the cohesive energy densities ρ_i. Their approach eliminated the assumption ($a_{ii} = a_{jj}$) that the repulsive interaction parameters between beads must be identical. The authors proposed an alternative method to estimate a_{ij} by:

$$\left(\delta_i - \delta_j\right)^2 = -r_c^4\alpha\left(\rho_i^2 a_{ii} + \rho_j^2 a_{jj} - 2\rho_i\rho_j a_{ij}\right) \tag{22}$$

where δ_i and δ_j are the solubility parameters of i and j particle components. The final dimensionless form of the equation is

$$\left(\delta_i - \delta_j\right)^2 = -\rho^2\alpha\left(a_{ii} + a_{jj} - 2a_{ij}\right) \tag{23}$$

Similar to Travis et al. [112], Goal et al. [23] calculated the a_{ii} or a_{jj} interaction parameters individually for both binary components, derived from the isothermal compressibility of the pure component by Equation (14) and $k^{-1} = 1 + \frac{2\alpha a_{ii}\rho}{k_B T}$ [23]. In addition, Kacar et al. [15] proposed that the like-like interaction parameters can be determined by achieving the pure liquid density for each bead type at the given pressure, using the following equation:

$$a_{ii} = \frac{p - \rho_{i,pure} k_B T}{\alpha \rho_{i,pure}^2 r_{DPD}^3} \tag{24}$$

In this equation, the pressure can be adjusted to control the overall compressibility of the mixture or by selecting a specific component and defining its compressibility. They expressed the following relations to describe the interaction parameters between unlike particles:

$$\Delta a_{ij} = \frac{p}{0.0454\left(a_{ii}\rho_i^{pure} + a_{jj}\rho_j^{pure}\right)}\chi_{ij} kT \tag{25}$$

$$\Delta a_{ij} = a_{ij} - a_{ij}, a_{ij} = \sqrt{a_{ii}a_{jj}} \text{ at } pr_{DPD}^3 \approx 23.8\, kT \tag{26}$$

By employing this approach to model beads that represent distinct chemically functional groups within a polymer, it is unnecessary to fulfill the condition of equal volume for each bead. The behavior of the beads, as described by this method, is consistent with Flory-Huggins theory and encompasses the Groot and Warren relationship as a special case that applies solely to beads with identical volumes [15].

1.3.2 | Physical Significance of DPD Parameters in Polymer Behavior

DPD is widely used to model polymer systems, with its key interaction parameters defining the thermodynamic and transport properties of the system. The three main forces in DPD each play a distinct role in determining the structural and dynamic behavior of polymers.

The conservative force parameter (a_{ij}) governs polymer-polymer and polymer-solvent interactions and is directly correlated to the Flory-Huggins interaction parameter (χ_{ij}). A higher a_{ij} value indicates stronger repulsion, leading to phase separation, while a lower a_{ij} value favors miscibility and homogeneous mixing [21]. This interaction parameter is fundamental in predicting polymer blend stability, self-assembly of block copolymers, and surfactant aggregation.

The dissipative force, controlled by the dissipation coefficient (γ), regulates hydrodynamic behavior, viscosity, and molecular relaxation times. Increasing γ leads to higher viscosity, mimicking the behavior of high molecular weight polymer melts and allowing DPD to capture viscoelastic and rheological properties in polymer solutions [113].

The random force ensures proper thermal fluctuations and maintains the system at the correct temperature. It is responsible for polymer diffusion and molecular motion, which is particularly relevant for polymer swelling, nanoparticle-polymer interactions, and chain conformations in solutions. By tuning random force, the diffusivity and self-assembly dynamics of polymer chains can be accurately represented [114].

1.4 | Hydrogen Bonding in DPD—Limitations and Enhancements

Hydrogen bonding plays a critical role in the structural and dynamic properties of biomolecular systems, polymeric materials, and soft matter. However, traditional DPD, with its soft repulsive force field, struggles to accurately capture the attractive and directional nature of hydrogen bonds. To address this limitation, various approaches have been proposed, including modified interaction potentials and multi-body force model techniques. The Morse potential, for example, introduces a short-range attractive interaction between donor and acceptor beads, offering computational efficiency but lacking explicit bond directionality [115–119]. Alternatively, multi-body force models account for local environmental effects, improving hydrogen bond network representation at the cost of increased computational complexity [120]. These advancements enhance the ability of DPD to model hydrogen bonding, though further refinements are necessary for achieving a balance between accuracy and efficiency in coarse-grained simulations.

1.5 | DPD and Bonded Forces

Alongside the interaction forces mentioned earlier for polymer modeling, it is also necessary to establish the force that links monomers together in linear chains. Fortunately, due to the advancement of DPD, it is relatively straightforward to model polymers by connecting DPD particles with spring forces [11, 121, 122, 123]. Various types of spring potentials can be employed, such as Hooke's law, finitely extendable nonlinear elastic springs, or more intricate force laws like Frenkel's springs. This force is usually explained as Hooke's spring;

$$\mathbf{f}_i^{(spring)} = \sum_j C\mathbf{r}_{ij} \tag{27}$$

The equation above calculates the total contribution of connected particles for particle i, with the spring constant selected to ensure that the average distance between connected particles corresponds to the maximum peak of the pair correlation function [18].

It was found that bond angle potentials were unnecessary in obtaining polymer microphase separation [124–126]. Consequently, bond angle potentials can be removed during the coarse-graining process, as they are not crucial for achieving polymer microphase separation. However, the bond angle potential within a DPD model is responsible for characterizing the level of molecular flexibility. Therefore, for systems where analyzing the elastic properties of the chains is critical, such as membranes, an appropriate bond angle potential should be incorporated [127–129].

1.6 | DPD and Polymer Dynamics: Challenges in Capturing Entanglements

Although polymers of arbitrary architectures and block copolymers can be modeled using the DPD method [18, 61], due to the soft interaction model, it is not expected that entanglements can be taken into account by the method. In fact, despite accurate and correct static properties resulting from DPD, dynamic properties, such as viscosity and diffusion coefficients of melts or polymer solutions, may not be properly simulated by DPD. Nevertheless, according to Groot and Warren [18, 61] DPD studies on block copolymer melts can be applied to determine the dynamical pathway in which a block copolymer melt approaches its equilibrium structure after quenching [61].

1.7 | Extending DPD for Free Surface Simulations: Many-Body DPD (mDPD)

Despite the broad applicability and success of DPD in addressing practical problems, the quadratic equation of state based on the conservative force lacks a van der Waals loop, and differs significantly from the equation of state for real fluids. Furthermore, since the dissipative and random forces act as a thermostat, the effective force between DPD particles remains purely repulsive due to the conservative force. Consequently, there are no attractive forces to bind the particles together, leading to a simulation box that becomes fully occupied by particles. While DPD is well-suited for studying systems with fluid interfaces, it is not feasible to investigate systems with free surfaces under these conditions [130, 131]. Several groups [131–133] have attempted to address this issue by modifying the original DPD method to incorporate the van der Waals loop into the equation of state, leading to the development of the many-body (or multibody) dissipative particle dynamics (mDPD) [130]. The mDPD method by Pagonabarraga and Frenkel [132] added an attractive force to DPD. The attractive force is independent of density, whereas the repulsive force is determined by a weighted average of the local density:

$$\boldsymbol{F}_{ij}^C = A_{ij}\omega_c(r_{ij}) + B_{ij}\left(\overline{\rho}_i + \overline{\rho}_j\right)\omega_d(r_{ij}) \tag{28}$$

The weight functions $\omega_c(r) = \left(1 - \frac{r}{r_c}\right)$ and $\omega_d(r) = \left(1 - \frac{r}{r_d}\right)$ are set to 0 for $r \geq r_c$ and $r \geq r_d$, respectively. The attractive component, $A_{ij}\omega_c(r_{ij})$ can be obtained by reversing the sign of the original force parameter, a_{ij}, $A_{ij} < 0$. The repulsion term for many-body interactions is expressed as self-energy per particle, with a quadratic relation to local density. $B_{ij}\left(\overline{\rho}_i + \overline{\rho}_j\right)\omega_d(r_{ij})$ is a many-body repulsive component with B>0. The density for each particle is defined as

$$\overline{\rho}_i = \sum_{j \neq i} \omega_\rho(r_{ij}) \tag{29}$$

$$\omega_\rho(r) = \frac{15}{2\pi r_d^3}\left(1 - \frac{r}{r_d}\right)^2 \tag{30}$$

The subsequent section examines how DPD and mDPD have been utilized to investigate various practical issues in polymer science and engineering, with the aim of encouraging greater adoption of these methods in this field.

2 | Molecular Self-Assembly

Recently, molecular self-assembly has emerged as a promising research field for creating complex and fascinating supramolecular structures [134–137], such as micelles [138–142], helices [143], fibers [144, 145], films [146, 147], ribbons [148], tubules

[149, 150], vesicles [151–154], and so on. These supramolecular structures have a diverse range of applications in different fields, including coatings [155, 156], tissue engineering [157, 158], drug delivery systems [159–162], and sensor devices [163, 164]. Polymeric self-assembled structures are only one type of these supramolecular aggregates formed from amphiphilic polymers with different molecular architectures in aqueous media [165–168]. Their exceptional properties as drug delivery vehicles have been recognized, including good biocompatibility, high stability, a simple preparation process, uniform sizes, easily modifiable surface groups, potential for multiple functions, and efficient drug loading [165, 169]. The substantial growth in the utilization of functional micelles as smart drug delivery systems, such as magnetic polymeric micelles [170], redox-sensitive micelles [171, 172], photo-responsive micelles [173], temperature-responsive micelles [174], ultrasound-sensitive micelles [175], and brain-targeted micelles, is attributed to their exceptional properties [176]. These micelles can respond effectively to a wide range of stimuli, making them increasingly important in the field.

However, studying the behavior of polymeric micelles with current experimental methods can be difficult, mainly due to their small size, typically ranging from 10 to 100 nm [177]. Computer simulations have emerged as a valuable and effective analytical tool for understanding experimental results related to polymeric morphologies, particularly in cases where detailed information on their behavior is difficult to obtain through current experimental approaches. Through simulations, additional insights into the dynamics, distributions, and ordering of these morphologies can be obtained [178–180]. In the last decade, DPD simulations have outperformed MD simulations by describing much larger systems for significantly longer times. In other words, DPD has become an organized and effective method that enabled the study of polymeric micelles' microstructure and their formation mechanism [141, 165, 181–186]. For instance, it was observed that the initial stages of micelle formation and amphiphilic copolymer micellization could occur within a few nanoseconds, while the final stage of micelle equilibration might take years [187]. There are several challenges to investigating the micellization kinetics experimentally because the very early stage is restricted by the spatial and temporal resolution of current scattering techniques, which can monitor only reasonably large micelles [188]. In the following, we highlight some examples of the vast body of research that has employed DPD simulations to study polymer self-assembly. The research has looked at different copolymer structures and their chemical properties, which are key to shaping the morphology, internal organization, and stability of polymeric self-assemblies.

2.1 | Linear Copolymers Self-Assembly

The process of self-assembly in linear amphiphilic block copolymers, when placed in certain solutions, has been deeply studied, resulting in a variety of different self-assembled structures [189]. The balance between the hydrophobic and hydrophilic segments, along with the design of the copolymer backbones, plays a critical role in determining the shape, internal structure, and stability of the resulting supramolecular structures. Due to its effectiveness in modeling polymeric self-assembly processes and capturing the corresponding morphology, the DPD approach has been frequently employed to study the self-assembly of amphiphilic copolymers, particularly linear ones.

Drug delivery is a key application of polymer self-assembly, particularly when using amphiphilic block copolymers. As a result, many studies have looked into how these copolymers self-assemble in the presence of drug molecules, aiming to achieve both self-assembly and drug encapsulation at the same time. For instance, Wang et al. [169] employed DPD simulations and coarse-grained models to investigate the self-assembly process of micelles loaded with Doxorubicin (DOX) using a linear copolymer of docosahexaenoic acid conjugated His10Lys10 (DHA-His10Lys10). The hydrophobic blocks of this amphiphilic copolymer were composed of docosahexaenoic acid (DHA) and histidine (H), while lysine (K) made up the hydrophilic block. The researchers determined the DPD interaction parameters of the segments by using Equation (21), where a_{ij} is expressed as χ_{ij}. They calculated χ_{ij} from the Hildebrand solubility parameters δ_i and δ_j, which were calculated via all-atom MD simulations [190], using the following equation

$$\chi_{ij} = \frac{V_{bead}}{RT}\left(\delta_i - \delta_j\right)^2 \tag{31}$$

in which V_{bead} is the volume of a bead. According to the DPD modeling results, by the progression of the simulation, some DHA-His10Lys10 and DOX molecules aggregated and formed clusters of small size. At the end of the simulation, they observed that all the small clusters gathered and formed a stable and large micelle, such that all DOX molecules dispersed into the micelle, including a hydrophobic core of DHA-His10 blocks and a hydrophilic shell of Lys10 blocks (see Figure 1A). Min et al. [191] also implemented DPD simulations to systematically elucidate the self-assembly morphologies of drug delivery systems and the loading/release of DOX in amphiphilic tri-block copolymer PCL-PDEA-PSBMA/PEGMA (poly(ε-caprolactone)-*b*-poly(diethylaminoethyl methacrylate)-*b*-poly(sulfobetaine methacrylate) or poly (ethylene glycol methacrylate)) in aqueous solutions. They found that as the copolymer concentration increased, the self-assembled morphologies of PCL-PDEA-PSBMA and DOX remained spherical micelles, while PCL-PDEA-PEGMA transitioned from spherical to cylindrical and finally to lamellar micelles. This indicated that the PSBMA system was more stable than the PEGMA system. Additionally, they discovered that although both copolymer systems could self-assemble into core-shell-corona micelles, the corona layers in PCL-PDEA-PSBMA nanoparticles were homogeneous, whereas those in PEGMA nanoparticles were inhomogeneous. Luo et al. [192] examined the assembly of PAE-*g*-PEGLA copolymers, which include pH-sensitive poly(β-amino ester) grafted with hydrophilic PEG and hydrophobic poly(D, L-lactide), and their ability to load/release DOX·HCl. They found that in water, PAE-*g*-PEGLA formed irregular aggregates, while solvent exchange between THF and H_2O led to bilayer-structured vesicles. The hydrophobic PAE and PLA blocks clustered inside the membrane, and hydrophilic PEG blocks formed the membrane/H_2O interface. Stability increased with longer PLA blocks. DOX·HCl was loaded at pH 7 and released at pH < 7 due

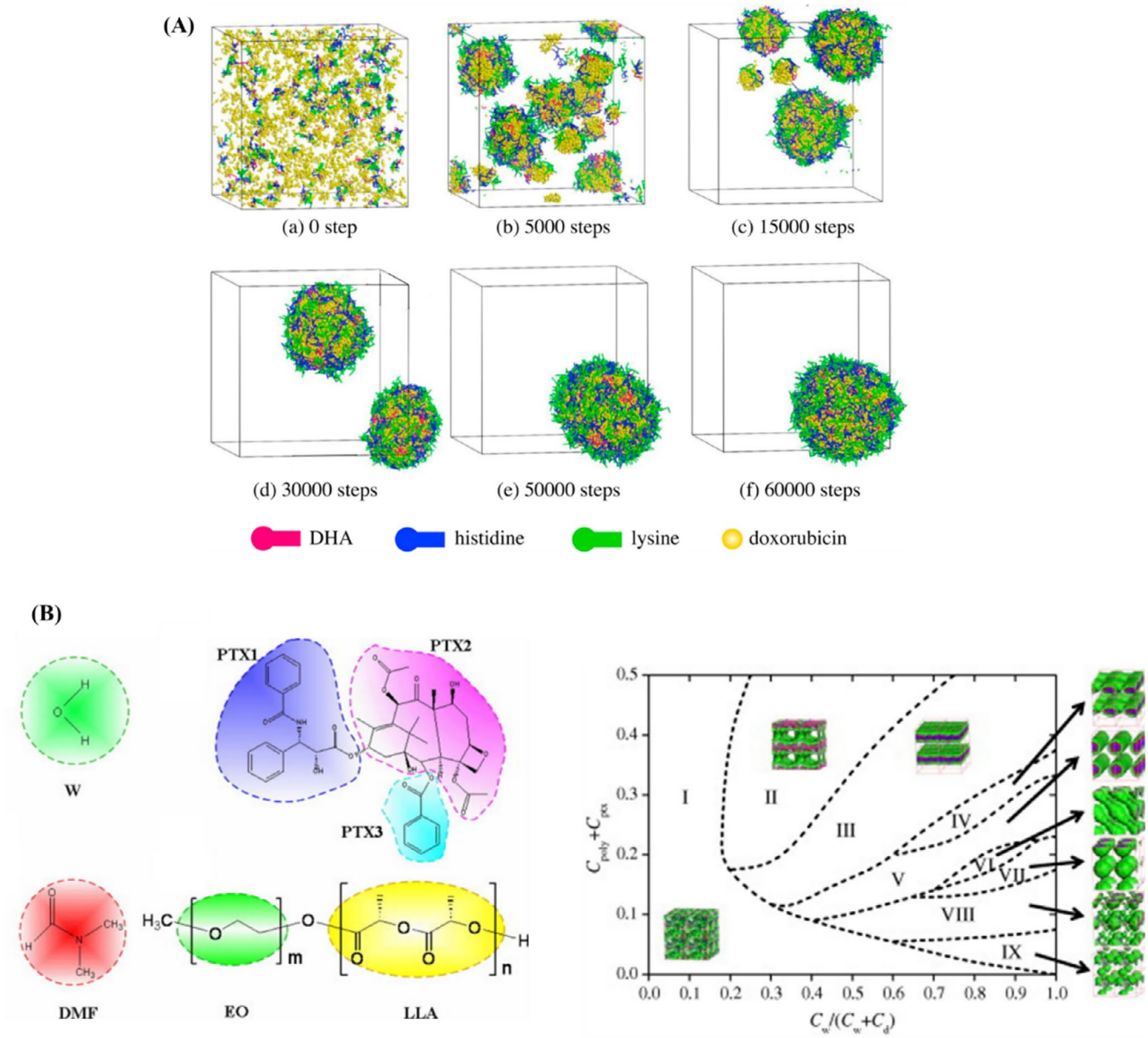

FIGURE 1 | Phase diagram predictions from DPD simulations; (A) Configurations of drug-loaded micelles at different simulated steps [169]. Reproduced with the permission of Elsevier, Copyright 2023. (B) Left panel: Schematic representation of the coarse-grained models of water, N,N-Dimethylformamide, paclitaxel, and PEO-*b*-PLLA, Right panel: Phase diagram as a function of $C_w/(C_w+C_d)$ and $C_{poly}+C_{ptx}$ for the ratio $C_{poly}/C_{ptx}=1.56$ [193]. Reproduced with the permission of Elsevier, Copyright 2023.

to protonation of the PAE blocks, making the membrane more permeable.

In another study, Luo et al. [194] integrated atomistic MD and DPD simulations to examine the loading and release of camptothecin (CPT) in a pH-sensitive diblock copolymer, consisting of hydrophobic poly(β-amino ester) (PAE) and hydrophilic methyl ether-capped poly(ethylene glycol) (PEG). For calculating the interaction parameter χ_{ij} between binary components *i* and *j*, they defined the mixing energies using atomistic MD simulations

$$\Delta E^{mix} = E_{ij} - \left(E_i + E_j\right) \tag{32}$$

in which E_{ij} is the potential energy of the binary mixture, and E_i and E_j are the potential energies of pure components i and j, respectively and ΔE^{mix} is mixing energy. They calculated the Flory-Huggins interaction parameters, χ_{ij}, as follows:

$$\chi_{ij} = \frac{\Delta E^{mix} V_r}{RT\Phi_i\Phi_j V} \tag{33}$$

Here V_r represents the average molar volume of the two-component types i and j, Φ_i and Φ_j denote the volume fractions of pure components i and *j*, respectively, T is the temperature, R is the gas constant, and V is the total volume of the system. Luo et al. [194] examined the micellization/demicellization of PAE–PEG and pH-sensitive loading/release of CPT. According to their DPD simulations, small spherical micelles were formed at a low concentration with their hydrophobic PAE-block in the core and PEG-block in a thin hydrophilic shell. By increasing the polymer

concentration, other morphologies of the aggregates, including disk-like micelles, vesicle structures, and bilayer structures, could also be observed. In the drug loading process, they observed that CPT molecules were adsorbed into small clusters formed by polymer chains, leading to an increase in cluster size, followed by CPT loading into larger micelles. After the protonation of PAE to PAEH, CPT molecules loaded in micelles (or vesicles) were released through a swelling-demicellization-release mechanism. Loading paclitaxel (PTX) in the self-assembled methoxy-poly(ethylene glycol)-poly(2-(N,N diethylamino)ethyl methacrylate)-polycaprolactone (mPEG-PDEA-PCL) (PDC) as a pH-responsive polymeric system was investigated by Li et al. [165] using both DPD simulations and experiments. The copolymer studied includes a pH-responsive segment, PDEA, which transforms into its protonated form, PDEAH+, in an acidic environment. They demonstrated that the high-low pH transition caused a significant difference between $\chi_{PDEA/H_2O}(2.89)$ and $\chi_{PDEAH+/H_2O}(-0.21)$ due to the hydrophobic-hydrophilic transition of PDEA to PDEAH+. DPD calculations revealed the dynamic process of PDC self-assembly and PTX loading in PDC micelles in a neutral environment. They suggested that the hydrophobic interaction between the PDC hydrophobic segments and the hydrophobic PTX molecules drove micelle formation and drug loading. However, the hydrophobic-hydrophilic transition of PDEA to PDEAH+ in an acidic environment was the leading factor in rapid PTX release. Guo et al. [193] also studied the phase behavior of paclitaxel loaded poly(ethylene oxide)-*b*-poly(L-lactide) (PEO-*b*-PLLA) copolymers in water and N,N-Dimethylformamide (DMF) from a mesoscopic point of view (see Figure 1B). The DPD results showed that the phase behavior of paclitaxel-loaded PEO_{11}-*b*-$PLLA_9$ in water and DMF was affected by the hydrophobic fractions and the solvent composition. To better understand the phase behavior, they studied the phase transitions at various C_{poly}(volume fraction of the copolymer) + C_{ptx} (volume fraction of drug) and solvents compositions (see Figure 1B). The resulting phase diagram consisted of nine distinct phases, each with different phase structures: (I) homogeneous disordered, (II) bi-continuous, (III) lamella, (IV) HPL (Hexagonal Perforated Layer), (V) rod, (VI) dumbbell, (VII) spherical structures with large and uniform size, (VIII) spherical structures with varying sizes, and (IX) spherical structures with small and uniform size. Wang et al. [195] conducted DPD simulations to investigate DCPD (dicyclopentadiene)-loaded micelles self-assembled from amphiphilic triblock pH-sensitive copolymers PEO-*b*-PDEAEMA-*b*-PMMA (poly(ethylene oxide)-*b*-poly(2-(diethyl amino)ethyl methacrylate)-*b*-poly(methyl methacrylate)). The self-assembly process formed a stable three-layered core-shell structure: core (DCPD), mesosphere (PMMA-PDEAEMA mix), and shell (PEO). They found that DCPD loading slowed aggregation and enhanced micelle stability without affecting micelle size. Simulations of the protonation process revealed that after protonation, DEAH beads migrated to the shell's surface, while MMA beads stayed in contact with DCPD beads. They proposed PEO-*b*-PDEAEMA-*b*-PMMA as a promising material as healing agent delivery system with desirable characteristics.

On the other hand, some researchers have directed their attention to the self-assembly of linear copolymers, focusing mainly on understanding the self-assembly process, the internal structure of the aggregates, and how these aggregates break apart, rather than exploring specific applications for the materials. This fundamental research is crucial as it lays the foundation for developing copolymer-based materials with desirable properties and functionalities. By comprehensively investigating the self-assembly of linear copolymers, researchers can gain insights into the molecular interactions that govern the formation of these aggregates, which can ultimately inform the design of copolymer-based materials for a wide range of applications. Below, we will describe some of those research studies.

Block copolymer-based microcapsules are stabilized by interface-driven forces when the system exceeds the critical micelle concentration, and various external factors, such as stimuli, dilution, and agitation, can influence their stability [196]. Covalent crosslinking between block copolymers has been established as an effective approach to creating nano-objects with prolonged retention times, which enhances the stability of nanostructures [197, 198]. In this regard, Wang et al. [199], developed a coarse-grained microcapsule model featuring a crosslinked shell of pH-sensitive diblock copolymers, PEO-*b*-PDEAEMA, enabling tunable particle permeability in response to pH variations. They used DPD simulations to investigate the formation and pH-responsive collapse of microcapsules from the self-assembly of a PEO-*b*-PDEAEMA/DCPD mixture. Their study demonstrated preferential DCPD loading in PEO-*b*-PDEAEMA polymers and explained the concentration-dependent encapsulation efficiency of DCPD. They found that as pH decreased, non-covalently bonded shells broke into small worm-like clusters due to increased self-repulsion of the protonated copolymers, while crosslinked nodes between blocks maintained stable polymer shells in acidic solutions.

Li et al. [200] investigated the micellization behavior of the copolymer methoxy-poly(ethylene glycol)-*b*-poly(ε-caprolactone)-*b*-poly(diethylaminoethyl methacrylate) (mPEG-PCL-PDEA) to elucidate the relationship between the number of pH-responsive units and micelle properties. At physiological pH (7.4), they observed that the hydrophilic PEG segment formed the outer shell of the micelle, encapsulating the hydrophobic core composed of PCL and PDEA blocks. However, when the pH decreased to 5.0, the amino groups in the PDEA block underwent protonation, leading to increased incompatibility with PCL. This incompatibility triggered a structural rearrangement, causing the PDEA block to migrate toward the micelle's outer layer. Furthermore, their study revealed that extending the PDEA block length resulted in a greater fraction of protonated PDEA shifting to the shell, displacing some PEG chains toward the core. As a result, the micelle's surface became predominantly covered by protonated PDEA, significantly altering its physicochemical properties (see Figure 2A).

Modifying the effective parameters of a system is one way to alter the properties and morphology of polymeric supramolecular structures. Another method is to introduce an additional polymeric component (such as a homopolymer or copolymer) to the system, which can also be used to fine-tune its properties and morphology. In this context, Zhao et al. [201] used the DPD method to investigate the self-assembly of the diblock copolymer poly(ethyl ethylene)-*b*-poly(ethylene oxide) (PEE-*b*-PEO) and the homopolymer poly(propylene oxide) (PPO)

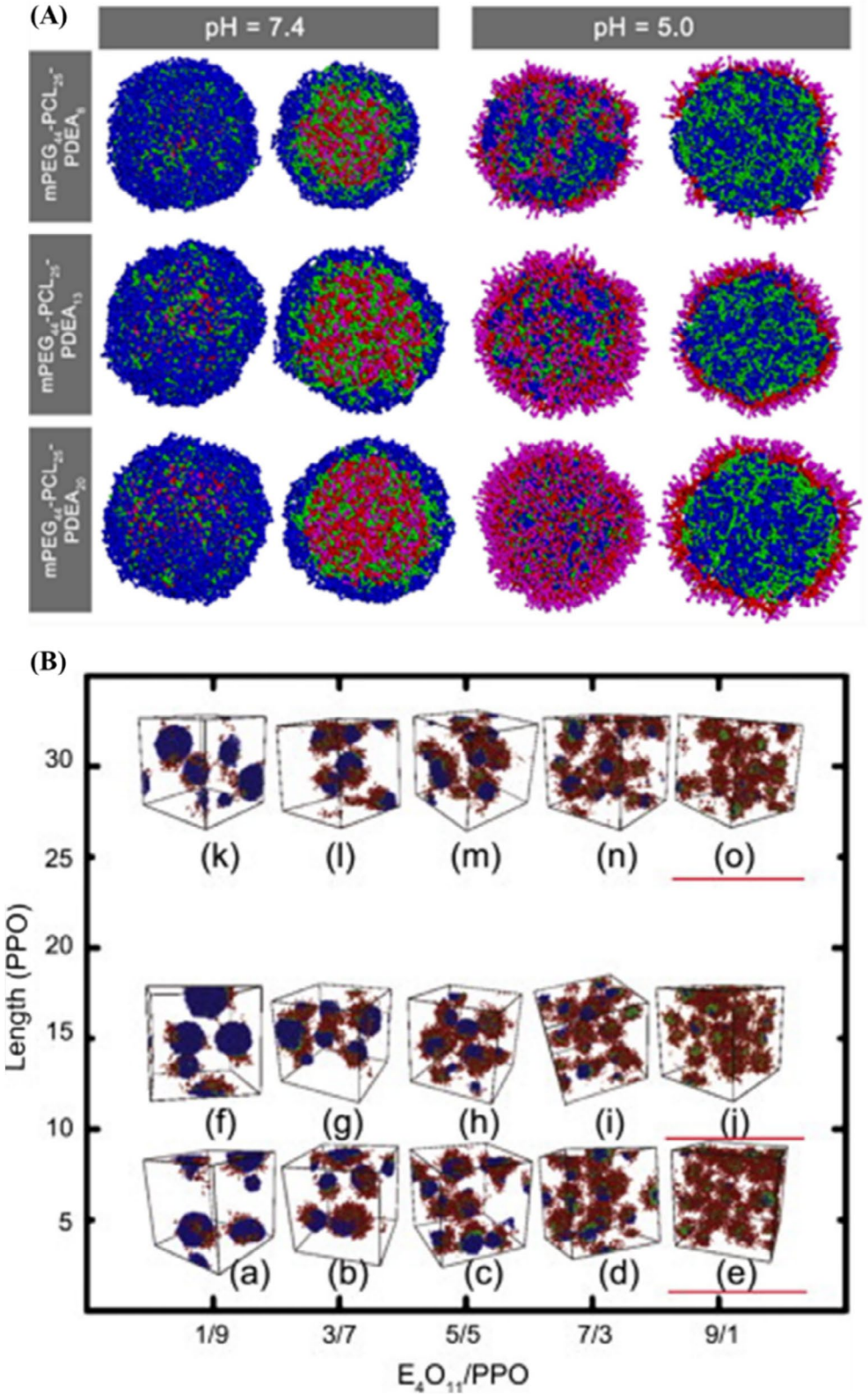

FIGURE 2 | (A) The final coarse-grained models of mPEG-PCL-PDEA micelles in water at pH 7.4 and pH 5.0 [200]. Reproduced with the permission of Elsevier, Copyright 2023. (B) Morphological phase diagram of the E_4O_{11}/PPO system, showing the effect of PPO chain length, volume fraction ratios, and molecular weights of PEE and PEO blocks (E_xO_y, where x and y are molecular weights divided by 1000) [201]. Reproduced with the permission of Elsevier, Copyright 2023.

in an aqueous solution. They determined the parameters for the polymer beads by utilizing the solubility parameters of the pure species. However, the interactions between polymer and water beads were estimated according to the energy mixing, using MD simulations to show the effect of hydrogen bonds, as follows:

$$\chi = V_{bead}\left(\frac{\Delta E_{mix}}{k_B T}\right) \tag{34}$$

$$\Delta E_{mix} = \varphi_A\left(\frac{E_{coh}}{V}\right)_A + \varphi_B\left(\frac{E_{coh}}{V}\right)_B - \left(\frac{E_{coh}}{V}\right)_{AB} \tag{35}$$

Here, ΔE_{mix} is the mixing energy, while φ_A and φ_B represent the volume fractions of the two components in the dilute solution. They calculated the cohesive energy E_{coh} using MD simulations as follows:

$$E_{coh} = \left(\sum_{i=1}^{N} E_{nb}^{isolated}(i) - E_{nb}^{N}\right)/N \tag{36}$$

where $E_{nb}^{isolated}(i)$ is the energy of non-bonding interactions for the i th isolated chain in vacuum and E_{nb}^{N} represents the non-bonded energy of the model with chains under periodic boundary conditions. Their simulation results revealed novel multi-compartment micelle structures that were not observed in experiments. They discovered that the chain length of PPO plays a critical role in determining the size of multi-compartment micelles. Specifically, when the chain length of PPO is shorter or longer than the PEE-*b*-PEO block, the formation of larger multi-compartment micelles can be easily observed (see Figure 2B).

Thermo-sensitive polymeric micelles are significant in various applications such as drug, gene, and siRNA delivery, and DPD has proven to be a useful tool in investigating their self-assembly and stimuli–response behavior. Rodríguez-Hidalgo et al. [202] identified the stability zones of stimuli-responsive polymeric micelles formed by poly(N-isopropylacrylamide-*b*-3-[N-(3-methacrylamidopropyl)-N,N-dimethyl]ammoniopropane sulphonate (PNIPA-*b*-PSPP)) diblock copolymer in water, triggered by temperature. Using thermal scanning, they detected five stability zones. In zone I, micelles had a PSPP core and PNIPA shell, while in zone V, reverse micelles had a PNIPA core and PSPP shell. In zone III, free unimer chains were dispersed in the aqueous environment. Two metastable zones (II and IV) showed low thermodynamic stability of the thermo-responsive micelles.

Using DPD, Li et al. [188] investigated the equilibrium properties and micelle formation kinetics in A_2B_3 and A_4B_x (x = 4, 6, 8) deblock copolymers, where A is hydrophobic and B is hydrophilic. Their study revealed that increasing hydrophobic interactions or reducing the length of the hydrophilic block resulted in a lower unimer concentration and a higher average aggregation number. Regarding micellization kinetics, they identified a three-stage process:

i. **Initial rapid aggregation**—Unimers quickly associate into small aggregates, leading to a sharp decrease in unimer concentration until it stabilizes.
ii. **Micelle growth phase**—Intermediate-sized micelles form through the fusion of smaller submicelles, progressively increasing aggregation numbers.
iii. **Equilibration and slow rearrangement**—The micelle size continues to grow gradually, driven by fusion-fission dynamics and unimer exchange, ultimately stabilizing the weight-average aggregation number.

Ma et al. [203] explored the structural characteristics of vesicles formed by amphiphilic multiblock copolymer ABABA (A hydrophilic, B hydrophobic) in a selective solvent using the DPD method. They examined the effect of temperature and solvent properties (a_{AS} with $a_{BS} = 75$), where lower temperatures represented a good solvent (smaller a_{AS}) and higher temperatures indicated a poor solvent (larger a_{AS}). They observed that as temperature increased, vesicle size and cavity size decreased, while membrane thickness increased. Additionally, they found that the hydrophilic/hydrophobic block ratio had a significant impact on aqueous cavity size, membrane thickness, and vesicle size (see Figure 3B). Chen et al. [204] also focused on the self-assembly of random copolymers and hydrophobic homopolymers using DPD simulations. The researchers noticed self-assembled micelles couldn't be formed solely by random copolymers due to the abundance of hydrophilic particles in the polymer chain. However, when a mixture of random copolymer and homopolymer chains was used, a self-assembled structure emerged, which consisted of a homopolymer core, a random copolymer corona, and a hydrophobic block interface (see Figure 4A). This study showed that micelle morphology and size can be controlled by adding homopolymers during self-assembly. In another study, they used DPD simulations to examine the self-assembly of the segmented random-block copolymer (A-*co*-B)-*b*-C in a selective solvent [205]. The researchers found that by adjusting the copolymer composition, interaction parameters, and overall copolymer makeup, they could control the self-assembly of (A-*co*-B)-*b*-B copolymers to form various aggregates, including spherical and rod-like micelles, as well as two-compartment micelles. These findings are valuable for developing methods to create specific micelle morphologies from segmented random-block copolymers. Using DPD simulations, Li et al. [206] proposed a 'covalent-bonding-forced orthogonal self-assembly' strategy to fabricate multi-geometry nanoparticles from block alternating copolymers. They found that diblock alternating copolymers $(AB)_x$-*b*-$(AC)_y$ could self-assemble in an orthogonal manner, forming single-geometry nanoparticles, which were then covalently linked to create multi-geometry nanoparticles. The success of this strategy relied on the incompatibility and critical molecular weight of each copolymer block. By controlling the composition of $(AB)_x$ and $(AC)_y$ blocks, they achieved various binary multi-geometry nanoparticles, such as channel-sphere, worm-vesicle, and lamella-sphere. Additionally, polymer concentration and the volume ratio of alternating copolymer blocks influenced the final nanoparticle structures, as shown in the volume ratio-block composition morphological phase diagram (Figure 4B).

Liao et al. [207] performed DPD simulations to investigate the self-assembled morphologies of two copolymer systems—poly(-lactic acid)-*b*-poly(ethylene glycol) (PLA–PEG) and poly(lactic acid)-*b*-poly(carboxybetaine) (PLA-PCB)—in aqueous solutions, with a focus on their potential as anti-biofouling materials. Their study explored the effects of polymer composition and concentration on the resulting self-assembled structures. The simulations revealed distinct morphological differences between the two systems. PLA–PEG copolymers predominantly

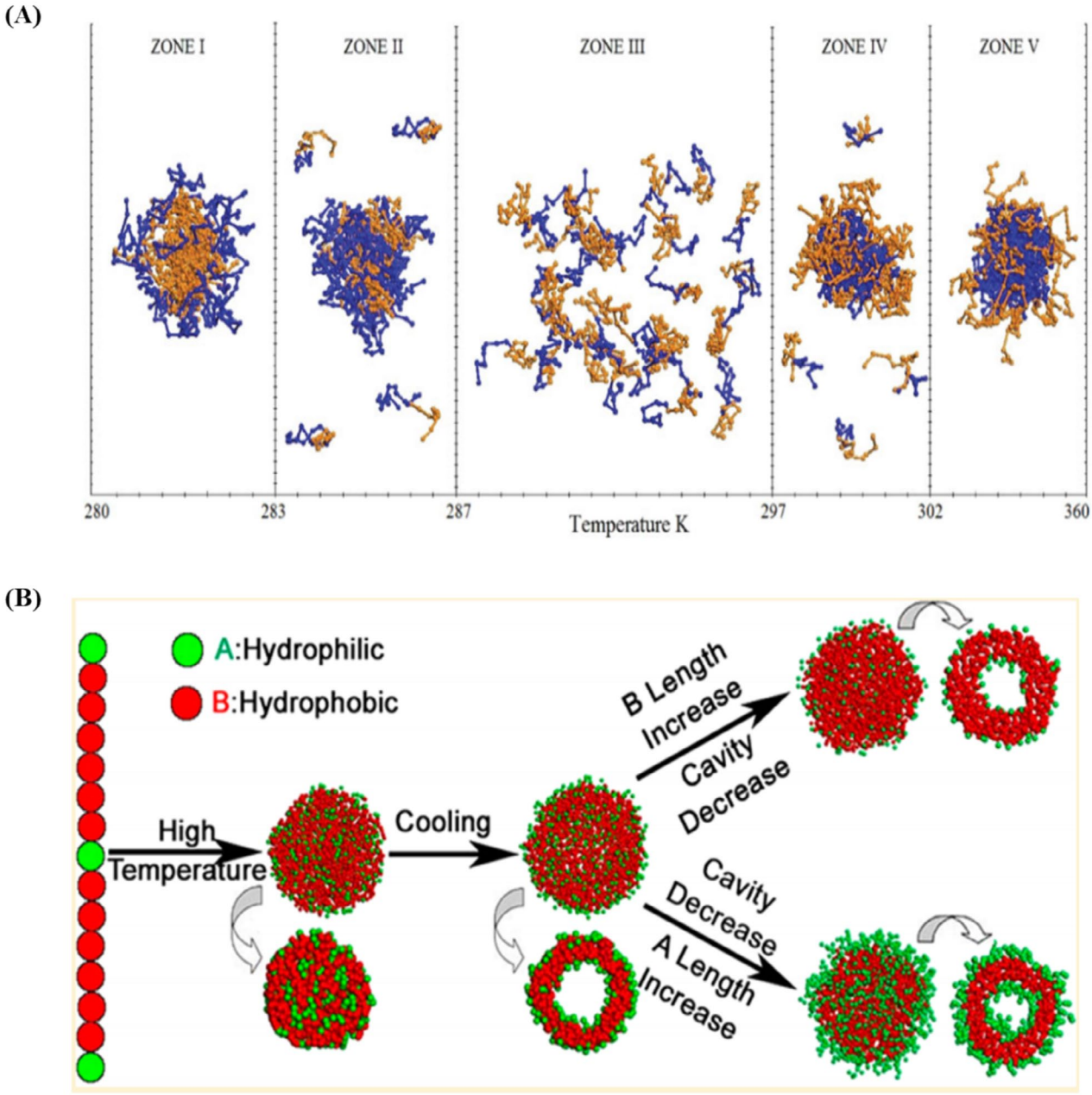

FIGURE 3 | Examples of temperature stability predictions from DPD simulations; (A) Micellar stability zones: (I & V) thermoresponsive micelles with core-shell structures (PSPP core/PNIPA shell or PNIPA core/PSPP shell), (II & IV) metastable zones with core-shell micelles coexisting with free unimer chains, and (III) free copolymer chains dispersed in the aqueous environment [202]. Reproduced with the permission of Taylor & Francis, Copyright 2023. (B) Effect of temperature and the blocks length on the vesicle structure [203]. Reproduced with the permission of the American Chemical Society, Copyright 2023.

formed core-shell structures, whereas PLA-PCB copolymers consistently assembled into onion-like and vesicle structures, regardless of their composition. Further analysis demonstrated that PCB provided greater stability than PEG in maintaining spherical morphologies. Additionally, the structural characteristics of the shell layers differed between the two systems (see Figure 5):

- PLA–PEG nanoparticles exhibited inhomogeneous shell layers, attributed to the amphiphilic nature of PEG, which leads to uneven surface distributions.
- PLA-PCB nanoparticles displayed homogeneous shell layers, owing to the strong hydrophilicity of the zwitterionic PCB block, which promotes uniform shell formation.

Multicompartment nanostructures are difficult to achieve with conventional block copolymer self-assembly. In this context, Wang et al. [208] developed a computational approach leveraging the cooperative assembly of diblock copolymer blends to design spherical and cylindrical compartmentalized micelles with complex internal structures. Their simulations explored self-assembly behaviors in pure AB, binary

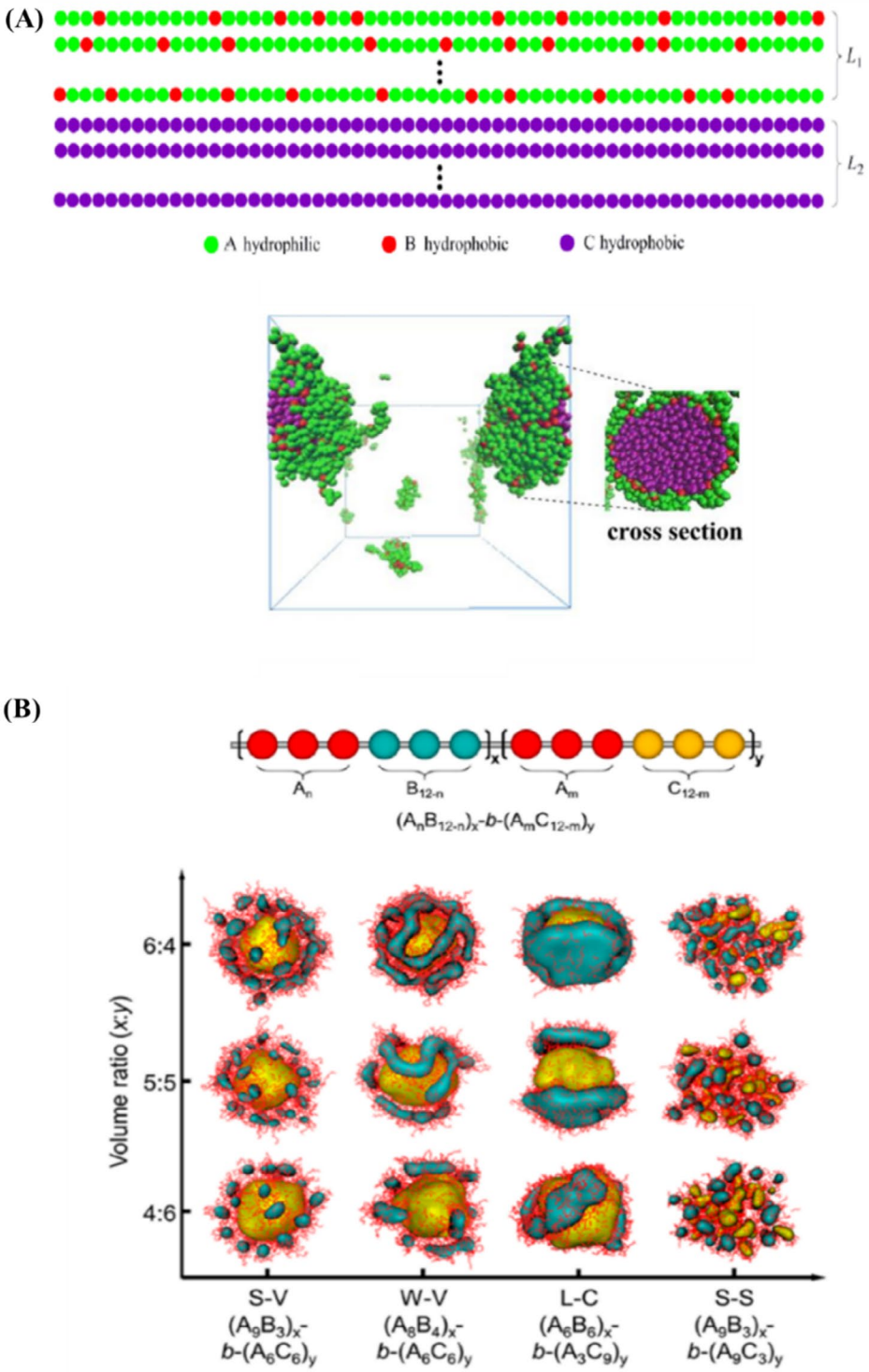

FIGURE 4 | (A) (Top Panel) Coarse-grained model of the random copolymer and hydrophobic homopolymer. Green (A) and red (B) particles represent hydrophilic and hydrophobic parts of the random copolymer, respectively, while purple (C) particles represent hydrophobic homopolymer. (Bottom Panel) Micelle morphology of a self-assembled structure composed of random copolymer and homopolymer chains ($L_1 = 54$, $L_2 = 30$) with DPD simulations at $a_{AS} = 25$, $a_{BS} = a_{CS} = 100$ [204]. Reproduced with the permission of Taylor & Francis, Copyright 2023. (B) Effect of block composition and volume ratio of $(AB)_x$ to $(AC)_y$ on multi-geometry nanoparticle architectures. Red coils represent hydrophilic A, cyan and yellow surfaces represent hydrophobic B and C. (S-V, W-V, L-C, S-S indicate sphere-vesicle, worm-vesicle, lamella-channelized micelle, and sphere-sphere, respectively) [206]. Reproduced with the permission of the American Chemical Society, Copyright 2023.

AB/AC, and ternary AB/AC/AD systems, where block A was hydrophilic, while blocks B, C, and D represented distinct hydrophobic segments. This approach led to the formation of a diverse range of nanostructures, including sponge-like, Janus, capsule-like, and onion-like micelles. A key finding of their study was the ability to fine-tune block interactions to manipulate micelle morphology and composition. By carefully adjusting segment compatibility, they demonstrated a controlled

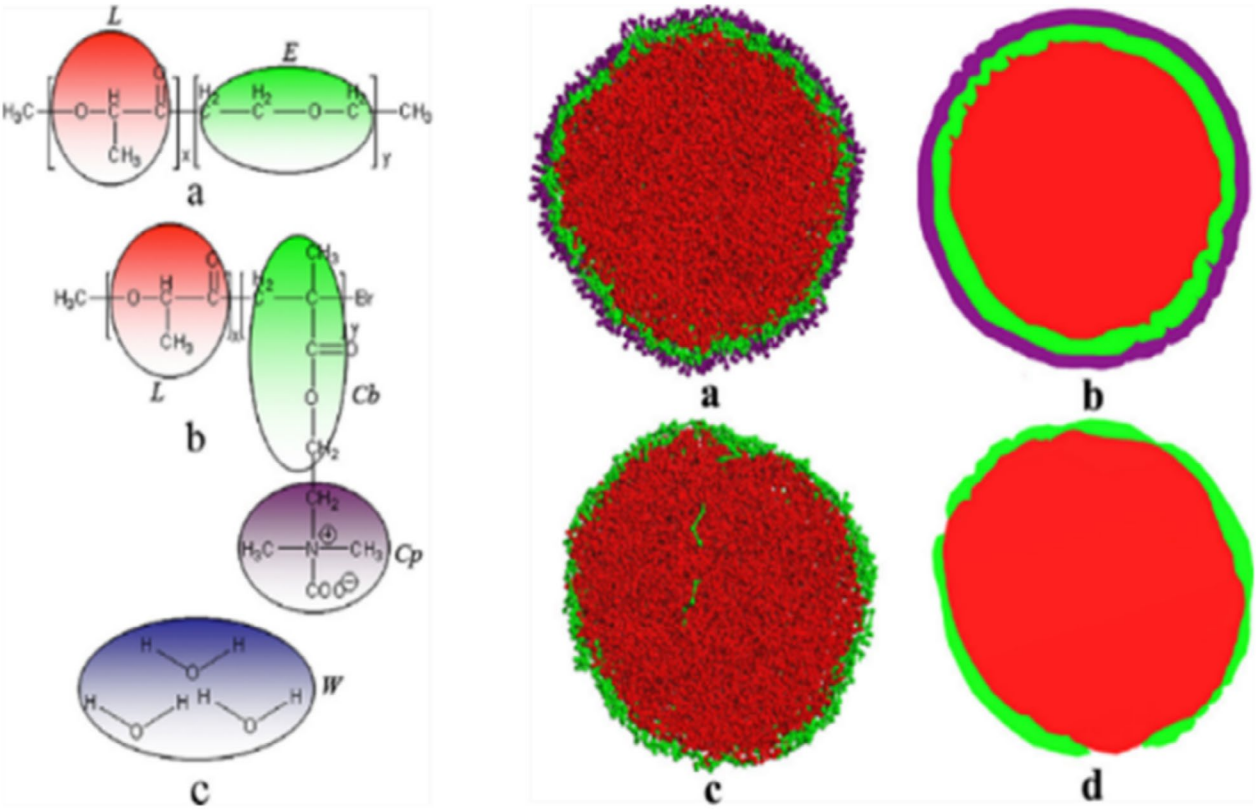

FIGURE 5 | Coarse-grained models of (Left Panel) (a) PLA–PEG and PLA–PCB (b); (Right Panel) (a) sectional view of PLA–PCB morphology, (b) slice for PLA–PCB, (c) sectional view of PLA–PEG morphology, and (d) slice for PLA–PEG [207]. Reproduced with the permission of the American Chemical Society, Copyright 2023.

transition between two distinct structural configurations in AB/AC/AD micelles:

- 'Pure shell/mixed core' morphology, where the outer shell consists of a single component while the core remains a heterogeneous blend.
- 'Mixed shell/pure core' morphology, where the shell incorporates multiple components while the core maintains uniform composition.

These results highlight a versatile strategy for designing tailored multicompartment micelles with precise control over internal organization, offering potential applications in drug delivery, nanoreactors, and biomimetic systems (see Figure 6).

To investigate the rapid self-assembly process of vesicles, which is challenging to observe experimentally and too slow for molecular dynamics simulations, Shillcock [60] utilized DPD simulations to examine the formation process of a typical linear amphiphile H3T6 (composed of three hydrophilic "Head" particles and six hydrophobic "Tail" particles). The simulations showed that this amphiphile underwent three distinct stages to self-assemble into a vesicle, and this transformation was concentration independent. The process began with a random dispersion of the amphiphiles in bulk water, which formed small spherical micelles after a few microseconds. These micelles gradually merged and transformed into quasi-planar bilayer patches, which required a certain amount of time for the micelles to grow large enough to form the planar membrane patches. Subsequently, there was an extended phase where the spherical micelles and planar bilayer patches diffused and merged gradually to form larger bilayer patches that eventually curled up to form closed vesicles. Arai et al. [209] investigated the formation of an onion-like vesicle using a minimalist model and DPD simulations, exploring the vesicle formation conditions. The study identified diverse self-assembled morphologies in Janus amphiphilic oligomer solutions and analyzed the influence of temperature, amphiphile concentration, and oligomer hydrophilicity on morphology. They also simulated a layer-by-layer water discharging process from the vesicle, resembling the "peeling-one-onion-layer-at-a-time" approach. The results showed that during the discharging process, water molecules in the center region were discharged first. With DPD simulations, Wang et al. [210] investigated the effect of terminal groups on the structure of vesicles formed by amphiphilic diblock copolymers, considering factors such as the number, location, and hydrophobicity of the terminal groups. Their findings showed that increasing the hydrophobicity of the terminal group reduced the vesicle cavity size and increased wall thickness. However, when the terminal group was located at the end of the hydrophilic block, increasing its hydrophobicity led to an increase in vesicle cavity size, while the wall thickness remained largely unchanged. Li et al. [58] used DPD simulations to study the transformation of vesicle shapes formed by triblock copolymers with a hydrophobic block in the middle and two hydrophilic blocks on the sides. By adjusting the repulsive parameters between the

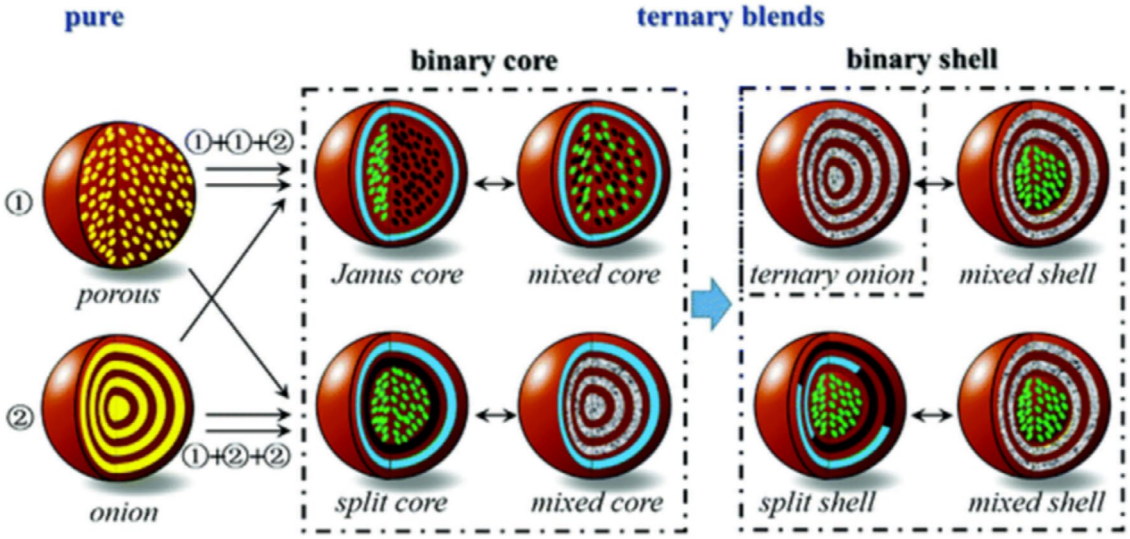

FIGURE 6 | Schematic of the cooperative self-assembly strategy of ternary diblock copolymer blends. The transition from 'pure' to 'ternary blend' shows the mixing of three diblock copolymers. Arrows between ternary micelles indicate transitions by altering block incompatibility. Brown domains represent hydrophilic blocks, while yellow, blue, dark, and green represent hydrophobic blocks; white-dark domains indicate hydrophobic block blends [208]. Reproduced with the permission of the Royal Society of Chemistry, Copyright 2023.

hydrophilic blocks to introduce spontaneous curvature, they modeled the asymmetric membrane of the vesicle. This approach led to the discovery of various complex vesicle shapes, including some previously unreported forms, such as starfish-shaped, toroidal, long rodlike, and inverted vesicles.

A giant vesicle resembling a cell-size membrane envelope mimics key characteristics of red blood cells, including their equilibrium biconcave shape and tumbling behavior under shear flow [211]. Therefore, membrane vesicles, as a popular model system, have been used to study membrane biophysics in general and red blood cell dynamics [212]. The shape changes of bilayer vesicles were investigated by using particle-based models of two-component amphiphilic diblock copolymers with the DPD approach. They started with a spherical vesicle and modified its shape by removing solvent particles from its interior and relocating them to the outer region. The simulations revealed a variety of complex vesicle shapes, including axisymmetric forms like spheres and dumbbell shapes, as well as non-axisymmetric shapes like pear, oblate, boomerang, and three- and four-armed starfish. The study demonstrated that shape transformations in lipid vesicles can also occur in polymer vesicles and that the DPD method is a simple yet effective approach for studying polymer vesicle behavior.

Mai et al. [213] investigated the phase behavior of polybutadiene-*b*-poly(ethylene oxide) (PB-*b*-PEO) copolymers in the ionic liquid [Bmim][PF_6] using DPD simulations (see Figure 7). Their study explored how copolymer concentration and the PEO/PB ratio influence self-assembled structures in an ionic liquid environment. At low copolymer concentrations, [Bmim][PF_6] acted as the continuous phase, with PB-*b*-PEO dispersed as isolated entities. However, as the PEO/PB ratio decreased, the self-assembled structures underwent a transition from spherical micelles to rod-like micelles, eventually forming vesicles. With increasing copolymer concentration, a diverse range of complex morphologies emerged, including wormlike micelles, branched lamellae, tubes, and platelets. In parallel, the role of the ionic liquid changed, transitioning from a continuous phase to a dispersed phase with microphase-separated structures. These micelle-like morphologies present promising applications in various industrial fields:

- **Membrane separation**—Enhanced control over phase separation.
- **Ion conductivity**—Tubular structures provide pathways for ionic transport.
- **Photoelectric material synthesis**—Microphase-separated IL regions offer potential in advanced material design.

The findings demonstrate the potential of PB-*b*-PEO copolymers in tailoring rheological properties and optimizing self-assembled architectures for functional applications in ionic liquid-based systems.

The transport of polymeric micelles between two immiscible phases, referred to as the micellar shuttle, is an intriguing phenomenon with considerable potential for industrial and pharmaceutical applications [214–216]. This process is reversible and strongly temperature-dependent. Soto-Figueroa et al. [217] utilized the DPD approach to study the micellization-demicellization process and micellar shuttle of PNIPAM-PEO (poly(N-isopropylacrylamide-block-ethylene-oxide)) copolymer in a biphasic system. They controlled the micellization-demicellization process and micellar shuttle by adjusting the temperature dependence of the solubility and interaction parameters of the chemical species involved (shown in Figure 8). Their simulations demonstrated that polymeric micelles migrated as a unit during the thermal process (Figure 8). They also found that at elevated temperatures, demicellization occurred in the ionic

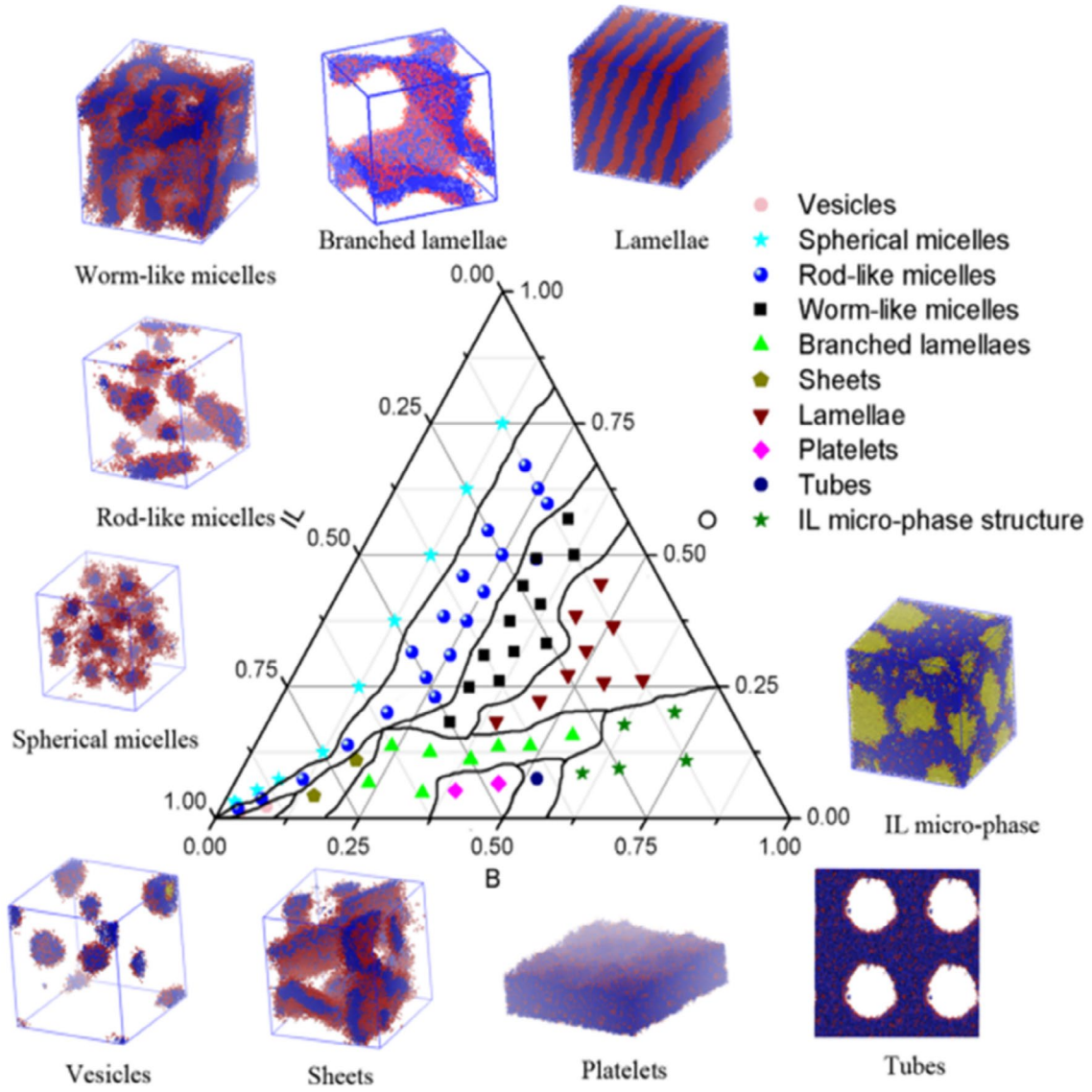

FIGURE 7 | Ternary phase diagram in vol% and corresponding structures at 298 K from DPD simulations. Blue denotes PB beads (B), red denotes PEO beads (O), and yellow denotes [Bmim][PF6] beads. Concentration is in volume fraction (vol%) [213]. Reproduced with the permission of the American Chemical Society, Copyright 2023.

liquid phase, and reduced interaction parameters caused micellar dissociation, increasing the solubility of diblock copolymer chains in the hydrophobic environment (Figure 8).

Summary:

To summarize, the following aspects of linear block copolymer self-assembly can be studied through DPD modeling:

1. The influence of solvent, copolymer composition, chain length, and chain chemistry on the self-assembly mechanism can be analyzed.
2. The internal structure and morphology of the self-assembled supramolecular structures can be observed.
3. Morphological phase diagrams can be constructed from DPD simulations of copolymers. The DPD model can be employed to investigate the encapsulation and release of small molecules, such as drugs.

2.2 | Star-Shaped Copolymers

Star-shaped polymers have gained attention as promising candidates for drug delivery applications due to their unique topology and outstanding physicochemical properties. Wu et al. [218] employed DPD simulations to examine micelle formation in a system with star-shaped polymers, analyzing the impact of the hydrophobic/hydrophilic block ratio on micellar structure and drug-loading efficiency, as well as the role of the pH-sensitive block ratio in drug release properties. The study examined loading DOX into four different topological structures of 4/6-herto-arm and 4/6-miktoarm star-shaped block polymers: $(PCL24)_2(PDEA16\text{-}b\text{-}PPEGMA19)_2$, $(PCL16)_3(PDEA14\text{-}b\text{-}PPEGMA10)_3$, $(PCL22\text{-}PDEA25\text{-}b\text{-}PPEGMA5)_4$, and $(PCL18\text{-}PDEA9\text{-}b\text{-}PPEGMA4)_6$. They found that under neutral conditions (pH = 7.4), increasing the hydrophobic/hydrophilic block ratio reduced micelle stability. Additionally, they observed that increasing the length of the pH-sensitive block (DEAH) improved drug loading performance in mikto-arm star-shaped polymeric micelles. In another study

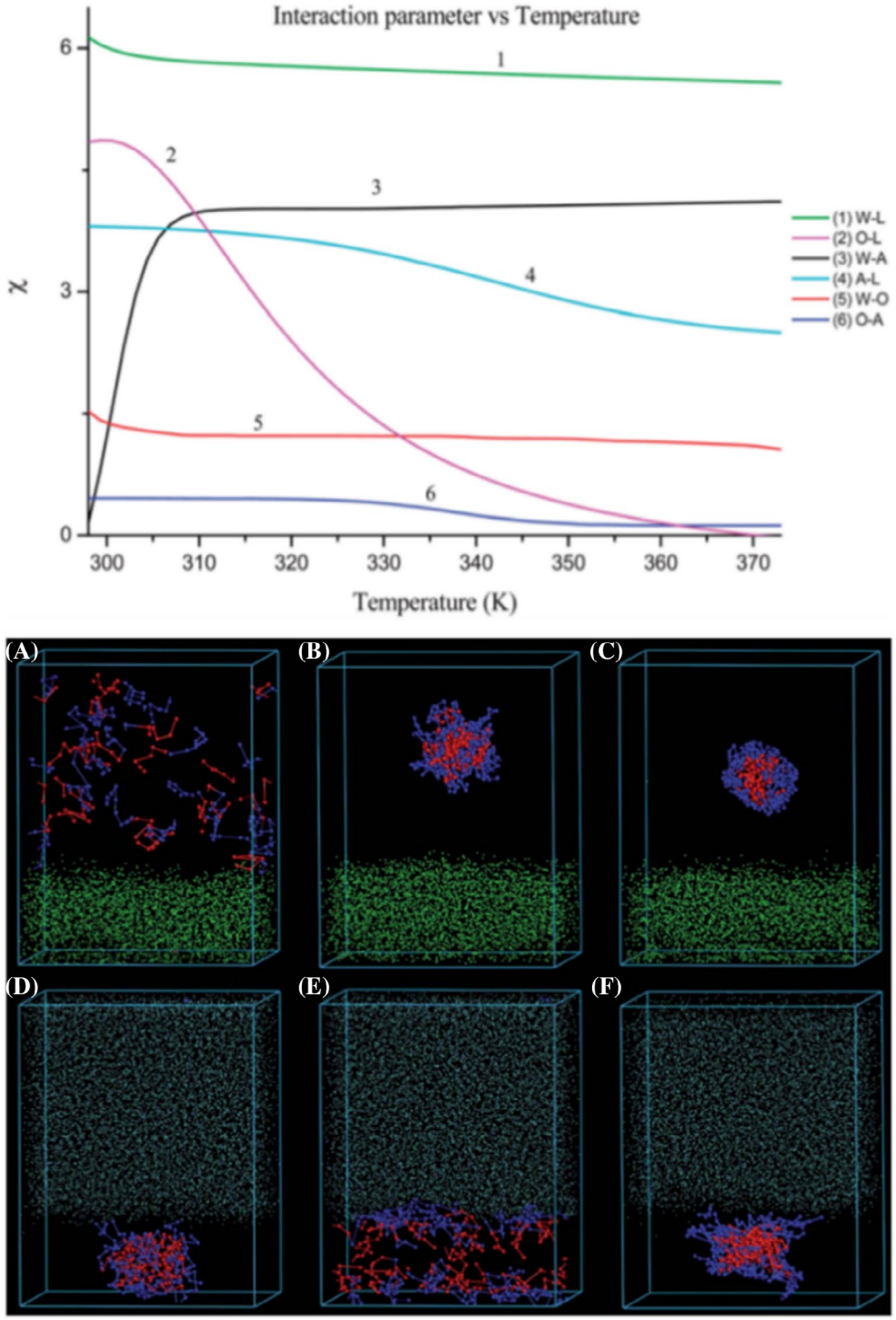

FIGURE 8 | (Top Panel) Interaction parameters of all chemical species in the micellization–demicellization process in a water/ionic-liquid system, obtained by Monte Carlo molecular simulations: W = Water molecules, L = Ionic liquid, A = PNIPAM segment, O = PEO segment. (Bottom Panel) Snapshots of the micellization–demicellization process and micellar shuttle in a water/[BMIM][PF6] system at different temperatures: (A) At 298 K, polymer chains are miscible in water; (B) micelles form in water at 303 K; (C) at higher temperatures, PEO blocks collapse and prepare for shuttle; (D) micellar shuttle to the ionic liquid phase at 333 K; (E) demicellization in ionic liquid at 346 K; (F) micelle formation at 333 K after temperature reversal [217]. Reproduced with the permission of the Royal Society of Chemistry, Copyright 2023.

on star-shaped polymers, Nie et al. [182] investigated the self-assembled structures of the pH-sensitive four-arm star triblock polymer poly(ε-caprolactone)-*b*-poly(2-(diethylamino)ethyl methacrylate)-*b*-poly(poly(ethylene glycol) methyl ether methacrylate) (4AS-PCL-*b*-PDEAEMA-*b*-PPEGMA) for DOX encapsulation using DPD simulations. This polymer system holds promising potential for hydrophobic anticancer drug delivery, enhancing cancer therapy. The system was self-assembled into micelles with DOX molecules in the core. Upon protonation of the amine groups in the polymer chains, PDEAEMA chains

became soluble in acidic solutions. By altering the pH, they observed different micellar morphologies after protonation of the PDEAEMA blocks. The study highlighted that the key factors driving these morphological changes were the sharp shift in the solubility parameter of the pH-sensitive blocks and micelle swelling.

Using DPD simulations, Chen et al. [219] examined the formation and degradation of multicomponent multicore micelles from two star copolymers ($A_2B_4B_4$ and $C_2B_4B_4$), and their dynamics. To examine the impact of interactions between the solvophobic A and solvophilic B segments, as well as between the solvophobic A and C segments, they created a morphological phase diagram based on A-B and A-C interaction parameters (Figure 9A). The study revealed several types of multicomponent multicore micelles: SCII (single core composed of A and C segments), MMII (multicore with A and C segment cores), MMI (multicore with either A or C segment cores), and MMRI (rod micelles with A or C segment cores). They found that the micelle formation process followed three stages: small aggregates → growth → micellization, while the degradation mechanism involved segment formation and diffusion, followed by core rearrangement. In another research work, Chen et al. [110] used DPD simulations to explore the self-assembly of a three-arm star-shaped polymer and identified a variety of complex colloidal particles. These included

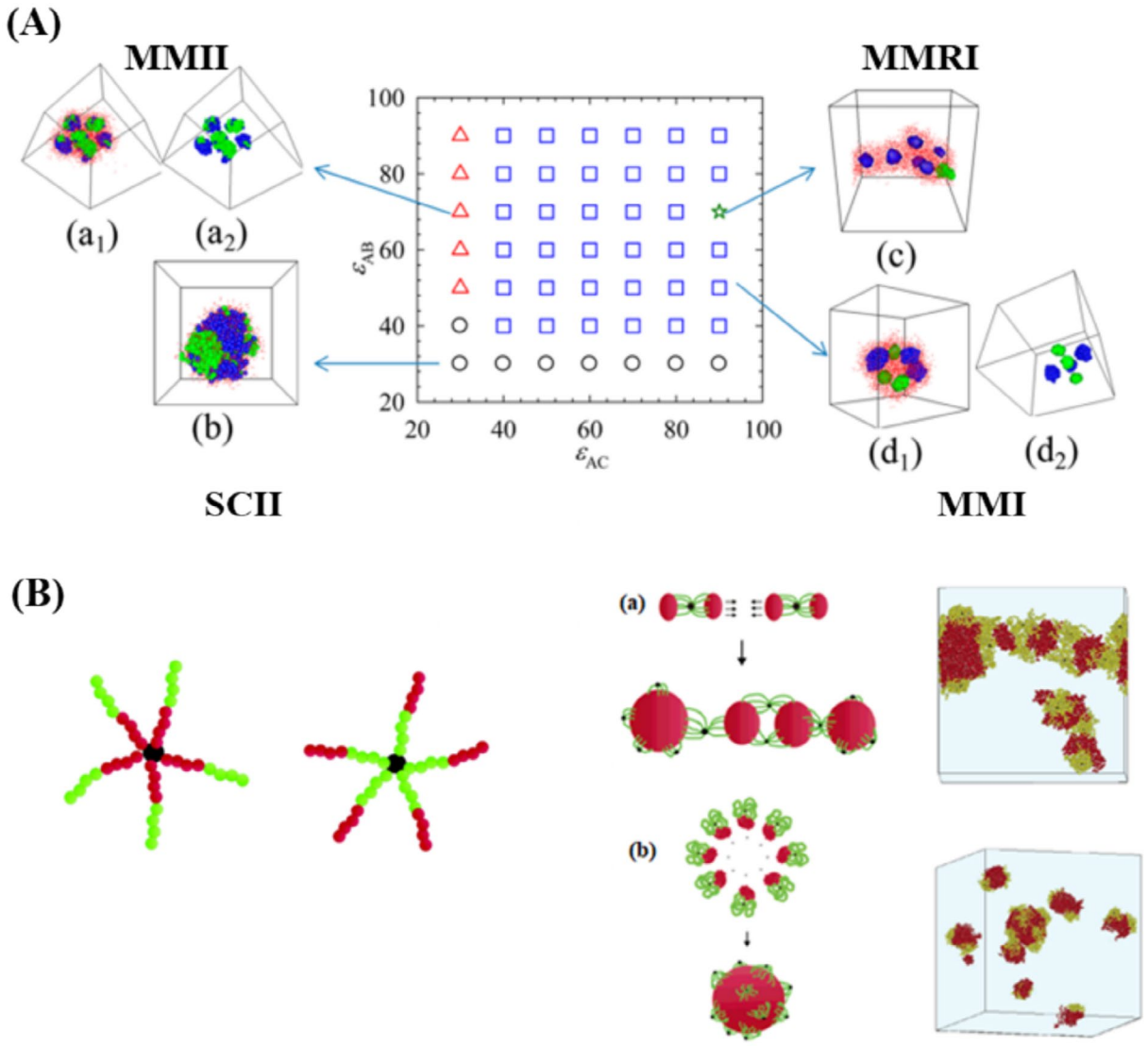

FIGURE 9 | (A) Phase diagram of self-assembled aggregates formed from a blend of two star copolymers ($A_2B_4B_4$ and $C_2B_4B_4$ in equimolar mixture) as a function of interaction parameters ε_{AC} and ε_{AB} ((Circles) Single-core micelles with cores of A and C segments (SCII); (Squares) Multicomponent multicore micelles with cores of A or C segments (MMI); (Triangles) Multicomponent multicore micelles with A and C segment cores (MMII); (Stars) Multicomponent multicore rod micelles with A or C segment cores (MMRI)). The micelle morphologies are shown for MMII (a_1, a_2), SCII (b), MMRI (c), and MMI (d_1, d_2). a_1 and d_1 show both the shell and core of the micelles, while a_2 and d_2 show only the cores. Green: A segments; Red: B segments; Blue: C segments [219]. Reproduced with the permission of the American Chemical Society, Copyright 2023. (B) Schematic representations of star-block copolymers: (Left Panel) $(BA)_n$ type and $(AB)_n$ type. (Right Panel) Morphologies of multiple $(AB)_n$ type star-block copolymers in a selective solvent with $L_A = 10$: (a) $L_B = 15$ (segmented worm micelles), and (b) $L_B = 30$ (core-lump micelles). Green bead: Solvophilic A, red bead: Solvophobic B, black bead: center of the star [221]. Reproduced with the permission of the American Chemical Society, Copyright 2023.

structures such as shell-single core, patchy particles with a central core, multicore, cylindrical layered, patchy particles with multiple cores, stacked layered with several patches on the surface, stacked layered, and stacked disk rods. Xin et al. [220] employed DPD simulations to study the formation of multicompartment micelles by blending star and linear triblock copolymers in solvents. The study found that both the blending ratio and copolymer composition significantly influenced micelle morphology. New morphologies, including toroidal micelles with ring/cogwheel cores and 'sphere-on-onion' micelles, emerged. The results showed that micelle size and structure could be controlled through different mixing options, providing a practical strategy for designing micellar structures.

Sheng et al. [221] performed DPD simulations to explore the self-assembled morphologies of star-block copolymers in dilute solutions. Their study focused on how block placement and solvent selectivity influence the resulting nanostructures. In a selective solvent for the A-block, they observed distinct morphological differences between $(BA)_n$ and $(AB)_n$ copolymers:

- In **$(BA)_n$ copolymers**, the solvophobic B-blocks aggregated at the core, while the solvophilic A-blocks extended outward, forming a corona-like structure.
- In **$(AB)_n$ copolymers**, the B-blocks did not remain confined to the core; instead, they formed aggregative domains on the periphery.

A particularly intriguing finding was the effect of B-block length on the self-assembled morphology:

- When B-blocks were sufficiently long, they clustered into a single domain, leading to an intramolecular Janus conformation.
- When the copolymer contained two distinct B-domains, the resulting structure resembled a worm-like morphology.
- The final Janus-like conformation consisted of a solvophobic core with solvophilic protrusions (lumps) on the surface, indicating a complex phase separation pattern (see Figure 9B).

These findings provide insight into the design of star-block copolymers with tailored self-assembled architectures, which may have potential applications in drug delivery, nanoreactors, and functional soft materials.

Summary:

DPD modeling can be used to study the self-assembly of star-shaped copolymers and investigate various aspects of their behavior. Specifically, DPD simulations allow researchers to explore:

1. How different polymer characteristics (e.g., number of arms, arm length, composition, and chemistry) affect the self-assembly mechanism.
2. The internal structure and morphology of the resulting supramolecular structures.
3. The creation of morphological phase diagrams that provide valuable insights into copolymer behavior.
4. The encapsulation and release of small molecules, such as drugs, occur within the self-assembled structures.

2.3 | Dendritic Polymers

Dendritic polymers, such as dendrimer multi-arm copolymers or hyperbranched multi-arm copolymers, show great potential as building blocks for self-assembled structures. These amphiphilic polymers consist of a hydrophobic (or hydrophilic) core and multiple hydrophilic (or hydrophobic) linear arms. Self-assembly of these polymers leads to the formation of various supramolecular aggregates with diverse structures and morphologies [160]. The following studies highlight how DPD modeling of dendritic polymers can be used to manipulate supramolecular interactions and self-assembly processes, resulting in the engineering of desired self-assembled structures. Tan et al. [163] applied DPD simulations to investigate the self-assembly behaviors of hyperbranched multi-arm copolymers with hydrophobic cores of varying degrees of branching. The study found that as the degree of hydrophilic branching increased, the morphology of the self-assembled copolymers transitioned from spherical micelles to wormlike micelles and, ultimately, to vesicles (Figure 10A). Low branching degrees led to cone microphase separation, forming spherical micelles, while moderate branching produced wormlike micelles through truncated cone separation. High branching resulted in cylindrical microphase separation, forming vesicles (Figure 10A). Kirkensgaard et al. [222] used DPD simulations to study the self-assembly of generic 2nd generation dendritic 3-miktoarm star copolymers (Figure 10B). Their results showed that ABC 3-miktoarm star terpolymers self-assembled into various cylindrical structures, progressing through different 2D Archimedean tiling patterns by adjusting molecular volume fractions. They found that incorporating a variably sized junction region enabled controlled tiling pattern formation, with one polygonal component forming a core-shell cylinder. Additionally, the study revealed a diverse phase diagram under asymmetric interaction parameters (Figure 10B). Similar to the previous article in another research work, DPD simulations have been used to investigate the vesicular self-assembly of amphiphilic hyperbranched multiarm copolymers in dilute aqueous solution by Wang et al. [223] The self-assembly mechanisms of branched polymersomes and conventional polymersomes from linear block copolymers were found to differ in a recent study. For branched polymersome copolymers, the commonly accepted process involves the aggregation of amphiphilic block copolymers into small spherical micelles, which then transform into sheet- or membrane-like structures, ultimately forming vesicles through membrane bending and closing. Unlike the vesiculation process of linear block copolymers, the study did not observe 'sphere-to-rod' and 'rod-to-membrane' transitions in the branched polymersomes, as the sphere transitioned directly to the membrane. In another study, Tan et al. [224] systematically explored the self-assembly of amphiphilic hyperbranched multi-arm copolymers in various solvents using DPD simulations. They obtained three phase diagrams and observed multiple morphological transitions for copolymer

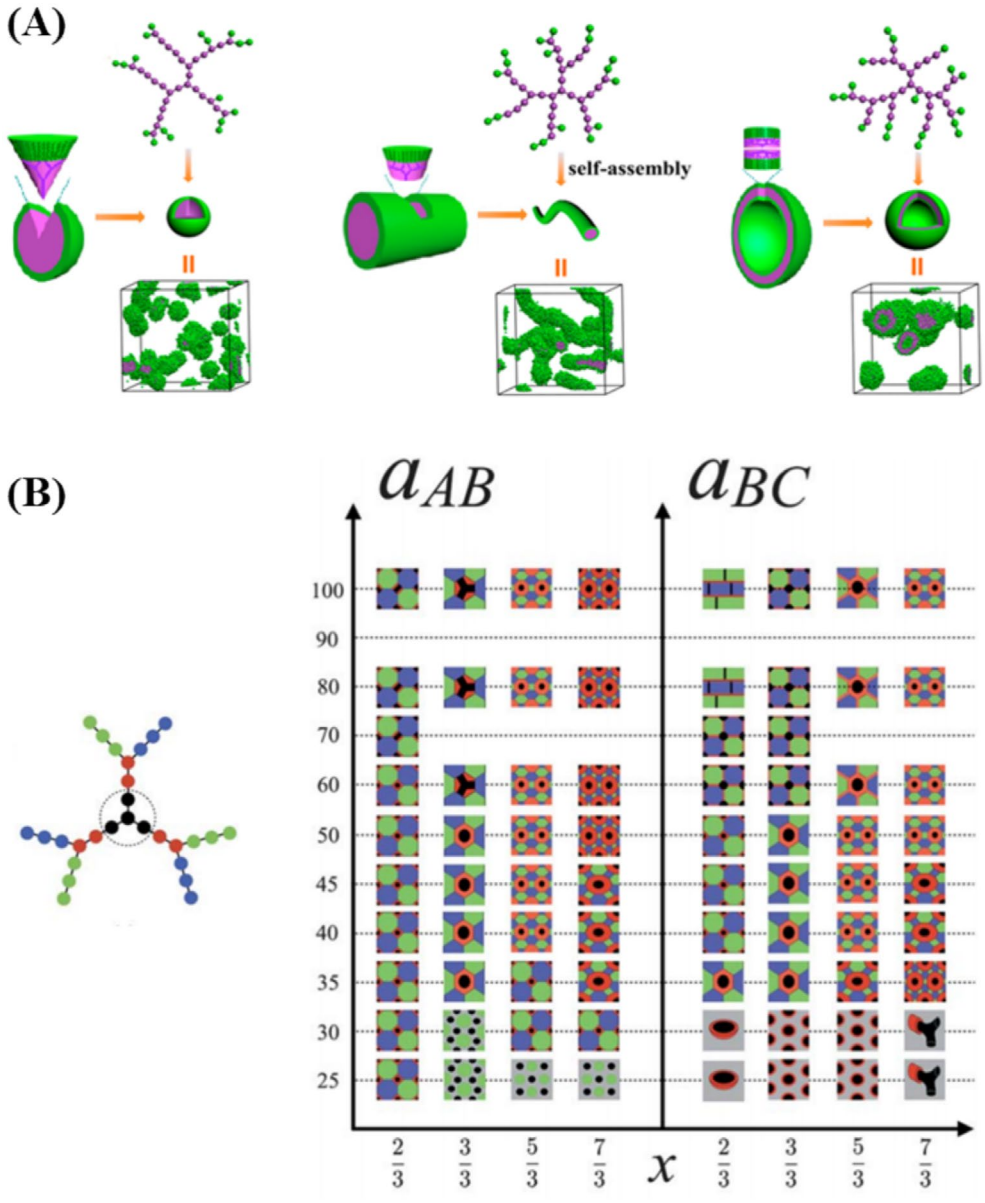

FIGURE 10 | (A) Morphology transformation in the self-assembly of HMCs with varying degrees of branching in the hydrophobic hyperbranched cores. Water beads are omitted for clarity. Purple beads represent the hydrophobic hyperbranched core, and green beads represent the hydrophilic linear arms [163]. Reproduced with the permission of the Royal Society of Chemistry, Copyright 2023. (B) (Left Panel) Model of a 2nd generation dendritic miktoarm star with $(n_L, n_A, n_B, n_C) = (1, 2, 3, 3)$, indicating bead counts for each color, excluding the central junction. Color code: L = black, A = red, B = blue, C = green. (Right Panel) Phase diagrams for two scenarios with asymmetric interaction parameters at four values of x, varying a_{AB}(with other pair interactions $a_{ij} = 45$) and a_{BC} (with other pair interactions $a_{ij} = 45$). x is the ratio of beads in the outer chains to those between the junction and branch point: $X = (n_L + n_A)/n_B$ [222]. Reproduced with the permission of the Royal Society of Chemistry, Copyright 2023.

architectures $A_{42}B_{20}$, $A_{42}(B_2)_{20}$, and $A_{42}(B_3)_{20}$, by controlling the hydrophilic linear arm length. For $A_{42}B_{20}$, the observed morphological transition followed the sequence: spherical micelles → mixture of spherical and worm-like micelles → worm-like micelles → membranes → vesicles → vesosomes. $A_{42}(B_2)_{20}$ exhibited a different pathway, progressing from spherical micelles → mixture of spherical and worm-like micelles → worm-like micelles → aggregates of spherical and worm-like micelles → helical micelles. Meanwhile, the $A_{42}(B_3)_{20}$ phase diagram revealed the transition: spherical micelles → small micelle aggregates → aggregates of spherical and worm-like micelles → helical micelles. Notably, this study revealed new structures, including aggregates of spherical and worm-like micelles, vesosomes, and helical micelles, in amphiphilic hyperbranched multi-arm copolymers.

Wang et al. [225] studied the micellization behavior of amphiphilic dendritic multi-arm copolymers in dilute solution using DPD simulations. Three models with different arm lengths were examined, each consisting of a dendritic core and several arms. The study applied parameters to describe the interactions between the core and arms (a_{AB}), core and water (a_{AC}) and arm and water (a_{BC}). The study revealed two self-assembly mechanisms for creating large multimolecular micelles: unimolecular micelle aggregation (UMA) and small micelle aggregation (SMA). In the UMA mechanism, dendritic multi-arm copolymers first

formed unimolecular micelles, which then combined to create large micelles. In the SMA mechanism, the copolymers self-assembled into microphase-separated small micelles, which later aggregated into larger micelles. The results showed that the microphase separation of dendritic multi-arm copolymers is influenced by the hydrophobicity of the dendritic cores and the incompatibility between the cores and the arms. The pH-responsive behavior of self-assembled amphiphilic dendrimers was surveyed by Yu et al. [226] studied the pH-responsive behavior of self-assembled amphiphilic dendrimers using a combination of DPD and atomistic simulations. They focused on an amphiphilic carboxyl-terminated polyester dendrimer (H_2O-COOH) in aqueous solution. The study showed that at low concentrations, the dendrimer's self-assembly morphologies changed as the degree of ionization of the carboxylic acid blocks decreased. The morphologies transitioned from unimolecular micelles to micro-phase-separated small micelles, wormlike micelles, sheet-like micelles, small vesicles, and finally large vesicles. The process was broken down into four stages: (1) random distribution of H_2O-COOH molecules, (2) aggregation into microphase-separated spherical micelles, (3) fusion of spherical micelles into small wormlike micelles, and (4) fusion of small wormlike micelles into long wormlike micelles. Using DPD simulations, Nie et al. [227] studied the pH-responsive behavior of dendritic polymers using DPD simulations, focusing on the relationship between the structure of pH-sensitive triblock polymers and drug release from micelles. Their findings showed that protonation of the pH-sensitive block triggered a transition from micelles to a 'fireworks-like' three-layer structure, which facilitated drug release through channels formed in the micelles. Based on their results, the researchers proposed several design principles: (i) the length of the hydrophilic block influences drug release and distribution in micelles, (ii) the pH-sensitive block length significantly affects drug release, and (iii) the impact of hydrophobic block length on drug release varies depending on drug distribution in the micelles.

Lin et al. [228] conducted DPD simulations to examine the self-assembly behavior of amphiphilic linear-dendritic block copolymers (LDBC), specifically R_X-dendr $[B_y\text{-}Y_3]_n$, in a selective solvent. Their study identified seven distinct self-assembled morphologies, including spherical, worm-like, and cylindrical micelles, as well as vesicles. The observed structural transitions were influenced by factors such as the generation number, block lengths, and π-π interactions. As the generation number increased, the self-assembled structures evolved from nanofibers to polymersomes, demonstrating a systematic shift in morphology (see Figure 11). The study also highlighted the importance of π-π interactions in stabilizing specific structures, particularly cylindrical and vesicular assemblies. In addition to these morphological transitions, the researchers investigated the impact of UV irradiation on the self-assembled structures. Exposure to UV light induced a conformational change in the azobenzene (Y-block) units, increasing their hydrophilicity. This alteration disrupted the balance between hydrophobic and hydrophilic interactions, leading to the deformation of spherical polymersomes into irregular vesicles. Further exposure resulted in membrane rupture and distortion, as the structural instability caused by the altered Y-block conformation intensified (see Figure 11). These findings provide valuable insights into the stimuli-responsive behavior of LDBC systems, demonstrating their potential for applications in drug delivery, nanocarriers, and light-responsive materials.

Summary:

In summary, DPD modeling can be used to study various aspects of dendritic copolymer self-assembly, including the impact of dendritic polymer characteristics on the self-assembly mechanism, monitoring the internal structure and morphology of supramolecular structures, generating morphological phase diagrams, and investigating the encapsulation and release of small molecules such as drugs.

2.4 | Comb- and Brush-Like Copolymers

DPD simulations were used to study structural transitions of vesicles formed by comb-like block copolymers with a semi-flexible backbone by Wang et al. [17] They studied the structural transitions of vesicles formed by $A_6(B_2)_3$ and $C_6(D_2)_3$ comb-like block copolymers, where A and C are hydrophobic and B and D are hydrophilic. By adjusting the interaction parameters between components, they explored how amphiphilicity and solvent selectivity affect the system. The researchers found that line tension plays a critical role in determining vesicle fission pathways. Additionally, they observed that tube-like vesicles tend to transform into layered micellar structures, while onion-shaped vesicles transition into reverse onion-shaped vesicles. Comb-like block copolymers were also investigated by Liu et al. [229] They studied the dynamic evolution of vesicles formed by comb-like block copolymer-based tethered nanoparticles using DPD simulations. The results showed that the copolymers self-assembled into monolayer vesicles, which are promising candidates for drug encapsulation and controlled release. The fusion mechanism of these vesicles differed from that of vesicles formed by self-assembled comb-like block copolymers. While nanoparticles influenced the fusion process, they did not affect the fission pathway. The slow fusion was caused by large and rigid nanoparticles, a factor that could be reduced by adjusting the molecular structures to lessen surface tension fluctuations. In addition, the mismatch between different nanoparticles created additional surface tension, which sped up the fission process. Cheng et al. [230] studied the self-assembly behavior of amphiphilic asymmetric macromolecular brushes (Y15-graft-(Rx/By-*b*-Gz)) using DPD simulations in a selective solvent. The macromolecular brush consisted of a solvophobic Y-block backbone, solvophilic R-block side chains, and diblock side chains consisting of a solvophobic B-block and a solvophilic G-block (Figure 12A). Five types of vesicles were observed: porous aggregates, worm-like micelles, donut micelles, hamburger micelles, and unimolecular micelles. The morphological phase diagram for Y15-graft-(R1/By-*b*-Gz) showed six aggregate types: porous aggregate, unimolecular micelle, worm-like micelle, symmetric five-layered vesicle (type A polymersome), inverted asymmetric four-layered vesicle (type B polymersome), and asymmetric four-layered vesicle (type C polymersome) (Figure 12A). The study revealed that asymmetric polymersomes formed when both solvophilic blocks were attached separately to the backbone and side chain, while

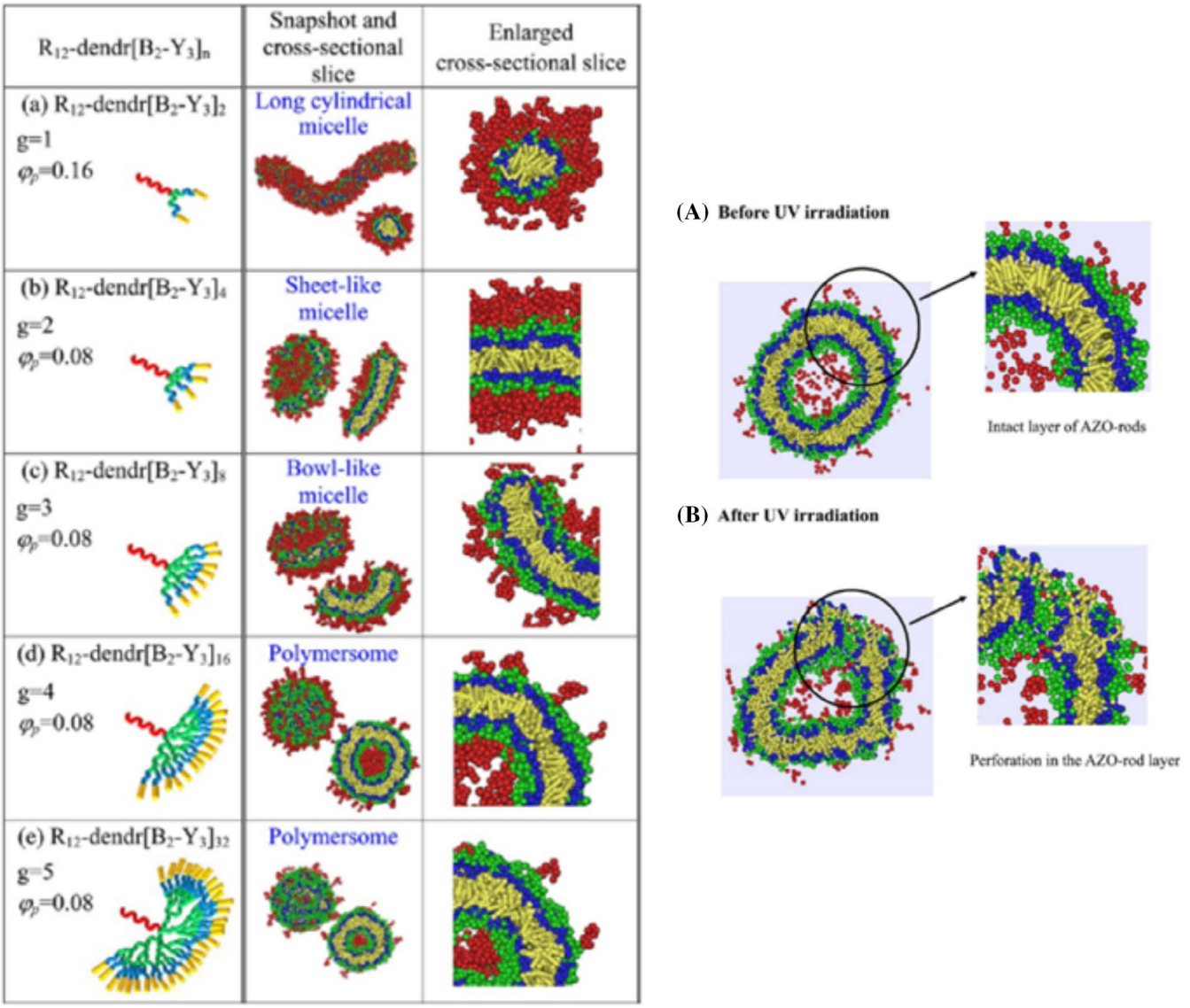

FIGURE 11 | (Left Panel) Generation-dependent aggregation behavior of amphiphilic linear-dendritic block copolymers, R_{12}-dendr[B_2-Y_3]$_n$, with aggregates represented by red (solvophilic PEG-block), green (solvophilic dendritic polyester), blue (solvophobic aliphatic block), and yellow (solvophobic azo-block) beads. Solvent beads are omitted. (Right Panel) Snapshots of vesicles formed by R_9-dendr[B_2-Y_3]$_{16}$: (A) before UV irradiation and (B) after UV irradiation. The polymersomes are represented by the same color code as above, with solvent beads omitted [228]. Reproduced with the permission of the American Chemical Society, Copyright 2023.

micellar aggregates formed when both solvophilic blocks were attached to either the backbone or side chain.

Summary:

To summarize, DPD modeling is a valuable tool for investigating different aspects of self-assembly in comb- and brush-like copolymers, including how their topological structure, composition, and chemistry affect the self-assembly process. Additionally, the internal structure and morphology of the resulting supramolecular structures can be monitored, and morphological phase diagrams can be generated through DPD surveys of the copolymers. Furthermore, the DPD model can be used to investigate the encapsulation and release of small molecules, such as drugs, in these systems.

2.5 | Cyclic Copolymer

Qian et al. [231] investigated the microphase separation behavior of cyclic diblock copolymers using DPD simulations. They created a phase diagram by fixing chain length while varying the composition fraction and χ-value (Flory-Huggins interaction parameters between blocks of cyclic diblock copolymers). The diagram predicted the order–disorder transition (ODT) point to be in the range of $40 < (\chi N)_{ODT} < 45$. By comparing the microphase morphology of linear A_3B_7 and cyclic c-A_3B_7 diblock copolymers, they found that cyclization had a significant impact on meso structures, influenced by the chain length of the cyclic copolymer. In the transition region between disordered and ordered phases, they observed micelle-like, liquid rod, and random network

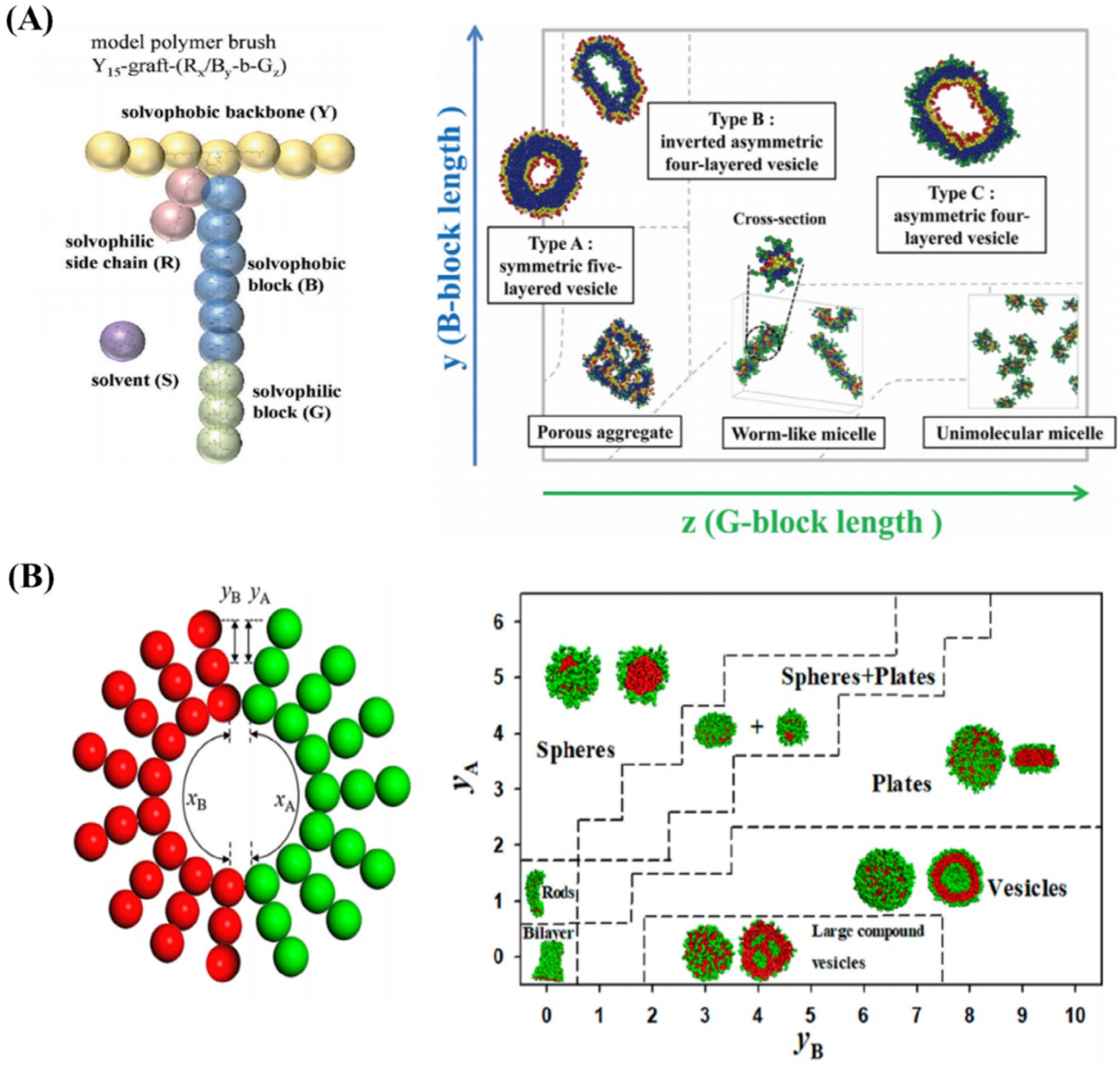

FIGURE 12 | (A) (Left Panel) PGMA-graft-(PEO/PS-*b*-PNIPAM) and its corresponding model polymer brush, Y15-graft-(Rx/By-*b*-Gz). (Right Panel) Morphological phase diagram of aggregates formed by polymer brush Y15-graft-(R1/By-*b*-Gz) [230]. Reproduced with the permission of the American Chemical Society, Copyright 2023. (B) Left Panel) Schematic of amphiphilic cyclic brush copolymers, with green beads (A) representing solvophilic components and red beads (B) representing solvophobic components. (Right Panel) Morphological snapshots for various lengths of solvophilic and solvophobic side chains [108]. Reproduced with the permission of the American Chemical Society, Copyright 2023.

structures, highlighting the complexity of microphase separation dynamics.

Xu et al. [232] simulated the microphase-separation behavior of graft-diblock copolymers using the DPD method. They found that the microphase-separation morphologies in graft-diblock copolymers differed significantly from those of linear copolymers with the same component volume fractions. By increasing or decreasing the graft fraction from 50%, the microphase-separation structures gradually transitioned to those of the corresponding linear copolymers. This highlights the significant effect of the graft fraction on the microphase-separation behavior of graft-diblock copolymer. Using DPD, Prhashanna et al. [233] investigated the self-assembly and chain exchange kinetics of micelles formed by diblock copolymers with a cyclic hydrophilic block ('tadpole polymer') and compared them to linear diblock copolymers with the same hydrophobic block and overall composition. They found that tadpole copolymers formed smaller micelles and exhibited faster chain exchange than linear copolymers. Interestingly, in mixed micelles (a blend of cyclic and linear copolymers), tadpole chain exchange slowed down, while linear chain exchange sped up compared to pure micelles, revealing a synergistic effect.

Cyclic brush copolymers, featuring a cyclic core densely grafted with outward-extending polymer brushes, have gained attention

as novel materials for both theoretical and applied research due to their distinct topology-driven properties [234–237]. Yang et al. [108] employed DPD simulations to investigate the self-assembled microstructures of amphiphilic cyclic brush block copolymers in solution. Their study revealed a diverse range of self-assembled morphologies, including plates, vesicles, bilayers, rods, and spheres, with the observed structures largely dependent on the solvophilic/solvophobic side chain lengths, backbone lengths, and grafting densities (see Figure 12B). They found that copolymers with greater backbone and graft asymmetry, particularly those with larger solvophilic components, exhibited a preference for structures with curved interfaces. This structural evolution followed a clear trend, transitioning from vesicles to plates and ultimately to spheres as the asymmetry increased. Similarly, higher grafting densities promoted the formation of highly curved morphologies, reinforcing the role of molecular architecture in dictating self-assembly behavior. These findings offer valuable insights into the design of cyclic brush copolymers with tunable morphologies, highlighting their potential for applications in nanostructured materials, drug delivery, and advanced coatings.

Summary:

The summary of what can be studied in cyclic copolymers self-assembly using DPD modeling is as follows:

1. The effect of the copolymers topological structures, composition, and chemistry on the self-assembly mechanism can be investigated.
2. The internal structure and morphology of the self-assembled supramolecular structures can be monitored.
3. Morphological phase diagrams can be valuable outcomes of DPD simulations of copolymers.

2.6 | T-, π- and H-Shaped Copolymers

T-shaped ternary liquid crystals (TLCs) are unique nonlinear amphiphilic supramolecules that have gained attention for their novel self-assembled microstructures [238] and various applications such as display devices [239], and semiconductors [240]. In this case, Liu et al. [241] employed DPD simulations to examine the phase behavior of T-shaped ternary amphiphiles, composed of rod-like cores linked to two incompatible end chains and side-grafted segments. They created three phase diagrams for systems with different terminal chain lengths, considering temperature and lateral chain length, and a normalized phase diagram of T-shaped amphiphiles in relation to f_L (the volume fraction of lateral chain) (Figure 13A). Their findings highlight critical factors such as shape, rigidity, connectivity, short-range repulsion, and segregation between components—each playing a vital role in replicating the fundamental characteristics of T-shaped liquid crystal systems. By employing DPD simulations, Chen et al. [242] used DPD simulations to investigate the assembly behavior of Π-shaped copolymers with a rigid rod backbone (A block) in a solvent. They analyzed how copolymer characteristics, such as the positions of junction points between coiled side chains (B blocks), copolymer concentration, and the repulsive parameters between coil and rod blocks, along with solvent properties, influenced the morphology. Their findings showed that altering these factors led to various morphologies, and by adjusting solvent selectivity and repulsive interactions between coil and rod blocks, they were able to create coil-block and rod-block cages. Harmat et al. [154] investigated the self-assembly of H-shaped block copolymers, focusing on how copolymer composition (middle block to branch length ratio) and solvent selectivity between the middle and branch blocks influenced the process. They observed a variety of assembly structures, including onion-like, vesicles, and multicompartment aggregates.

In general, the structure of polymeric assemblies is influenced by a range of parameters, such as copolymer architecture, chemistry, compositions, and amphiphilicity. By manipulating these parameters, different assembled structures with distinct morphologies and internal configurations can be obtained. The DPD method can address the question of how assembly structures are altered by varying these parameters through predictive mesoscale investigations, offering valuable guidelines for this field of study.

Summary:

DPD modeling can be employed to investigate various aspects of T-, π-, and H-shaped copolymers' self-assembly.

1. One area of research is the impact of copolymer topological structures, composition, and chemistry on the self-assembly mechanism. Through DPD simulations, researchers can examine how these factors influence the formation and stability of self-assembled structures.
2. Another aspect of self-assembly that can be studied using DPD is the internal structure and morphology of the self-assembled supramolecular structures. This information can provide insight into the thermodynamics of self-assembly and how different factors affect the formation of specific structures.
3. Additionally, morphological phase diagrams can be valuable outcomes of DPD surveys of the copolymers. These diagrams map out the different phases and morphologies that arise as a function of various parameters such as temperature, solvent composition, and copolymer concentration. These diagrams can aid in understanding the complex behavior of the self-assembled systems and offer a useful guide for designing materials with specific properties.

2.7 | Shape Amphiphiles

Shape amphiphiles are characterized by distinct components with incompatible packing geometries, including a hydrophilic head and a linear, hydrophobic polymeric tail (Figure 13B). While their structures resemble those of small surfactant molecules, their much larger size makes them unique. This size enables shape amphiphiles to self-assemble into various morphologies in selective solvents, leading to significant interest due to their unique properties and potential applications. In this regard, using the DPD method, Ma et al. [244] studied the self-assembly behavior of shape amphiphiles with one or more hydrophobic tails and a hydrophilic head. Their simulations showed that as the interaction parameter between the hydrophilic heads increased, the micellar morphology

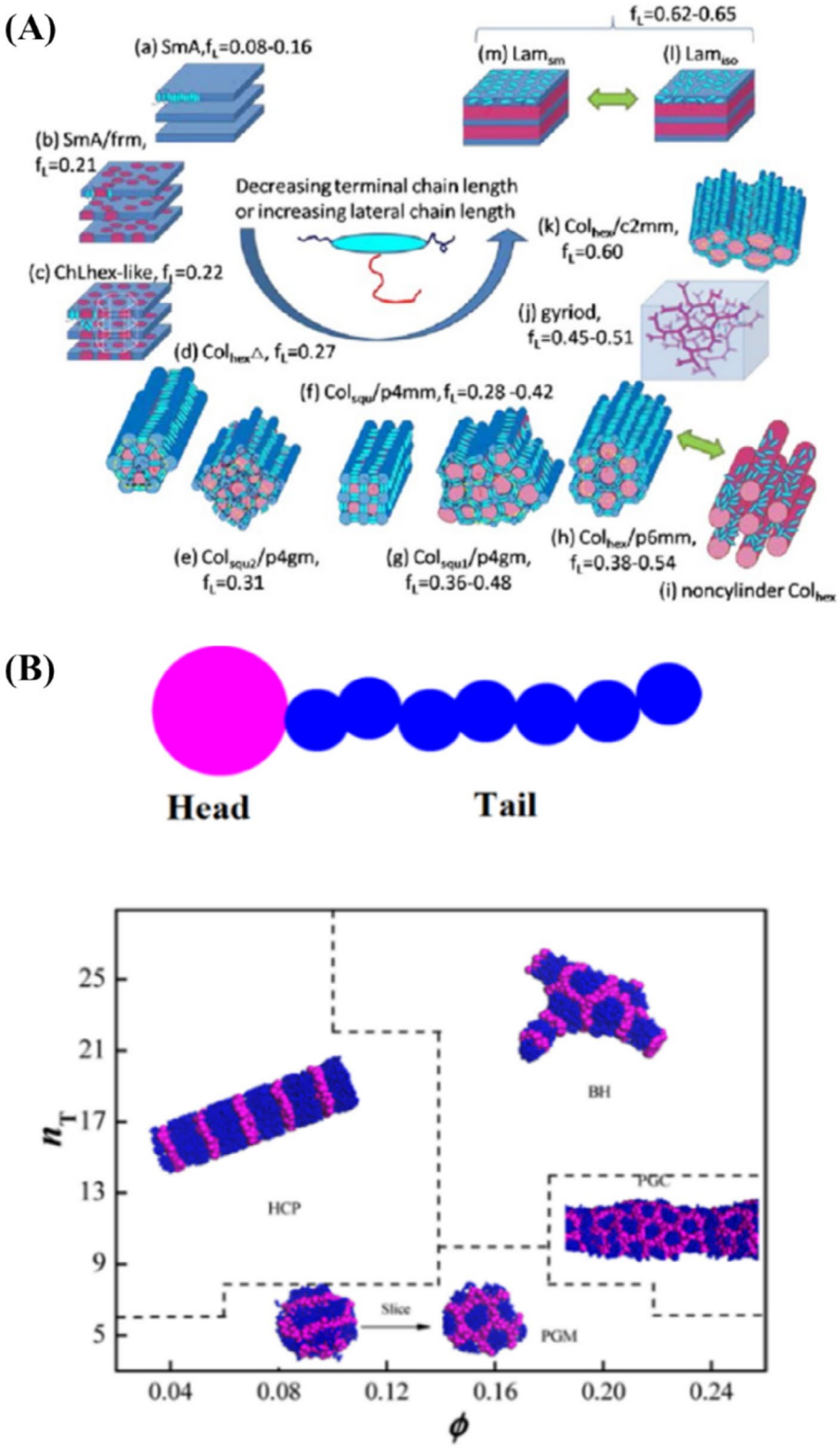

FIGURE 13 | (A) Phase transition sequence in T-shaped ternary amphiphiles as a function of f_L (volume fraction of lateral chains), with green arrows indicating temperature-driven structural changes [241]. Reproduced with the permission of the American Chemical Society, Copyright 2023. (B) Polymer with one head (HG) bead and n tail (T) beads; characteristic morphological snapshots of $T_n - H$ aggregates as a function of $T_n - H$ concentration (φ) and hydrophobic tail length (n_T) [243]. Reproduced with the permission of the American Chemical Society, Copyright 2023.

transitioned from vesicles to worm-like cylinders and eventually to spheres. The researchers identified eight distinct self-assembled morphologies: worm-like cylinders, spheres, vesicles, pupa-like micelles, disk-like micelles, layered-spherical micelles, segmented rod-like micelles, and micelles. These morphologies were influenced by factors such as hydrophobic tail length, hydrophilic head size, the hydrophilic head-solvent interaction parameter, and the number of hydrophobic tails. In another research work, they

investigated the self-assembly of surfactant-like amphiphiles composed of a hydrophilic head and a hydrophobic tail, using the DPD method [243]. Seven self-assembled morphologies were observed, including pomegranate-like micelles, (PGM), pomegranate-like columnar structures (PGC), sphere-like micelles (SM), disklike micelles (DM), hierarchical colloidal polymeric (HCP) structures, branched hybrid structures (BH), and vesicles. The formation of these structures was affected by multiple factors, including the interaction parameter between the hydrophilic head and solvent, the length of the hydrophobic tail, the size of the hydrophilic head, and the polymer concentration. To form an HCP structure, polymer lengths had to be greater than 9 monomers and polymer concentrations below 0.16, with a fixed $a_{HS} = 25$ and $a_{HS} = 25 > 30$ (Figure 13B). The results showed that micelles with smaller hydrophilic heads behaved like amphiphilic diblock copolymers, while larger heads shifted the behavior toward amphiphilic triblock or miktoarm star-like copolymers.

Summary:

Using DPD modeling, researchers can explore various aspects of self-assembly in shape-amphiphile copolymers.

1. Specifically, they can investigate the impact of the copolymer properties, such as topological structures, composition, and chemistry, on the self-assembly mechanism.
2. Additionally, DPD simulations can enable researchers to monitor the internal structure and morphology of the self-assembled supramolecular structures.
3. Finally, researchers can use DPD to construct morphological phase diagrams that provide valuable insights into the behavior of the copolymers during self-assembly.

2.8 | Liquid Crystalline Polymers

Liquid crystalline polymers (LCPs) have been extensively studied through DPD simulations due to their exceptional properties and self-assembly behavior. Understanding their self-assembly is crucial because LCPs can form various liquid crystalline phases, including nematic, smectic, columnar, and cholesteric structures. The polymer's architecture, chemical structures, mesogenic units, flexible spacers, and hydrophobic tails are key factors that control these self-assembled structures. LCPs are widely used in optics, polymer fibers, energy storage, and actuators. Thus, predicting and controlling their size, morphology, and self-assembly structures is crucial for optimizing their performance in these applications.

In this context, Li et al. [245] conducted a study using DPD simulations to investigate the microphase separation of side chain liquid crystalline (SCLC) block copolymers. The copolymer consisted of flexible A and B segments with rigid C side chains grafted onto them, with A, B, and C blocks being incompatible. They found that the phase structures of SCLC copolymers could be modulated by adjusting the lengths of the A and C blocks and the graft number. The observed mesophases included spheres, cylinders, gyroids, and lamellae. Additionally, they discovered that the packing order of the C side chains increased with decreasing temperature or longer rigid C side chains. The molecular structures of the SCLC copolymers are shown in Figure 14A. Gong et al. [246] developed a coarse-grained model for triphenylene-based side-chain discotic liquid crystalline polymers (SDLCPs) (Figure 14B) and utilized DPD simulations to examine how composition and structural factors—including molecular weight, spacer length, and aliphatic tails—affected self-assembly behavior. They observed eight mesophases: hexagonal columnar–amorphous (Colh-Am), nematic columnar–amorphous (Colne-Am), nematic columnar–clustered (Colne-Clu), nematic columnar–columnar (Colne-Col), random columns–amorphous (Colran-Am), random columnar–clustered (Colran-Clu), amorphous–amorphous (Am-Am), and sphere–amorphous (Sph-Am) (Figure 14B). They found that intracolumnar self-assembly patterns based on discrete columnar stacks (DCS) were present in Colh-Am, Colne-Am, and Colne-Clu, while Colne-Col and Sph-Am exhibited different packing modes. The study also indicated that forming ordered mesophases in SDLCPs requires moderate to strong incompatibility between mesogenic cores and their substituents, along with appropriate peripheral aliphatic tails.

Summary:

The use of DPD simulations to study liquid crystalline polymers provides valuable insights into their self-assembly behavior. The following aspects can be explored:

1. The impact of the polymer's topology, composition, and chemistry on the self-assembly mechanism can be studied.
2. The internal structure and morphology of the self-assembled supramolecular structures can be visualized and analyzed.
3. The generation of morphological phase diagrams, which can provide a comprehensive overview of the different self-assembled phases formed by the polymers, is a significant outcome of DPD modeling.

Thus, the DPD approach can provide valuable information on the self-assembly of liquid crystalline polymers, including morphology, liquid crystalline phase alignment, and molecular configurations. Understanding these characteristics is crucial for developing high-performance materials with tailored properties that meet the requirements of various applications.

2.9 | Hybrid Organic/Inorganic Materials

Huang et al. [247] presented a DPD simulation of polymer-directed mineralization of inorganic particles, focusing on the aggregation of hydrophobic nanoparticles using double hydrophilic block copolymers (DHBCs). One block of the DHBCs was more attractive to the nanoparticles, while the other was repulsive. They observed three typical structures: nearly spherical aggregates when DHBC concentration (C_{DHBC}) < 0.5, hexagonally packed cylinders at $C_{DHBC} \approx 0.5$, and ordered lamellae at $C_{DHBC} = 0.9$. In the range $0.5 < C_{DHBC} < 0.9$, a disordered structure was detected. The ordered lamellae formation mechanism involved the progression from a disordered structure to disordered lamellae and eventually to parallel-oriented ordered lamellae. Their results provide molecular-level insights

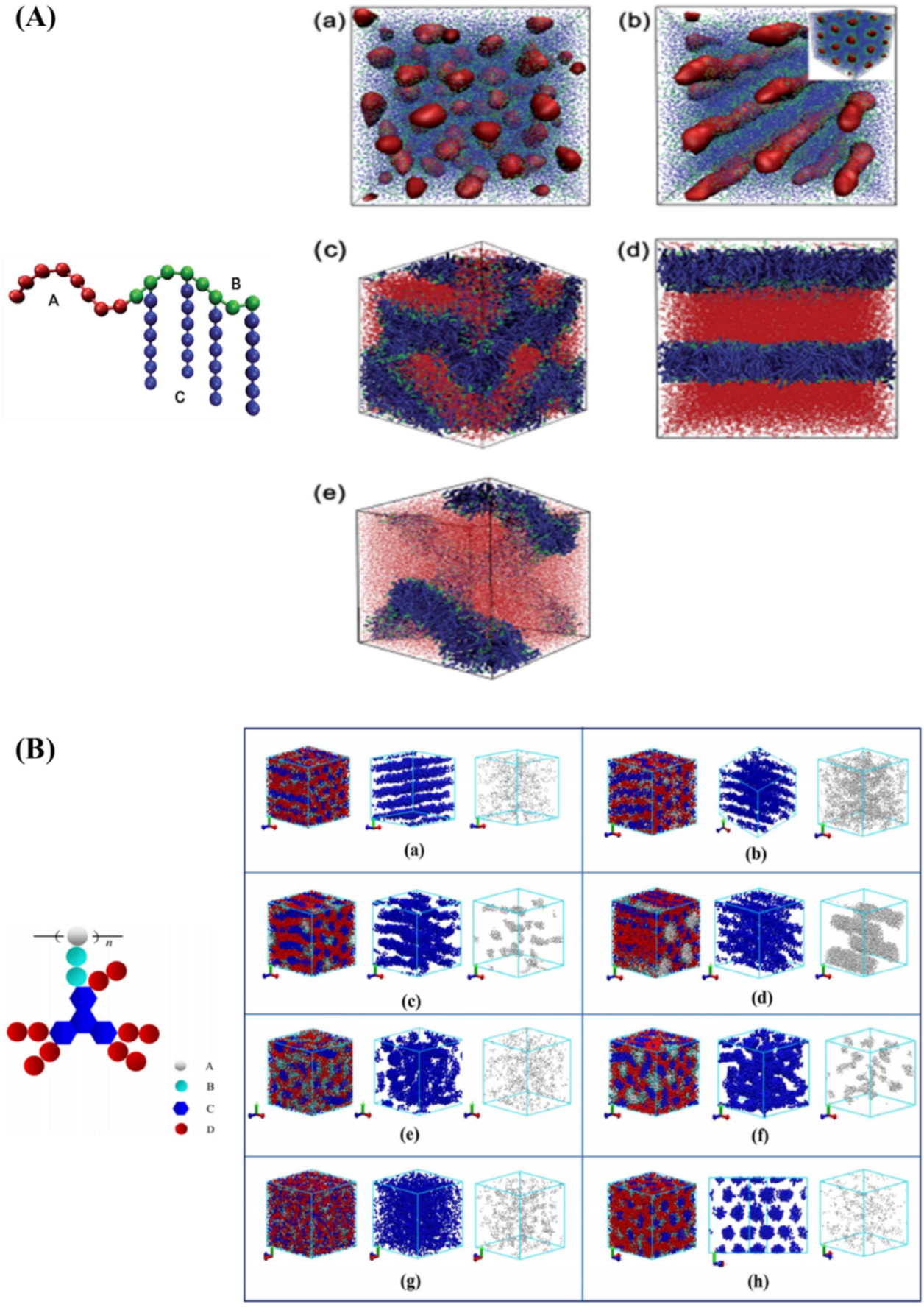

FIGURE 14 | Legend on next page.

FIGURE 14 | (A) Coarse-grained model of SCLC block copolymers, with red, green, and blue beads representing flexible A blocks, flexible B blocks, and rigid C side chains, respectively. (Right Panel) Simulated structures formed by SCLC block copolymers with $N_B = 8$, $N_C = 6$, and $n = 4$. From (a) to (e), A block lengths (N_A) are 4, 8, 24, 48, and 80, respectively. Red, green, and blue colors represent A, B, and C blocks, respectively [245]. Reproduced with the permission of the Royal Society of Chemistry, Copyright 2023. (B) (Left Panel) Coarse-grained model of triphenylene-based SDLCPs $(A_k B_l C_4 D_{5xm})_n$, with beads: A (light gray), B (cyan), D (red), and n as DP. (Right Panel) Self-assembled phases of SDLCPs under various conditions: (a) Colh-Am, (b) Colne-Am, (c) Colne-Clu, (d) Colne-Col, (e) Colran-Am, (f) Colran-Clu, (g) Am-Am, (h) Sph-Am. Each phase shows all beads (left), discotic mesogenic core beads (middle), and polymer backbone beads (right) [246]. Reproduced with the permission of the American Chemical Society, Copyright 2023.

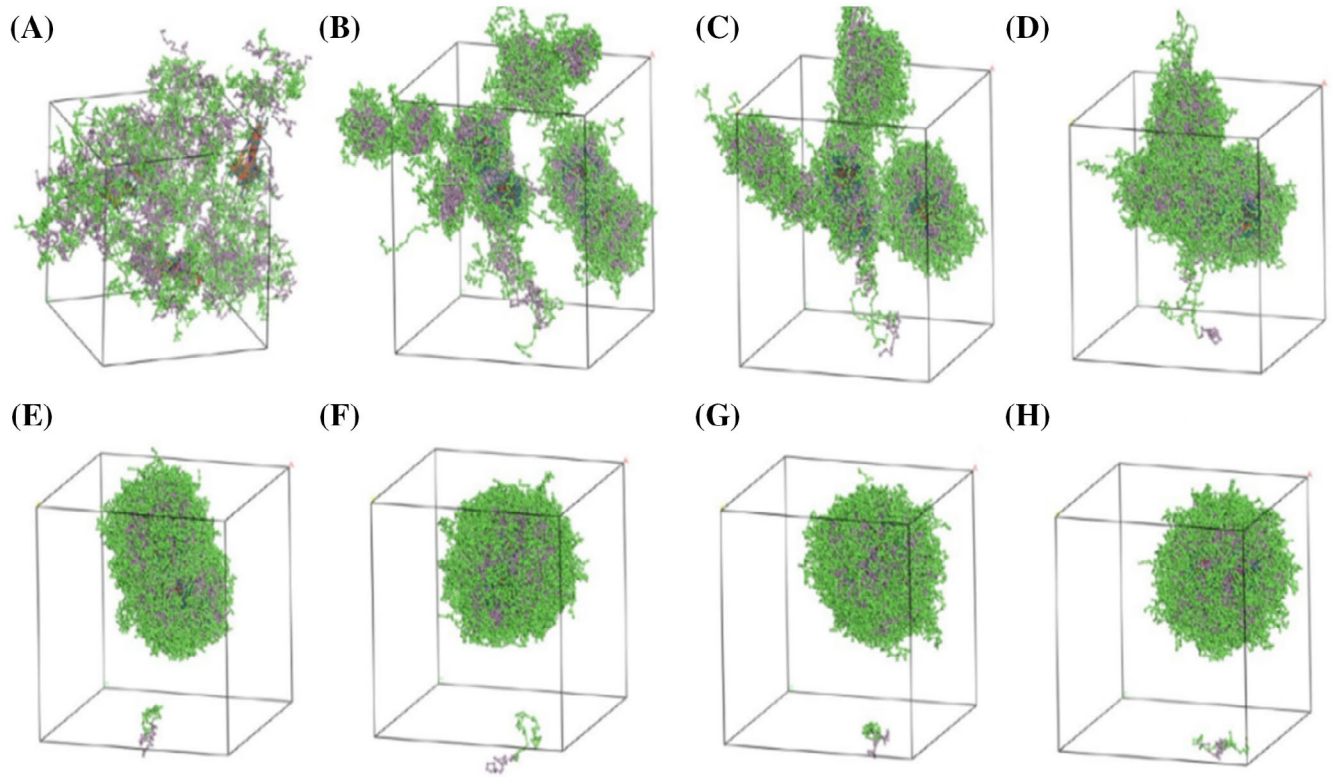

FIGURE 15 | The dynamic process of QD-loaded PS-PEO block copolymer assembly at different simulated steps: (a) 0, (b) 5000, (c) 10,000, (d) 20,000, (e) 30,000, (f) 40,000, (g) 50,000, and (h) 100,000 steps [254]. Reproduced with the permission of the American Chemical Society, Copyright 2023.

for designing hybrid organic/inorganic materials with tailored morphology.

While single-component nanomaterials, such as quantum dots (QDs), offer potential for in vivo applications [248, 249], issues of nonspecific adsorption and aggregation limit their use [250, 251]. To solve this problem, their surfaces should be modified to improve their biocompatibility and biodistribution in vivo. PEO and its derivatives have extensively been applied for surface modification [252, 253]. In this regard, Li et al. [254] investigated the self-assembly dynamics of PS-*b*-PEO (poly(styrene-*b*-ethylene oxide)) block copolymers and quantum dots (QDs) in an aqueous solution using DPD simulations. The QDs consisted of a CdSe semiconductor core coated with trioctylphosphine oxide (TOPO). They observed four sequential stages in the formation of composite nanoparticles (CNPs) (Figure 15): (1) random distribution of components, (2) assembly of polymer chains and QDs into small clusters, (3) merging of small spheres into larger aggregates, and (4) stabilization into assembled micelles. The resulting micelles had a hydrophilic PEO shell and hydrophobic PS core.

Hpone Myint et al. [255] used a DPD model with varying polymer-solvent interactions to simulate the encapsulation of spherical nanoparticles (NPs) in PS_{17}-*b*-PEG_{33} block copolymer micelles during a rapid transition from a good solvent (THF) to a poor solvent (water) for PS and NP. Their study aimed to investigate the effects of nanoparticle concentration and polymer composition on micelle formation and coagulation times. The simulations showed that as the number of hydrophobic PS beads increased, the micelle formation time decreased. Conversely, the coagulation time increased with a higher number of hydrophilic PEG beads. Ma et al. [256] studied nanoparticle self-assembly using DPD, focusing on the aggregation behavior of nanoparticles in hybrid assemblies made from amphiphilic block copolymers tethered to nanoparticles in solution. They studied how the number of arms in tethered copolymers, hydrophobic block length, and nanoparticle-hydrophobic block interactions

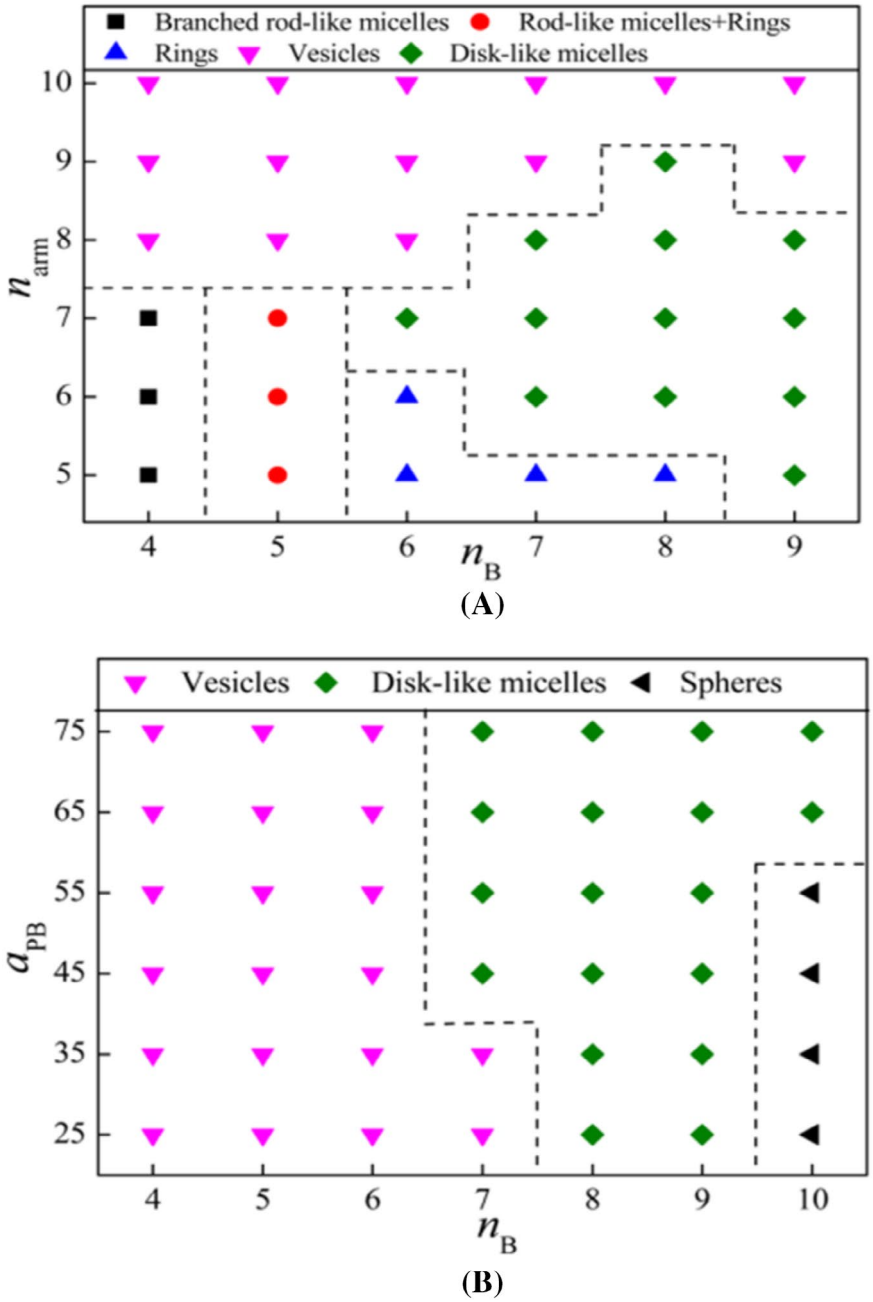

FIGURE 16 | (Top Panel) Morphological phase diagram of aggregates formed by model polymer as a function of tethered arm number (n_{arm}) and hydrophobic chain length (n_b). (Bottom Panel) Phase diagram of aggregates formed by eight-arm tethered nanoparticle $P(BnA1)_8$ as a function of interaction parameter (a_{PB}) between nanoparticle (P) and hydrophobic block (B) and hydrophobic chain length (n_B), with fixed $a_{PA}=65$ [256]. Reproduced with the permission of the American Chemical Society, Copyright 2023.

influenced self-assembly. Their simulations revealed structures such as branched rod-like, disk-like, ring-like, spherical micelles, and vesicles (as shown in Figure 16).

Summary:

The following are the key aspects of hybrid organic/inorganic polymeric materials that can be studied using DPD modeling:

1. The impact of the topological structures, composition, and chemistry of the molecules on the self-assembly mechanism can be examined.
2. The internal structure and morphology of the self-assembled supramolecular structures can be observed.
3. Morphological phase diagrams can be generated to provide a better understanding of the self-assembly behavior.

2.10 | Copolymer Self-Assembly in Confined Space

The self-assembly of block copolymers under confinement has gained increasing attention due to its ability to disrupt structural symmetry, leading to the formation of new nanostructures that cannot be achieved through other methods [257].

The diverse internal microphase-separated nanostructures formed by block copolymers in confinement hold significant potential for applications such as drug delivery systems, dielectric resonators, and catalyst carriers [258, 259]. Copolymer self-assembly in confined spaces has been studied by the DPD method to predict morphologies, configuration, and alignment of the separated microphase. For instance, Petrus et al. [260] performed DPD simulations of lamellar- and cylinder-forming diblock copolymers confined in planar slits to examine the competing effects of physical adsorption and confinement on self-assembly. They varied slit widths and copolymer-bead wall interactions with different affinities. Phase diagrams revealed that, depending on slit width and copolymer-wall interaction, A5B5 and A4B6 systems initially formed perpendicular and parallel lamellar phases with varying lamellae numbers. Mixed lamellar phases were also observed, featuring perpendicular lamellae in the center or attached to a wall, along with adsorbed layers or parallel lamellae near the wall. The phase diagrams showed that the more asymmetric the copolymer, the more asymmetric its corresponding phase diagram (see Figure 17A). Nikoubashman et al. [261] studied the phase behavior of PS-PHMA (polystyrene-*b*-(n-hexyl methacrylate)) diblock copolymers confined in thin films using DPD with an advanced coarse-graining approach. Their findings revealed that the minority block (PS) formed cylindrical microdomains to reduce contact with the majority block (PHMA). With increasing film thickness, these domains transitioned from a perpendicular to a parallel orientation relative to the substrate. Regarding microphase separation in confined places, the micro-phase separation and morphologies of the diblock copolymer in a nanosphere with different sizes and interfacial energy were studied by Feng et al. [262] Their results indicated that the morphology of the diblock copolymer in a nanosphere is significantly affected by nanosphere size and surface properties. For the symmetric diblock copolymer A_5B_5 within a neutral-surfaced nanosphere, the structure primarily formed distorted lamellae (see Figure 17B). As the radius increased, the morphology transitioned from mushroom-like to helical and then to a bi-continuous mesostructure with uniform microdomains. For a non-neutral surface, the mesostructure formed onion-like or core-multi-shell structures. For the asymmetric diblock copolymer A_3B_7, the morphology was heavily dependent on the volume ratio.

Hierarchical structures, found in nature in materials like collagen and abalone nacre [263–265], are also being explored in applications such as smart coatings, biosensors, and fuel cells [266]. Block copolymers are capable of self-assembling into these hierarchical microstructures [267], advancing the formation of multi-length-scale microstructures [268]. For lamellar microstructures self-assembled from diblock copolymers in confinement, the number and orientation of layers relative to solid surfaces depend on the film thickness [269–271].

In this regard, Zhang et al. [272] used DPD simulations to study the hierarchical microstructures self-assembled from linear $A(BC)_n$ multiblock copolymers in thin films confined between two solid substrates selective for A blocks. They examined two cases based on interaction strengths: (1) where $a_{AB} \leq a_{AC}$, and (2) where $a_{AB} > a_{AC}$. In both cases, either parallel or perpendicular lamellae-in-lamellae structures were observed. They found that as the film thickness (Δ) increased, large-length-scale structures changed from single to double periodicity, and small-length-scale structures transitioned from parallel to perpendicular. For case (1), the sequence of transformations included $L_3 1$, $L_\perp 1$, $L_5 1$, $L_3 2 \perp L_\perp 1$, and $L_5 2$, while for case (2), the sequence was $L_\perp 1 \rightarrow L_5 1 \rightarrow L_7 1 \rightarrow L_\perp 2 \rightarrow L_5 1 // L_\perp 1 \rightarrow L_5 2$ (see Figure 18). $L_x Y$ refers to a film with Y parallel lamellae, each containing x layers, while $L_\perp Z$ describes Z perpendicular lamellae. $L_x Y \perp L_\perp Z$ includes Y parallel lamellae and Z perpendicular lamellae, with the parallel lamellae positioned perpendicular to the perpendicular ones. Finally, the $L_x Y // L_\perp Z$ film is similar to $L_x Y \perp L_\perp Z$ but with parallel and perpendicular lamellae arranged parallelly.

Summary:

The following summarizes what can be explored in confined copolymer self-assembly using DPD modeling:

1. The impact of copolymer and substrate composition and chemistry on the self-assembly process can be examined.
2. The internal structure and morphology of the resulting supramolecular structures can be observed.
3. The creation of morphological phase diagrams is a useful result of DPD analysis of the copolymers.

3 | Polymer Solutions

Polymer solutions, composed of long macromolecular chains and small solvent molecules, are of significant practical and theoretical importance, as many polymers are produced, handled, or utilized in solution form [273–277]. Polymer solutions are essential in the production of various products, including fibers, films, adhesives, paints, and other materials made from polymers [278–280]. The DPD modeling method can provide insight into the behavior of polymers in solutions by covering a large range of time and length scales. By using this approach, it is possible to study configurational, dimensional, and dynamic aspects of polymer chains in solvents. In an interesting research study, Zhao et al. [281] conducted DPD simulations to investigate the diffusion behavior of rigid-chain polymers in isotropic solutions. The rigid rods were modeled as consecutive DPD particles, and their Brownian motion was examined in the presence of solvent particles. Their results for both rotational and translational diffusion aligned with the predictions of the Kirkwood theory [282, 283]. In the semi-dilute range of isotropic solutions, Zhao et al. observed that the rotational and translational diffusion of rigid-chain polymers became more complex due to entanglement effects. They found that the asymptotic scaling law for the radial diffusion coefficient $D_r \sim (\nu L^3)^{-2}$ (where ν is the number of polymers per volume and L is the polymer length) appeared only at high concentrations within the semi-dilute range. This scaling law corresponds to the formation of a fully enclosed tube, as predicted by the Doi-Edwards theory [81]. Their analysis of velocity auto-correlation functions (VACFs) offered new insights into the diffusion of rigid polymer rods in isotropic solutions. They found that motion parallel to the long axis followed one-dimensional non-interacting Brownian motion, governed by

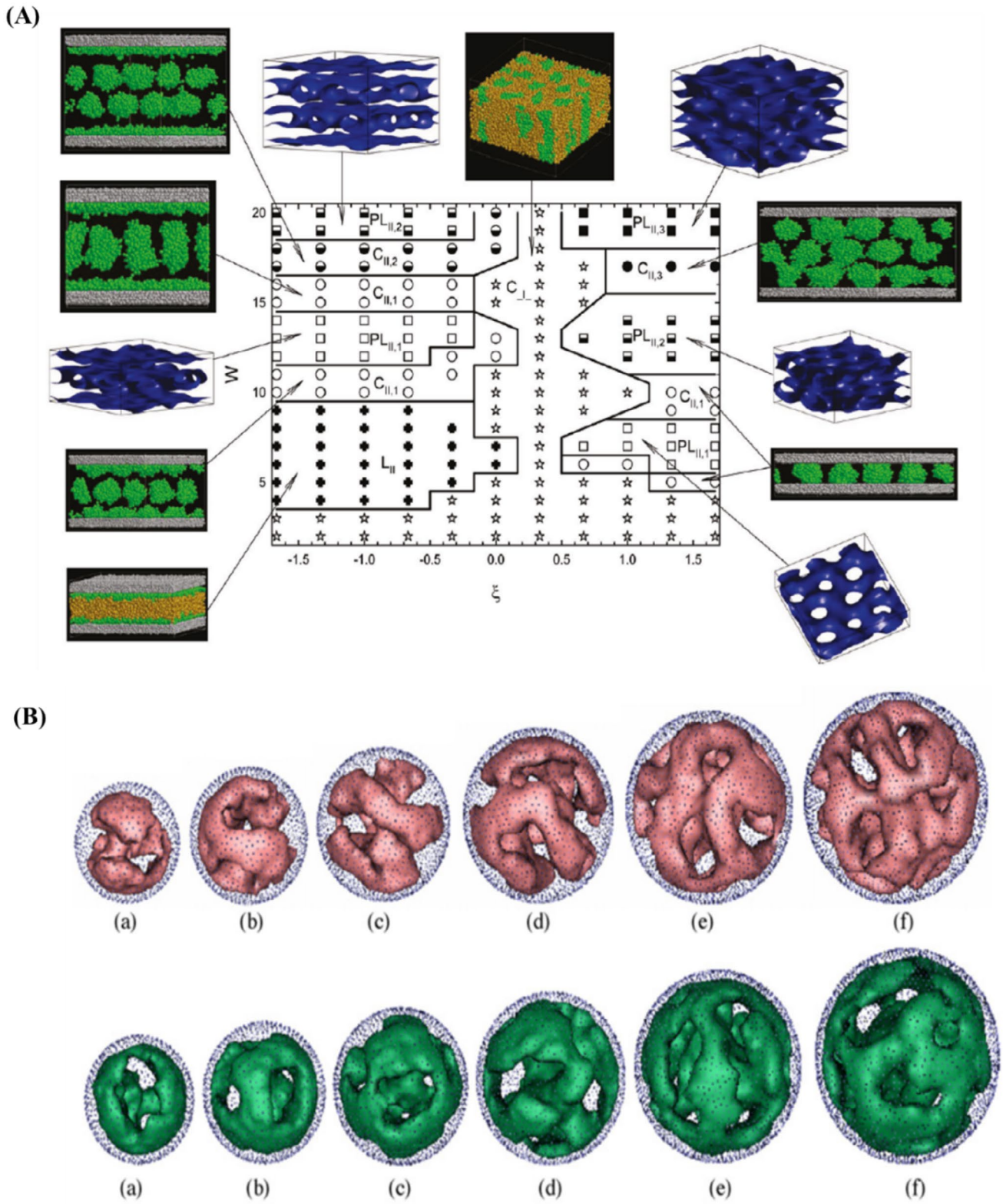

FIGURE 17 | (A) Phase diagram of the A_3B_7 system confined in planar slits, with simulation configurations for various phases. W represents slit width and ξ denotes bead phobicity toward the walls. Symbols indicate simulation results and solid lines represent microphase separation boundaries. Phases include perpendicular cylindrical ($C_{\perp}$), parallel cylindrical ($C_{\parallel}$, ν), parallel lamellar ($L_{\parallel}$), and parallel perforated lamellar ($PL_{\parallel}$, ν). Green and gold spheres represent A- and B-beads, respectively, and gray spheres represent wall-beads [260]. Reproduced with the permission of the American Chemical Society, Copyright 2023. (B) In figures (a–f) at the top, the systems feature natural A-blocks described by an iso-surface ($a_{AA} = a_{BB} = 25$, $a_{AB} = 35$, $a_{AsN} = a_{BsN} = 70$). Below, figures (a–f) are associated with systems containing nanospheres with non-neutral surfaces, where A-blocks have parameters ($a_{AA} = a_{BB} = 25$, $a_{AB} = 35$, $a_{AsN} = 90$, $a_{BsN} = 70$) and B-blocks are described by an iso-surface [262]. Reproduced with the permission of Elsevier, Copyright 2023.

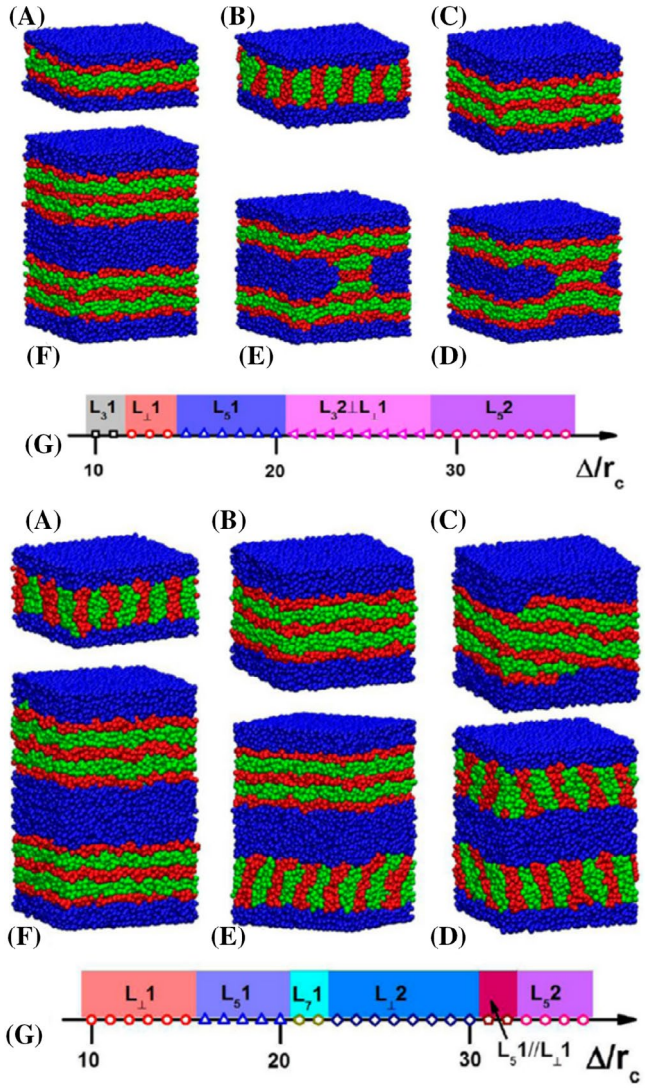

FIGURE 18 | DPD predictions of hierarchical structures; (Top Panel) Hierarchical microstructures self-assembled from $A(BC)_3$ multiblock copolymer thin films: (A) $L_3 1$, (B) $L_\perp 1$, (C) $L_5 1$, (D, E) $L_3 2 \perp L_\perp 1$, and (F) $L_5 2$. (G) One-dimensional diagram for hierarchical microstructures as a function of Δ/r_c. Film thicknesses for parts a to f are 11, 13, 17, 22, 24, and 32, respectively. The interaction parameters are $a_{AB} = a_{AB} = 80$, $a_{BC} = 400$, $a_{AW} = 25$, and $a_{BW} = a_{CW} = 200$. (Bottom Panel) Hierarchical microstructures self-assembled from $A(BC)_3$ multiblock copolymer thin films: (A) L⊥1, (B) L51, (C) L71, (D) L⊥2, (E) L51// L⊥1, and (F) $L_5 2$. Blue, red, and green represent A, B, and C particles, respectively. Wall particles omitted. (G) one-dimensional diagram for hierarchical microstructures as a function of Δ/r_c with thickness of 13, 19, 21, 28, 32, and 36, respectively. The interaction parameters are $a_{AB} = 160$, $a_{AC} = 80$, $a_{BC} = 400$, $a_{AW} = 25$, and $a_{BW} = a_{CW} = 200$ [272]. Reproduced with the permission of the American Chemical Society, Copyright 2023.

medium-induced friction, while perpendicular motion was described as Brownian motion with a dynamic confining potential, consistent with the recently modified tube theory.

DPD simulations by Wu et al. [284] investigated the impact of polymer chain length and stiffness on the phase separation dynamics of semi-dilute polymer solutions. They found that shorter, more flexible chains led to a crossover in the growth exponent from 1/3 to 2/3, indicating a shift from diffusion-dominated coarsening to interfacial tension-driven flow. Longer chains, regardless of stiffness, exhibited a growth exponent of 1/4 in the diffusion-dominating regime, attributed to chain entanglement. Shorter but stiffer chains diffused in a rodlike pattern with a growth exponent of 1/6, corresponding to transient gel coarsening. Increasing both chain length and stiffness required larger repulsion between the polymer and liquid to trigger phase separation, with stiffer and longer chains forming a network that delayed the crossover from diffusion to flow-driven domain growth.

At the theta point, a typical polymer in solution behaves as an ideal chain, separating good and poor solvent qualities [285]. The theta point in equilibrium thermodynamics can be defined using various methods, such as the gyration radius and the second-order virial coefficient [279]. For the same species, the theta point determined by nondynamic methods can vary significantly [286]. The conformational changes resulting from internal motions fluctuate to reach the most probable distribution [287], which makes the dynamic behaviors of the polymer chain the key factor in determining the condition of the theta point. Liu et al. [288] studied the polymer chain dynamics by gradually changing the solvent quality from good to poor using DPD simulations. They found that the dynamic structure factor S(q,t) exhibited different behaviors at different solvent qualities (see Figure 19A). In a good solvent, S(q,t) (at $qR_g \sim 1$) (here q is the wavenumber (the length of the wave vector), and R_g (is the gyration radius of the polymer chain) decayed exponentially with fluctuations due to internal motion. Near the coil-to-globule transition, decay slowed due to strong internal motion, while in a poor solvent, it dropped quickly to zero before fluctuating longer. At the transition point, chain conformation relaxed through a slow mode, identified via spectral density. In infinite chain length, the coil-to-globule transition closely approximated the theta point.

Summary:

The DPD modeling approach enables the study of several aspects of polymer solutions, including:

1. The impact of polymer characteristics, composition, topological structure, and polymer/solvent chemistry on their diffusivity and dynamics within the solution
2. Behavior and dynamics of polymer chains in various solution regimes

4 | Polymer Blends

Polymer blending is a widely used technique to create new polymer materials by combining two or more existing polymers without the need for chemical reactions or new molecules [290–292]. Despite its usefulness, polymer blending often results in poor mixing due to low entropy gain upon mixing. This typically leads to phase-separated structures with weak interface interactions between the different polymer components, resulting in blends with poor mechanical properties [293–296]. Compatibilizers, also known as interfacial modifiers or emulsifiers, are used

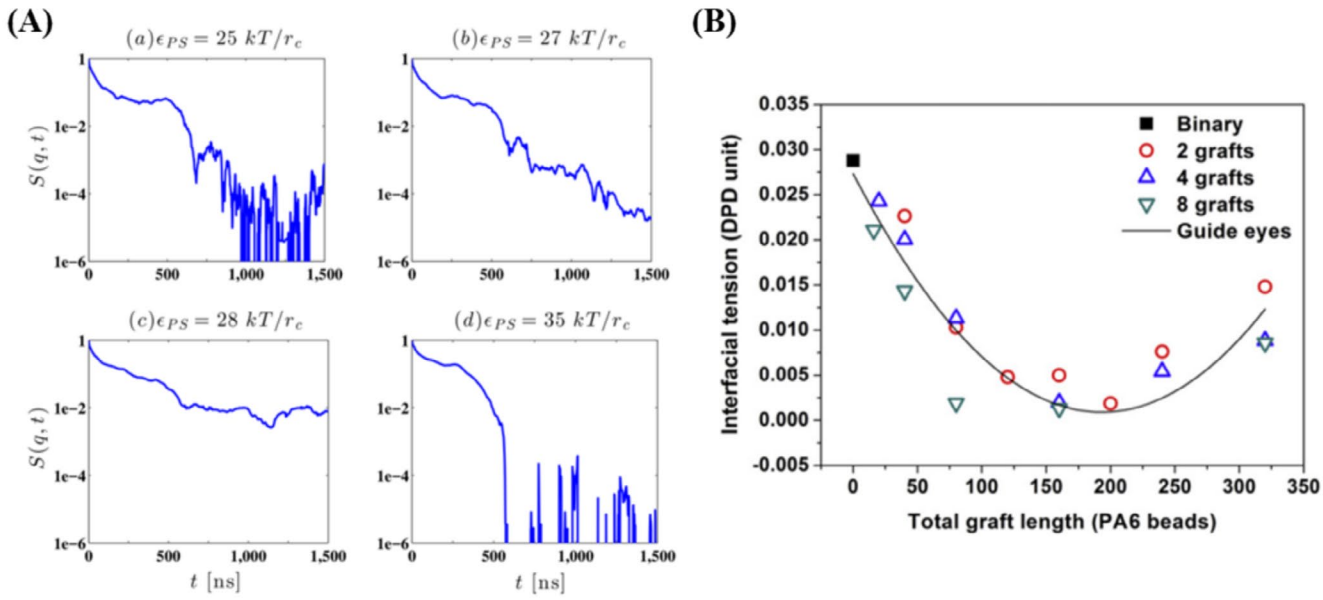

FIGURE 19 | (A) Dynamic structure factor of a polymer chain ($N = 240$) in water solvent as a function of time: (a) good solvent, (b) transition point, and (d) poor solvent [288]. Reproduced with the permission of the American Chemical Society, Copyright 2023. (B) Effect of the total PA6 graft length on the interfacial tension [289]. Reproduced with the permission of Elsevier, Copyright 2023.

to enhance interfacial adhesion and reduce interfacial tension between immiscible components in polymer blends. Block and graft copolymers are common examples of compatibilizers that help slow down the phase coarsening process in the blend [297–301]. DPD modeling is a valuable technique for exploring microphase separation in polymer blends and identifying methods to enhance blend homogeneity with compatibilizer agents. Several research studies have employed the DPD modeling approach to investigate polymer blends, as outlined in the following sections. In a study by Wang et al. [289] DPD simulations were used to study the compatibilization of immiscible polymer blends of polystyrene (PS) and polyamide 6 (PA6), with PA6-*g*-PS copolymers as compatibilizers. The graft copolymer anchored the interfaces, accelerating morphological development and creating a more uniform blend with smaller dispersed phase domains. They found that interfacial tension decreased initially with increasing PA6 graft length, reaching a minimum before rising again, as shown in Figure 19B. Gooneie et al. [302] employed the DPD method to investigate the equilibrium morphology of immiscible PP(polypropylene)/PA11(polyamide-11) blends with carbon nanotube (CNT) inclusions. The researchers found that high aspect ratio CNTs exhibited self-assembly at the interface, forming honeycomb-ordered structures, while CNTs with low aspect ratios were dispersed randomly throughout the blend. The interfacial tension distribution was measured by calculating the distribution of pressure differences across the interface, revealing localized oscillations of pressure differences only in the vicinity of the CNT. The researchers also observed that the pressure differences of low aspect ratio CNTs were greater than those of high aspect ratio CNTs due to their more effective interactions with the dispersed phase resulting from their random dispersion.

Block copolymers can spontaneously organize into ordered structures through microphase separation when in a molten state. This segregation is driven by both enthalpic and entropic thermodynamic interactions, which govern the separation of the copolymer's components. The strength of the enthalpic interactions is described by the Flory-Huggins interaction parameter, χ, which is inversely proportional to temperature. Typically, χ is represented as $\chi \approx AT^{-1} + B$, where A and B correspond to the entropic and enthalpic contributions, respectively [303, 304]. Entropic interactions in microphase separation arise from configurational and translational chain displacements and are influenced by architectural constraints, polymerization degree (N), and copolymer composition. The mean-field theory (MFT) of Leibler [305] microphase separation in asymmetric diblock copolymers is governed by the balance between enthalpic and entropic forces, which the reduced parameter χN can describe. This phase transition is termed the order–disorder phase transition (ODT). This phase transition is known as the order–disorder phase transition (ODT). Several segregation regimes have been identified based on the degree of incompatibility: weak segregation limit (WSL), intermediate, and strong segregation limit (SSL) [306]. Fredrickson and Helfand [307] extended Leibler's result by incorporating fluctuation effects using a method developed by Brazovskii [308]. This led to the prediction of a phase transition between different ordered structures, known as the order–order transition (OOT) [309, 310]. The thermal behavior induced by the characteristic ordered state of block copolymers is a key area of interest in the study of microphase modification.

In this regard, in an interesting research work, Soto-Figueroa et al. [311] conducted mesoscale simulations to investigate the phase transitions of poly(styrene)-poly(isoprene) diblock copolymers in the bulk state. By varying the system's composition, they observed the formation of different ordered microphases, including body-centered-cubic (BCC), hexagonally packed cylinders (HPC), alternating lamellar (LAM), and ordered bicontinuous double diamond (OBBD). The microphases were subjected to thermal cycles to assess their thermodynamic stability. The results showed that the microphases were thermodynamically

unstable due to enthalpic and entropic interactions. The BCC microphases disappeared at higher temperatures, and the HPC microphase underwent an order–order transition to BCC during heating. The transition occurred in stages: microdomain undulation, microphase modification, breakdown of undulated microdomains, and thermal stabilization of poly(styrene) microdomains in a newly ordered state, consistent with Leibler's weak segregation limit theory.

Summary:

One can study the microphase separation in polymer blending by investigating various factors such as the composition of polymer chains, their topological structures, concentrations, and polymer/solvent chemistry using DPD modeling.

5 | Charged Polymeric Systems

Due to the soft nature of the DPD repulsive force, there is a chance that DPD beads could overlap in space during simulation. If point charges are used to account for electrostatic effects, the potential energy would become infinite and the system would collapse when two charged beads overlap. To avoid this divergency, Groot [74] used a charge distribution normalization $f(r)=\frac{3}{\pi R_e^3}\left(1-\frac{r}{R_e}\right)$, for $r<\mathrm{R_e}$, where $\mathrm{R_e}$ is a smearing radius. Groot applied the method of solving the electrostatic field on a lattice to calculate electrostatic forces [312]. However, Melchor [313] proposed to adopt the Slater type distribution, $f(r)=\frac{q}{\pi\lambda^3}\exp\left(-\frac{2r}{\lambda}\right)$, to describe the charge distribution in DPD beads and remove the divergence at $r=0$. Thus, using Ewald techniques, the electrostatic force between beads i and j is represented as

$$F_{ij}^{E}=\frac{\Gamma q_i q_j}{4\pi r_{ij}^2}\left[1-\exp\left(-2\beta r_{ij}\right)\left(1+2\beta r_{ij}\left(1+\beta r_{ij}\right)\right)\right]\hat{\boldsymbol{r}}_{\boldsymbol{ij}} \quad (37)$$

Here, $\Gamma=e^2/\left(k_B T\varepsilon_0\varepsilon_r R_c\right)$, where e is the elementary charge, ε_0 is the vacuum permittivity, ε_r is the relative permittivity of medium, q is the charge number, $\beta=5r_c/8\lambda$, and λ is the decay length of charge. In this context, Hao et al. [109] investigated the self-assembly behavior of zwitterionic copolymers, docosahexaenoic acid–b-poly(γ-benzyl-L-glutamate)–b-poly(carboxy betaine methacrylate) (DHA–PBLG–PCB), and examined the loading and release mechanism of the anticancer drug DOX using DPD simulations. In their system, the PCB monomer featured a positively charged quaternary ammonium group (NH_4^+) and a negatively charged carboxylate group (COO^-). Under physiological conditions (20°C–40°C, 1 atm, pH 6–8), the carboxylate group remains negatively charged but becomes neutral (−COOH) upon protonation in acidic environments. The PCB was divided into three types of beads: the backbone (B), and side chains (N under physiological pH or C under acidic pH). They investigated the effects of polymer concentration, drug content, and pH on polymeric micelles by using DPD simulations with Melchor's [313] approach to treat the electrostatic forces. The simulations revealed the self-assembly of DHA–PBLG15–PCB10 into core–shell micelles, where DOX could be encapsulated in the micelle under physiological pH but released in acidic conditions. Due to protonation/deprotonation of PCB monomers, the system showed significant morphological changes in different pH environments, demonstrating its pH responsiveness.

Zhai et al. [314] systematically predicted the phase diagram and morphology of diblock copolyelectrolytes using a modified DPD simulation framework that incorporated both explicit electrostatic interactions and ion diffusion dynamics. To account for the local charge concentration effect at the mesoscale, they applied the Slater smearing charge distribution, following Melchor's approach [313], to avoid overlaps between oppositely charged particles. The researchers explored several experimentally adjustable factors, including the Flory-Huggins parameter, block volume fraction, and dielectric constant charge fraction. They introduced a new method called the 'diffusivity tensor' to predict ion diffusivity asymmetry along primary microdomain orientations, enabling efficient mapping of phase-specific ion transport. Their findings showed that higher dielectric constants increased ion diffusivity by reducing electrostatic attraction between the charged block and counterions, facilitating easier ion diffusion across block microdomain interfaces. Lisal et al. [315] investigated the pH-dependent self-assembly of poly(2-vinylpyridine)-*b*-poly(ethylene oxide) (P2VP – PEO) in aqueous media using DPD simulations. In neutral and alkaline solutions, copolymers with deprotonated or minimally protonated P2VP blocks formed multimolecular spherical core-shell micelles with insoluble P2VP cores. However, when P2VP protonation exceeded 25%, the micelles dissociated into single chains in acidic media. Lisal et al. [316] also employed DPD simulations to investigate the reversible self-assembly of symmetrical block copolymers, composed of a hydrophobic block and an ionizable polyelectrolyte block of equal length, in aqueous solutions. They explored the self-assembly and characteristics of core-shell micelles as a function of the degree of ionization, hydrophobicity of the non-ionized block, and block compatibility. Their findings showed that as the degree of ionization increased, the micelles underwent extensive dissociation. Sindelka et al. [317] used DPD simulations to study the electrostatic co-assembly of diblock copolymers with a neutral water-soluble block and either positively or negatively charged polyelectrolyte blocks in non-stoichiometric aqueous mixtures. They observed core-shell structures with inter-polyelectrolyte complex cores and neutral shells, finding that non-stoichiometric mixtures led to lower association numbers, charged cores, and unassociated excess chains.

Luo et al. [192] combined MD and DPD simulations to study the vesicular self-assembly of amphiphilic grafted copolymers and their ability to load and release doxorubicin hydrochloride (DOX·HCl). The investigated copolymers, PAE-*g*-PEGLA, consisted of pH-sensitive poly(β-amino ester) (PAE) grafted with hydrophilic poly(ethylene glycol) (PEG) and hydrophobic poly(D,L-lactide) (PLA). Their findings revealed that vesicle formation proceeded through an aggregation-rearrangement mechanism, in which small polymer clusters initially formed, then underwent structural rearrangement, eventually merging into bilayer-structured vesicles. At physiological pH (7.0), DOX·HCl was encapsulated within the vesicle interior, with loading efficiency increasing as polymer concentration rose.

However, at acidic pH (< 7.0), protonation of the PAE blocks rendered them hydrophilic, disrupting membrane integrity and significantly enhancing vesicle permeability, which facilitated the release of DOX·HCl. The study further demonstrated that vesicle stability increased with longer PLA blocks, as the enhanced hydrophobic interactions suppressed DOX·HCl release. To achieve a controlled release profile, the researchers proposed a hybrid vesicle system composed of two different copolymers, which resulted in a moderate and tunable release rate of DOX·HCl. These findings provide important insights into the design of pH-responsive nanocarriers for drug delivery, demonstrating how molecular architecture can be tailored to optimize drug loading, stability, and release kinetics.

Javan Nikkhah et al. [162, 186] implemented an integrated mesoscale model to design a nanocapsule based on block copolyelectrolytes for the oral administration of Trastuzumab, a monoclonal antibody used in breast cancer treatment. Their system was engineered to shield the antibody from the harsh conditions of the gastrointestinal tract while ensuring selective release in the more neutral environment of the intestine, where drug absorption is optimal. To accurately simulate electrostatic interactions within the copolyelectrolyte system, they implemented Melchor's approach [313], incorporating Slater-type charge density distributions to represent local charges on the polyelectrolyte chains with high precision. Their simulations revealed that at acidic pH (3.0), the nanocapsule formed a tightly packed core-shell structure, which provided strong protection for the encapsulated antibody. However, at neutral pH (7.0), the structure underwent partial disassembly and reorganization into a weaker shell, facilitating antibody release in the intestinal environment. Additionally, their model demonstrated how key structural parameters, such as the block length ratio of the copolyelectrolyte chains, played a crucial role in determining the efficiency of drug protection and controlled release. By offering a detailed mechanistic understanding of polyelectrolyte-based encapsulation, this study provides valuable design principles for the development of targeted oral antibody therapy, paving the way for more effective and stable antibody-based treatments in cancer therapy.

Summary:

The DPD modeling technique can be employed to investigate several aspects of charged polymers, such as the impact of polymer composition, charge fraction, and chemistry on the self-assembly mechanism. Additionally, DPD simulations can enable monitoring of the internal structure and morphology of self-assembled supramolecular structures. Another valuable outcome of DPD analysis of copolymers is the ability to generate morphological phase diagrams.

6 | Polymer Interfaces

Extensive research is being conducted on polymer-solid interfaces, as they play a crucial role in various applications such as polymer coatings, hybrid materials, lubrication, adhesion, etc. [318–323] The presence of a solid substrate that confines a polymer is expected to impact the polymer's properties, including mechanical properties and glass transition temperature [318, 324–326]. While the DPD method enables the study of polymer/solid interfaces on a scale comparable to experiments and yields valuable insights beyond the reach of experimental methods, DPD studies of interfaces are challenging; the soft repulsive nature of DPD interactions can lead to polymer beads penetrating the solid substrate at the interface, resulting in unrealistic geometries. To prevent overlap and address this artifact, reflective boundary conditions can be implemented, where beads bounce back upon reaching the solid substrate, thereby preserving realistic geometries [327, 328], or increase the repulsion between liquid and surface beads artificially [329]. As an alternative, increasing the density of surface beads relative to the bulk can help prevent the penetration of polymer beads into the wall, ensuring more realistic interface behavior [330, 331]. Using the last procedure, Kacar et al. [15] studied epoxy-alumina interfaces and their interactions. Modeling liquid–solid interactions in DPD has been a persistent challenge, particularly in deriving coarse-grained DPD parameters from atomistic simulations. To overcome this, atomistic MD and DPD can be coupled through the surface excess parameter, as explained below:

$$\Gamma = \int_{-\infty}^{L_s} \rho(z)dz + \int_{L_s}^{\infty} \left[\rho(z) - \rho_{bulk}\right]dz \tag{38}$$

where $\rho(z)$ and ρ_{bulk} are the polymer bead number densities in the z dimension and the bulk-phase, respectively, and L_S represents the surface's location. The DPD polymer-solid interaction parameters were found by equating Γ_{DPD} (Equation 38) with Γ_{MD} from atomistic MD. After this parametrization, Kacar et al. [15] identified strong, attractive interactions between unreacted epoxy and amine functional groups at the alumina surface. After cross-linking, beads transformed into different functional groups, altering their interactions. The study showed that cross-linking started in the bulk region, but as equilibrium neared, cross-linked beads migrated to the interface. To investigate the properties of cis-1,4-polybutadiene chains interacting with a silica surface, Maurel et al. [332] employed a multiscale strategy. Using a bottom-up approach, they derived structure-based coarse-grained potentials from atomistic simulations through the Iterative Boltzmann Inversion method. DPD models were then used to study the initial stage of polymer chain adsorption onto the silica surface at varying separation distances. The conformational properties of the chains were examined using the normalized parallel and perpendicular components of the squared radius of gyration. Results showed that as the chains neared the silica surface, the parallel component approached 1, while the perpendicular component decreased significantly, indicating chain flattening against the surface. The study was extended to examine the impact of surface coverage on the adsorption of free chains onto a grafted surface. They observed that as surface coverage increased, the overlap between free and grafted chains disappeared, resulting in the formation of two distinct phases: polymer brush and free chains. Cheng et al. [89] modeled polyisoprene natural rubber brushes in mixtures of good and bad solvents (benzene-acetone) to investigate the conformations of polymer brushes in binary solvents using DPD simulations. They found that, unlike the globule-coil transition in single chains, the collapsed-to-expanded transformation in polymer brushes occurred gradually in the good solvent

with higher mole fractions (x_B), particularly at low grafting densities (Figure 20A). They found that similar to globule-to-coil transitions in single chains, entropy gain overcame cohesive forces between polymer segments during collapsed-to-expanded transformations in polymer brushes.

Scacchi et al. [335] used DPD simulations to investigate the self-assembly behavior of linear amphiphilic diblock copolymers on a hydrophilic surface. Their study focused on how variations in block length ratios influence both the surface coating properties and the internal organization of the assembled films. Their simulations revealed that asymmetric copolymers with short hydrophobic segments exhibited enhanced wetting, leading to better surface coverage. In contrast, nearly symmetric diblock copolymers formed more stable and highly ordered thin films, suggesting that the balance between hydrophilic and hydrophobic interactions plays a crucial role in determining film morphology and stability. These findings provide valuable insights into the rational design of surface coatings, offering guidelines for developing tailored nanostructured films for applications in protective coatings, biomedical interfaces, and functional surface modifications.

Hasheminejad et al. [336] employed DPD simulations to investigate the self-assembly of three-component polymeric coatings on hydrophilic surfaces, revealing critical composition-dependent behaviors. The study focused on a system comprising an amphiphilic di-block co-polymer, a hydrophobic polymer, and a hydrophilic stabilizer, modeling interactions relevant to poly(styrene-*co*-n-butyl acrylate) and starch-based coatings. A key finding was the role of the amphiphilic di-block *co*-polymer in determining coating morphology—symmetric block ratios promoted uniform lamellar structures, while asymmetric configurations resulted in advanced patterning. Additionally, the presence of excess free stabilizer was shown to disrupt film homogeneity, which could compromise coating performance. These results align with experimental observations of block length-dependent assembly behaviors, phase separation, and microstructural properties. The study provides a mesoscale mapping of polymer assembly responses, offering valuable insights for designing optimized barrier coatings with controlled spreading and stability on hydrophilic substrates.

Berezkin et al. [333] used DPD simulations to investigate the formation of thin films from mixtures of two compositionally symmetric diblock copolymers. Their study focused on how film thickness and selective block adsorption to the substrate influence macro-phase distribution and lamellae orientation within the assembled structures. Their simulations revealed distinct phase separation behaviors depending on film thickness. In thinner films, lateral phase separation occurred, resulting in domain structures with distinct compositional regions (see Figure 20B). In contrast, thicker films exhibited a three-layer structure, consisting of two short copolymer-rich layers near the interfaces and a long copolymer-rich layer at the core. The orientation of lamellae within the short copolymer-rich layers was largely dictated by the surface selectivity of the substrate, demonstrating how interfacial interactions play a key role in structural organization. Additionally, their study suggested that the introduction of a low-molecular-weight copolymer could serve as an effective strategy for controlling domain orientation without requiring complex chemical modifications of the substrate. These findings offer valuable insights for the design of thin-film coatings with tunable nanostructures, particularly in applications requiring precise control over phase separation and material properties in functional coatings, nanolithography, and advanced surface engineering.

Ramírez-Gutierrez et al. [334] used DPD simulations to investigate the influence of acrylic acid (AA) functionalization on the wetting behavior of water on poly(dimethylsiloxane) (PDMS) surfaces within microfluidic channels. Their study focused on how varying the concentration of AA particles grafted onto the PDMS surface modulates surface hydrophilicity and wettability. Their simulations demonstrated that increasing the amount of AA on the PDMS surface led to a gradual rise in surface hydrophilicity, as evidenced by a progressive decrease in the water contact angle (see Figure 20C). This modification allowed for precise control over wetting properties, providing a direct correlation between AA concentration and water-surface interactions in an oil medium. By quantifying the wetting behavior under different functionalization conditions, the study highlighted an effective strategy for tuning surface properties in microfluidic applications, particularly in systems where controlled fluid behavior is critical. These findings offer valuable design insights for optimizing surface modifications in lab-on-a-chip devices, biomedical microfluidics, and fluid transport technologies, demonstrating how AA grafting can serve as a straightforward approach to enhancing PDMS surface wettability without requiring complex material alterations.

Weng et al. [337] explored the self-healing and dewetting dynamics of a polymer nanofilm on a smooth, partially wetting surface using the mDPD method. The initial polymer film configuration was achieved by adjusting the attractive parameter (A_{ij}) between solid and liquid beads to result in a total wetting surface. They then studied the dewetting process by switching the attractive parameter to a value that produced partial wetting surfaces with a contact angle θ_Y. Their simulations identified three dewetting phenomena: (i) spinodal decomposition, (ii) nucleation and growth, and (iii) metastable self-healing. They examined the effects of surface wettability (θ_Y), the polymer film thickness (h_0), and the radius of the dry hole (R_0) on the film dewetting phenomena. They found that as surface wettability decreased (increasing θ_Y), the critical film thickness associated with the nucleation/self-healing crossover (h_c) increased, allowing the self-healing process to maintain the film's metastability. Li et al. [338] investigated the evaporation and surface-induced morphology changes of $A_{10}B_{10}$ diblock copolymer thin films using mDPD simulations. To initiate evaporation, they rapidly increased the height of the simulation box, creating a vacuum to allow solvent movement toward the upper wall. The simulations revealed various morphologies, including lamellar structures (perpendicular or parallel to the surface), sphere-like morphology, and disordered configurations. They demonstrated that the morphology of the diblock copolymer thin films depended on the interactions between the copolymer components, surface interactions, and solvent vapor.

Yang et al. [339] employed mDPD simulations to investigate the film morphology and wetting stability of 3μ-ABC terpolymers ($A_yB_yC_z$) on both nonselective and selective substrates. Their

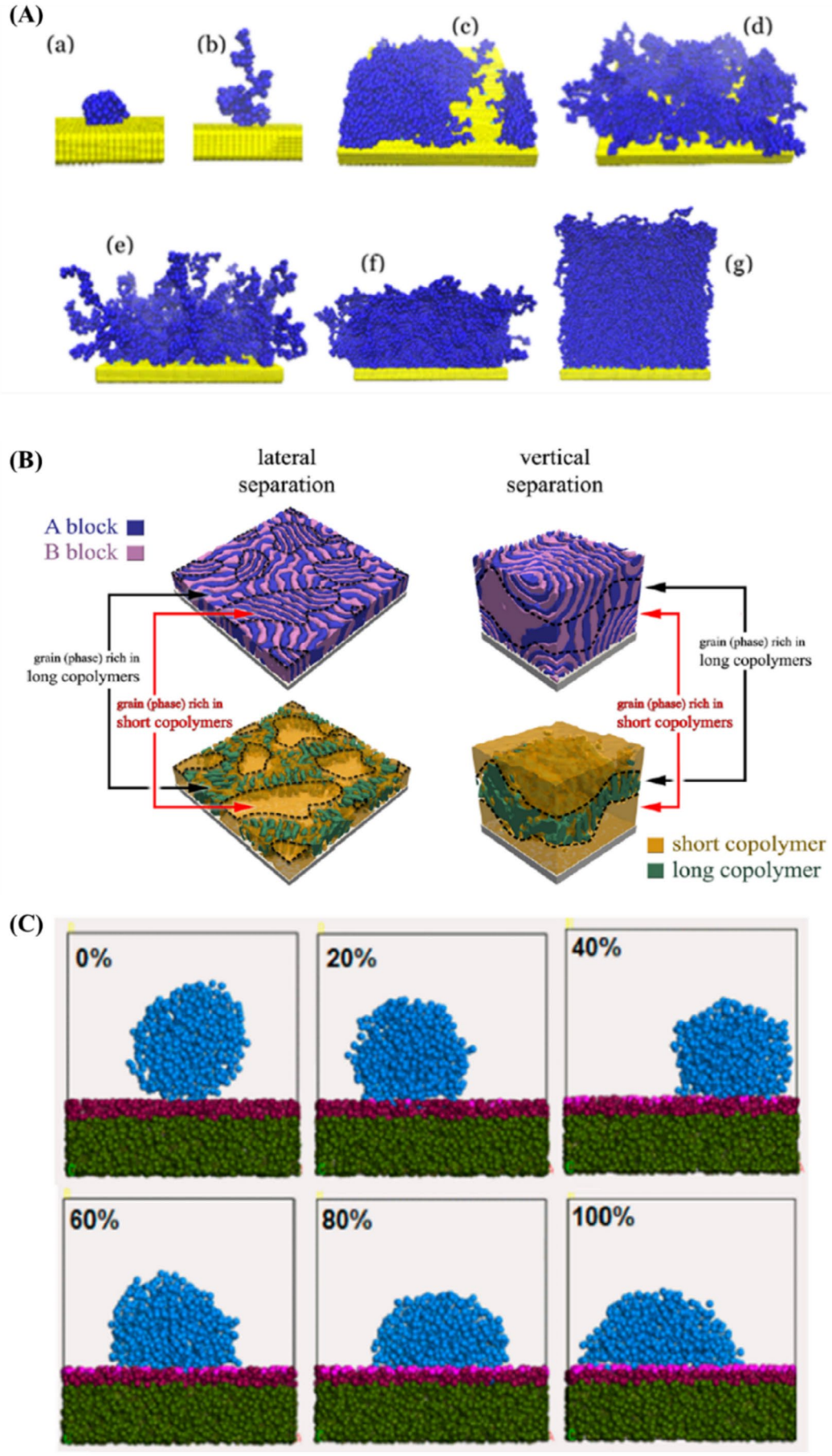

FIGURE 20 | Legend on next page.

FIGURE 20 | (A) Snapshots of modeled PINR conformations in binary solvent (solvent not shown). (a) Globular single tethered chain, $x_B = 0$; (b) coiled single chain, $x_B = 1$; (c) low density brush ($\rho s = 0.12\,nm^{-2}$) in collapsed state, $x_B = 0$; (d) semi-expanded brush at $x_B = 0.4$; (e) fully expanded brush in good solvent, $x_B = 1$; (f) dense brush ($\rho_s = 0.88\,nm^{-2}$) forms a uniform polymer layer in bad solvent, $x_B = 0$; (g) dense expanded brush ($\rho_s = 0.88\,nm^{-2}$, $x_B = 1$) [89]. Reproduced with the permission of the American Chemical Society, Copyright 2023. (B) Schematic of lateral and vertical macrophase separation in the copolymer mixture. Dashed lines represent phase boundaries between regions rich in short and long chains [333]. Reproduced with the permission of the American Chemical Society, Copyright 2023. (C) DPD simulation snapshots of water droplets (blue) on PDMS (violet) with varying AA concentrations (pink). Silicone oil beads are removed for clarity [334]. Reproduced with the permission of the American Chemical Society, Copyright 2023.

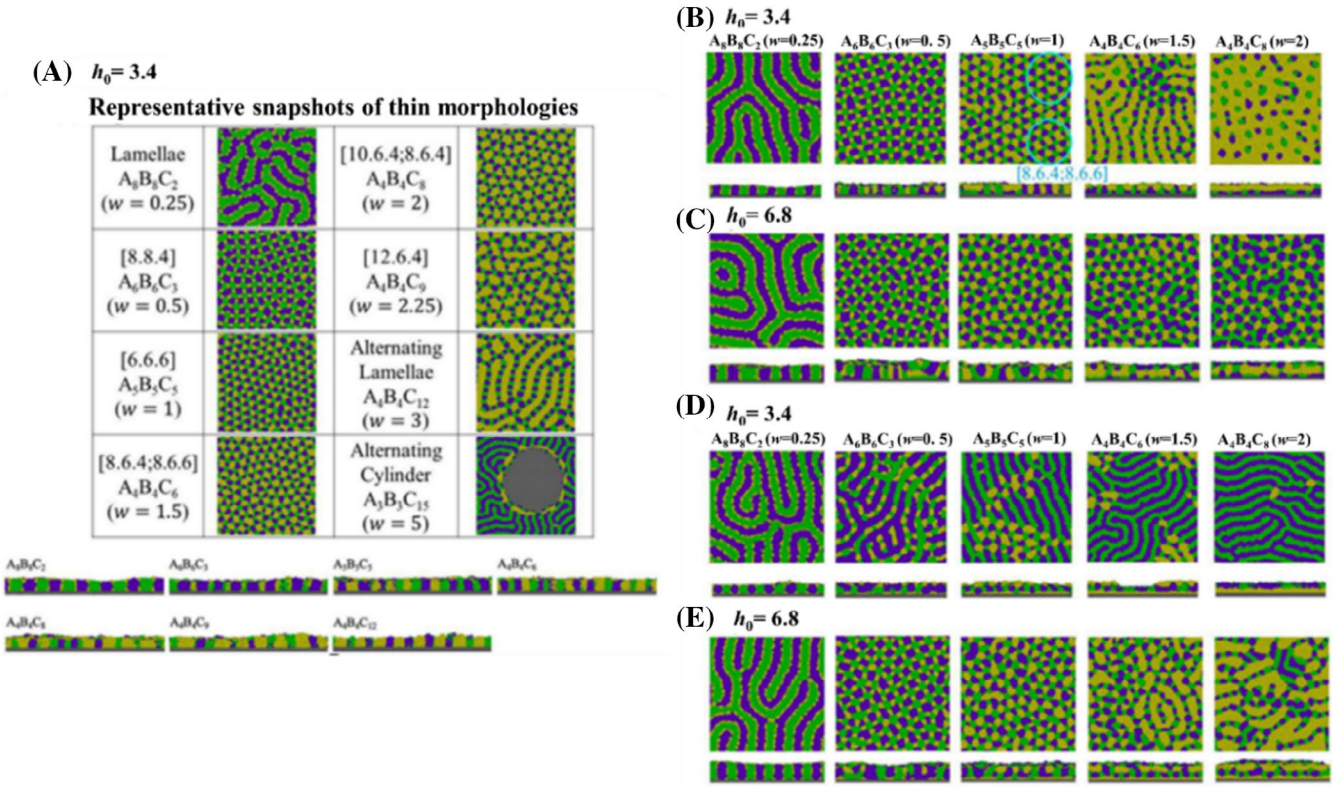

FIGURE 21 | Film morphologies (top and side views) on nonselective surfaces (a) with film thickness $h_0 \approx 3.4$, and on selective substrates with weaker ($a_{CS} = -25$) and stronger ($a_{CS} = -45$) attractions to C-arms. Initial film thicknesses: (b) $h_0 = 3.4$, (c) $h_0 = 6.8$ for weaker attraction, and (d) $h_0 = 3.4$, (e) $h_0 = 6.8$ for stronger attraction [340]. Reproduced with the permission of the American Chemical Society, Copyright 2023.

study focused on how the length ratio of the C-arm to the A-arm (w = y/z) influenced self-assembled structures and wetting behavior, with w ranging from 0.25 to 5. Their simulations revealed a systematic morphological transition as w increased. At lower values of w, the copolymers primarily formed lamellar structures. As w increased, the morphology evolved into various Archimedean tiling pattern, before ultimately transitioning back into alternating lamellae at the highest values (see Figure 21). This structural transformation highlighted the influence of arm length asymmetry on nanoscale organization within the thin films. To analyze wetting stability, the researchers introduced a dry hole into the system and observed three distinct outcomes: (i) a growing hole (nucleation and growth), (ii) a shrinking hole (self-healing), and (iii) a stable hole, each determined by the polymer composition and substrate interactions. On selective substrates, where the attraction to the C-block was weaker, the morphology remained largely unchanged compared to nonselective substrates when $w < 1$. At $w = 1$, a small fraction of the Archimedean tiling pattern began to interfere with the C-arms, an effect that became more pronounced at $w = 1.5$. When w reached 2, the Archimedean tilings completely disappeared as the C-arms became fully covered, leading to a return to lamellar structures (see Figure 21). These findings provide valuable insights into the design of terpolymer-based coatings, offering guidelines for tuning surface morphology, wetting properties, and self-healing behavior in thin-film applications, functional coatings, and nanostructured materials.

Summary:

DPD/mDPD modeling can be utilized to investigate various aspects of interfaces, including:

1. Examining the interfacial interaction between polymers/copolymers and substrates by analyzing the effect of their composition and chemistry.

2. Monitoring the internal structure and morphology of self-assembled supramolecular structures of polymers at the interface.
3. Studying the thin-film formation mechanism and morphology.
4. Investigating the wetting behavior of substrates by simulating contact angle tests.

7 | Polymer Rheology

DPD simulation can be divided into two main categories: equilibrium simulations, where material properties are analyzed at rest, and non-equilibrium simulations, where external fields are applied to DPD particles to reproduce rate-dependent fluid properties. Equilibrium simulations typically yield thermally stable results in simple periodic boundary conditions, while non-equilibrium simulations provide insights into polymer rheology behavior. However, non-equilibrium DPD simulations may be prone to two types of artifacts: (1) the Lees-Edwards boundary condition may not maintain stable profiles at the boundaries in the velocity direction, and (2) out-of-equilibrium simulations may affect the DPD thermostat and hence the thermal stability of the calculations [88, 341, 342]. Various research works have focused on investigating polymer rheology through DPD simulations [329, 343–345]. Using the DPD method, Chen et al. [346] studied the behavior of polymer drops in a shear field using periodic boundary conditions. Their study revealed non-Newtonian behavior, including shear thinning and normal stress differences, using the FENE (finitely extensible nonlinear elastic) chain model. They observed that both the viscosity and first normal stress difference of the polymer followed a power-law relationship with shear rate. In a separate study on polymer gels, they found that these materials, consisting of covalently or physically cross-linked polymers swollen with solvent, exhibited low toughness and weak mechanical response to strain rate, which limited their practical applications [347, 348].

Sliozberg et al. [349] examined the influence of physical entanglements on polymer gel performance, particularly when the solvent molecular weight was sufficient to entangle with the polymer network. In their DPD simulations of polymers, conservative force, F^C, derived from the excluded volume potential U_{WCA} (Weeks Chandler Andersen excluded volume potential [350]), and included a contribution from bonded particles (U_{FENE} (the finitely extensible nonlinear elastic (FENE) potential)), $U_{FENE/LJ}(r) = U_{FENE}(r) + U_{WCA}(r)$. They showed that the presence of a high-molecular-weight solvent led to entanglement with the polymer network, resulting in a time-dependent modulus that was higher than that of gels without entanglement. Schneider et al. [351] studied the precipitation of polymer solutions using the explicit solvent DPD method, focusing on the impact of slip springs on aggregation dynamics. They examined 1% solutions of chains with varying lengths, where 50% of the solvent was suddenly replaced with antisolvent to induce precipitation. Their results revealed that during aggregation, a network-like structure formed with globular polymers bridged by elongated chains. They also explored the effects of entanglements by adding different numbers of slip springs to the precipitating chains.

Zheng et al. [352] conducted mesoscopic simulations using DPD to investigate the behavior of star polymer melts adsorbed onto solid surfaces under shear flow. To accurately capture the structural rigidity and deformation dynamics of star polymers, they introduced a bond-angle potential between the polymer arms, ensuring sufficient rigidity while still allowing deformation under shear stress. Additionally, to prevent bond crossings caused by the soft repulsion of beads, they implemented a segmental repulsion force between non-consecutive bonds. This force was defined as $f_{ij}^{segm} = a_{ij}^{s}\omega^{s}(d_{ij})\widehat{d}_{ij}$, with a_{ij}^{s} is the interaction parameter between bonds i and j, $\omega^{s}(d_{ij})$ a soft weighting function and d_{ij} the minimal distance between the two segments of bonds i and j. Their simulations revealed distinct adsorption and mobility behaviors between linear and star polymers at the solid surface. Linear chains closely followed the no-slip boundary condition, adhering to the surface without significant mobility differences. However, higher-functionality star polymers exhibited a markedly different behavior: due to their more spherical conformations, their centers of mass remained farther from the surface, causing them to move slower than the solid substrate itself (Figure 22A). This difference in adsorption behavior highlights the role of polymer architecture in determining interfacial dynamics under shear. These findings provide valuable insights into the flow behavior of polymer melts, particularly in applications involving lubrication, coatings, and nanocomposite materials, where controlling polymer-surface interactions is crucial for optimizing rheological and tribological properties.

8 | Polymeric Membranes

Polymeric membranes are extensively studied for applications in desalination, wastewater treatment, biopurification, solvent recovery, gas and liquid phase pollutant capture, and gas separations. The advantages of polymers in membrane development include their cost-effectiveness, ease of processing, and abundance, making them an attractive choice for membrane technology. The chemistry–processing–structure–performance paradigm underscores the importance of polymers in advancing membrane technology. In this context, DPD modeling has been utilized to study polymeric membranes, and it provides valuable insights into the structure and behavior of these membranes. Vishnyakov et al. [107] proposed a novel DPD model for hydrated Nafion membranes, incorporating explicit electrostatic forces between charged polymer fragments and dissociated counter-ions. The hydration level, λ, was defined as the number of water molecules per sulfonate group forming the cation bead. The study explored the evolution of self-assembled morphology as hydration increased, with simulations conducted for hydration levels λ ranging from 2.25 to 18. The results indicated a classical percolation transition from isolated water clusters to a 3D hydrophilic channel network (see Figure 22B). With increasing hydration, isolated clusters merged into a worm-like network, eventually forming interconnected spherical clusters.

Wu et al. [354] studied the hydrated morphologies of 3 M PFSA (3 M perfluorosulfonic acid) membranes using DPD simulations, observing similar behavior in water clusters with increasing hydration levels. In addition to hydration, they also examined the effects of molecular weight (MW)

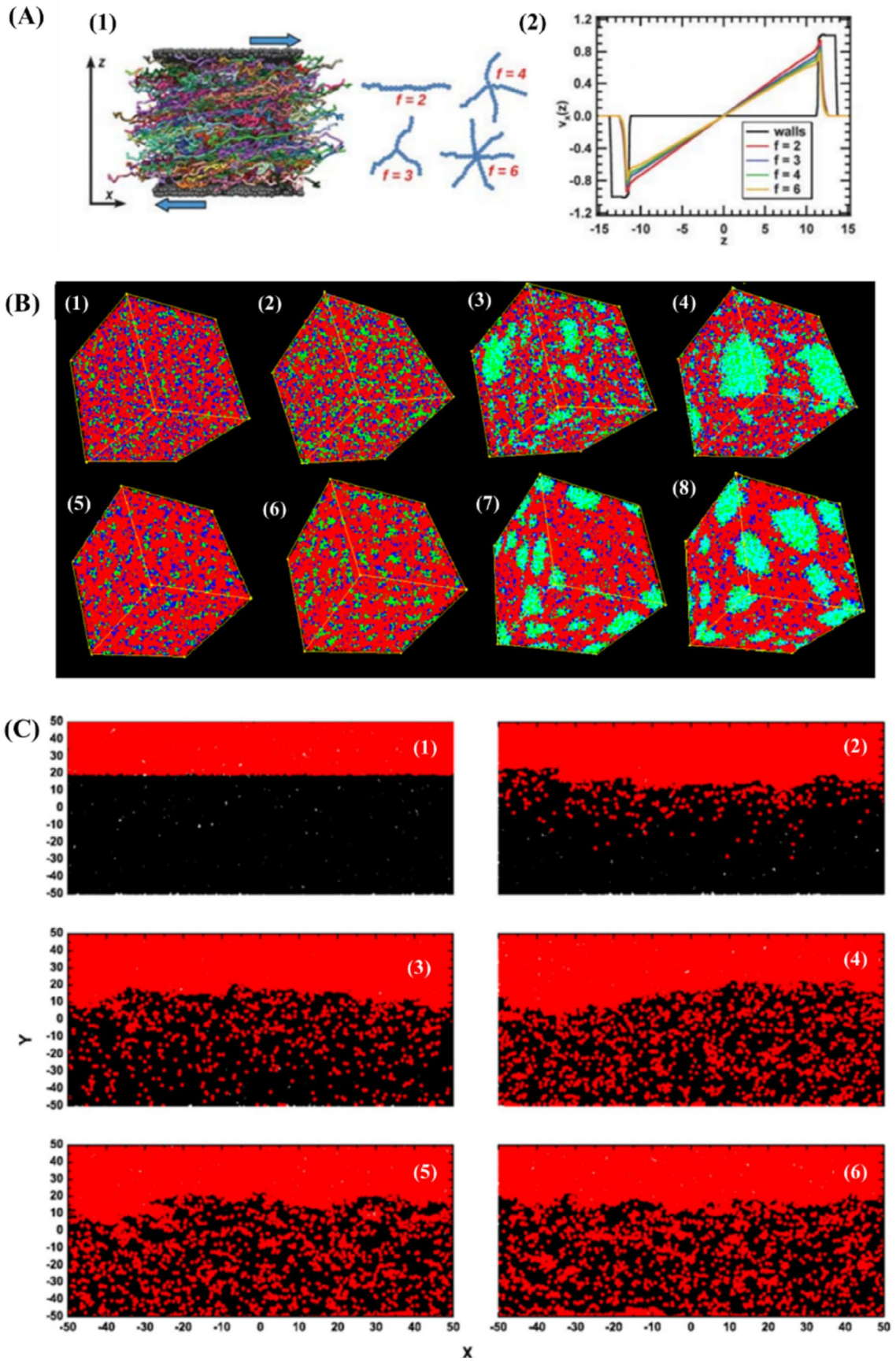

FIGURE 22 | Legend on next page.

FIGURE 22 | (A) Configuration of linear polymer chains (f = 2) confined between two solid walls, with random colors for better visualization. (Right Panel) Velocity $v_x(z)$ as a function of functionality f. The velocity profile imposed on the walls is shown for comparison [352]. Reproduced with the permission of the Royal Society of Chemistry, Copyright 2023. (B) Snapshots of nanophase separation in hydrated Nafion: $M_{eq} = 1144$ (top) and 1744 (bottom). Hydration level $\lambda = 2.25$ (**B(1), B(5)**), 6 (**B(2),B(6)**), 9 (**B(3),B(7)**) and 13.5 (**B(4),B(8)**). The Nafion skeleton and perfluoroether sidechain beads are depicted in red, sulfonate groups in dark blue, counterions in green, and water beads in light blue [107]. Reproduced with the permission of the American Chemical Society, Copyright 2023. (C) Morphology of the polymer/solvent/nonsolvent ternary system (with the polymer chain length $N = 100$) at **(1)** $t = 0$; **(2)** $t = 900$; **(3)** $t = 4900$; **(4)** $t = 29, 900$; **(5)** $t = 44, 900$; and **(6)** $t = 60, 000$. The red color represents the nonsolvent, while the black color indicates the polymer chains that make up the membrane [353]. Reproduced with the permission of Elsevier, Copyright 2023.

and equivalent weight (EW) on morphology. They found that a longer PTFE (poly(tetrafluoroethylene)) backbone, corresponding to higher MW, promoted an elongated form in the water-rich ionic phase. Conversely, a higher EW, linked to a lower ion exchange capacity (IEC), resulted in lower water uptake, as water aggregation into fewer but larger clusters became more complex. Huang et al. [355] used DPD simulations to study the mesophase evolution of a PMP (poly(4-methyl-1-pentene))-diluent system, analyzing the effects of diluent and PMP concentration. Their findings showed that: (1) using a good diluent like DOP (dioctyl phthalate) led to smaller, well-connected pores, while poor diluents like DPE (diphenyl ether) or DBP (dibutyl phthalate) resulted in larger, less interconnected pores; (2) a mixture of good and poor diluents created larger, more interconnected pores in the membrane morphology; and (3) excessively high PMP concentration and poor diluent use resulted in hollow fiber membranes (HFM) with lower diffusivity. Tang et al. [356] conducted DPD simulations to examine how introducing a second diluent influences membrane formation in polymer-diluent systems undergoing thermally induced phase separation (TIPS), with a focus on polypropylene/oleic acid (PP-OA) systems. The simulation was conducted in two phases: initially, the polymer solution was placed between neutral substrates at a high temperature (473.15 K) to allow relaxation, followed by rapid cooling to 273.15 K. The results showed that adding a second diluent, like dimethyl phthalate (DMP) or diethyl phthalate (DEP), altered the TIPS process from solid–liquid (S–L) phase separation to liquid–liquid (L–L) phase separation. For systems like PP/OA, which typically undergo S–L phase separation upon quenching, it was found that selecting a second diluent with good compatibility with the primary diluent but poor compatibility with the polymer is beneficial. This combination of diluents can be used as a new effective diluent for membrane preparation via TIPS. Wang et al. [353] to examine the impact of solvent conditions and polymer chain lengths on membrane formation via immersion precipitation, a phase inversion process in a polymer/solvent/nonsolvent ternary system [357]. Their findings revealed a mechanism where late-stage domain coarsening followed early-stage spinodal decomposition at the membrane surface. Initially, a thin polymer solution film was placed in a nonsolvent bath. As the solvent diffused out and the nonsolvent replaced it, spinodal decomposition occurred (see Figure 22C). Once phase regions in the polymer matrix reached their maximum size, hydrodynamic flow driven by interfacial tension promoted domain coalescence.

Summary:

In polymer membrane modeling, the DPD method allows exploration of how polymer/copolymer and substrate composition, as well as chemistry, influence membrane formation and morphology.

9 | Chemical Reactions-Polymerization

The idea of simulating reactions using DPD is particularly suitable for designing polymerization reactions. In this regard, Liu et al. [358] a method to construct several living polymerization models [359, 360]. In their approach, the chain termination step is omitted, allowing for the continuous growth of polymer chains. The polymerization rate r_P and the reaction probability P_r are related as follows,

$$r_P = -\frac{d[M]}{dt} = \frac{[P^*]P_r}{\tau} \tag{39}$$

where $[M]$ is the concentration of free monomer, $[P^*]$ is the growth centers concentration, and τ is the reaction time interval. To link the reaction model with DPD simulations, they incorporated the reaction probability concept, which controlled the timing of each reaction step throughout the process. Their approach involved selecting a free monomer within the interaction radius if an active end encounters several of them during each reaction time interval τ. From there, a random number P is generated, and if it is less than the reaction probability P_r, the active end determines whether to connect with the chosen monomer (as shown in Figure 23A). If they do connect, the bond information is updated by modifying the spring forces between them. They believed that varying reaction probabilities corresponded to different reaction rates or reaction activation energies (refer to Figure 23A). Additionally, by adjusting the initiator density and selecting different polymerization probabilities, they were able to produce polymer brushes.

Wang et al. [361] conducted a study on star architecture copolymers' polymerization-induced self-assembly (PISA) process using a reaction model and DPD simulations. This process involved the dissolution of solvophilic macro-CTAs and solvophobic monomers in a selective solvent, followed by self-assembly through copolymerization of the monomers. Macro-CTA was represented by A3C in their experiments. When monomer D approached an active end C within a reaction radius R ($R = 0.8\ r_c$), it had a specific probability (P_r) with the nearest monomer D. Upon bonding, monomer D transformed into a solvophobic bead B, and the solvophobic chains always ended with the active end C. The reaction probability P_r was controlled by generating random numbers between 0 and 1. If a random number was less than P_r, the active ends bonded with the nearest monomers, with P_r determining the polymerization rate. The results demonstrated that the PISA of these copolymers could directly generate porous vesicles, with star-shaped architecture promoting their

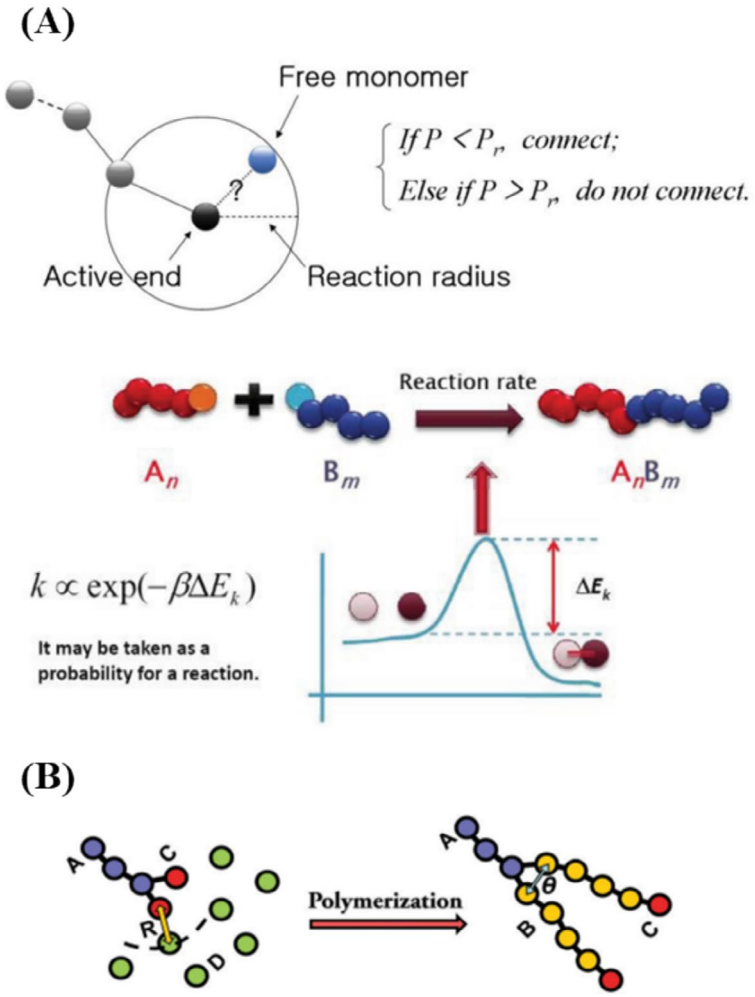

FIGURE 23 | (A) Top panel: Schematic of the reaction process controlled by the reaction probability. Bottom panel: Illustration of the relationship between reaction probability and kinetic reaction activation energy [358]. Reproduced with the permission of Elsevier, Copyright 2023. (B) Schematic of the reaction model: Solvophilic beads A (purple), solvophobic beads B (yellow), active ends C (red), and monomers D (green) [361]. Reproduced with the permission of the Royal Society of Chemistry, Copyright 2023.

formation more effectively than linear copolymers. The study also revealed that the steric effect of two solvophobic chains was a key factor in the formation of the porous vesicles. Overall, this research provides valuable insights into the PISA of star-shaped copolymers, offering a foundation for the experimental development of porous nanomaterials.

10 | Polymeric Composites

Polymer nanocomposites consist of polymer matrices and fillers, which display enhanced macroscopic properties compared to bulk or pure polymer. The extent of improvement in the properties is closely related to the size, shape, and chemistry of the filler, as well as their microscopic spatial organization [362, 363]. The DPD method has been increasingly utilized for studying polymer composites in recent times [364]. DPD has become a useful tool for exploring the properties of polymer composites. By simulating polymeric matrices, DPD can provide insight into interfacial interactions between the matrix and fillers, filler orientation, composite morphology, and mechanical properties. This knowledge can aid in tailoring the properties of composites for specific applications. Below, we will discuss some DPD-based investigations focused on polymer composites. Hu et al. [365] employed DPD simulations to explore nanocube and nanoplatelet self-assembly in a polymer matrix. Their goal was to comprehend the aggregation mechanism of organophilic nanoparticles and the dispersion of organophobic ones. The study also investigated the influence of polymer matrix chain length on aggregation behavior. The findings showed the self-assembly of organophilic nanocubes, with the mean aggregation number increasing for shorter polymers but decreasing for longer ones as the matrix polymer chain length increased (see Figure 24A). Depletion attraction was a key factor in the interparticle interactions of two nanoparticles, driving the aggregation of organophilic ones. Simulation results revealed that the aggregation of organophobic nanoparticles primarily stemmed from the entropy gain in polymer matrices. Despite expectations of organophobic nanoparticles aggregating due to nanoparticle/polymer compatibility, simulations indicated a decrease in the mean aggregation number with longer matrix polymer lengths (see Figure 24A).

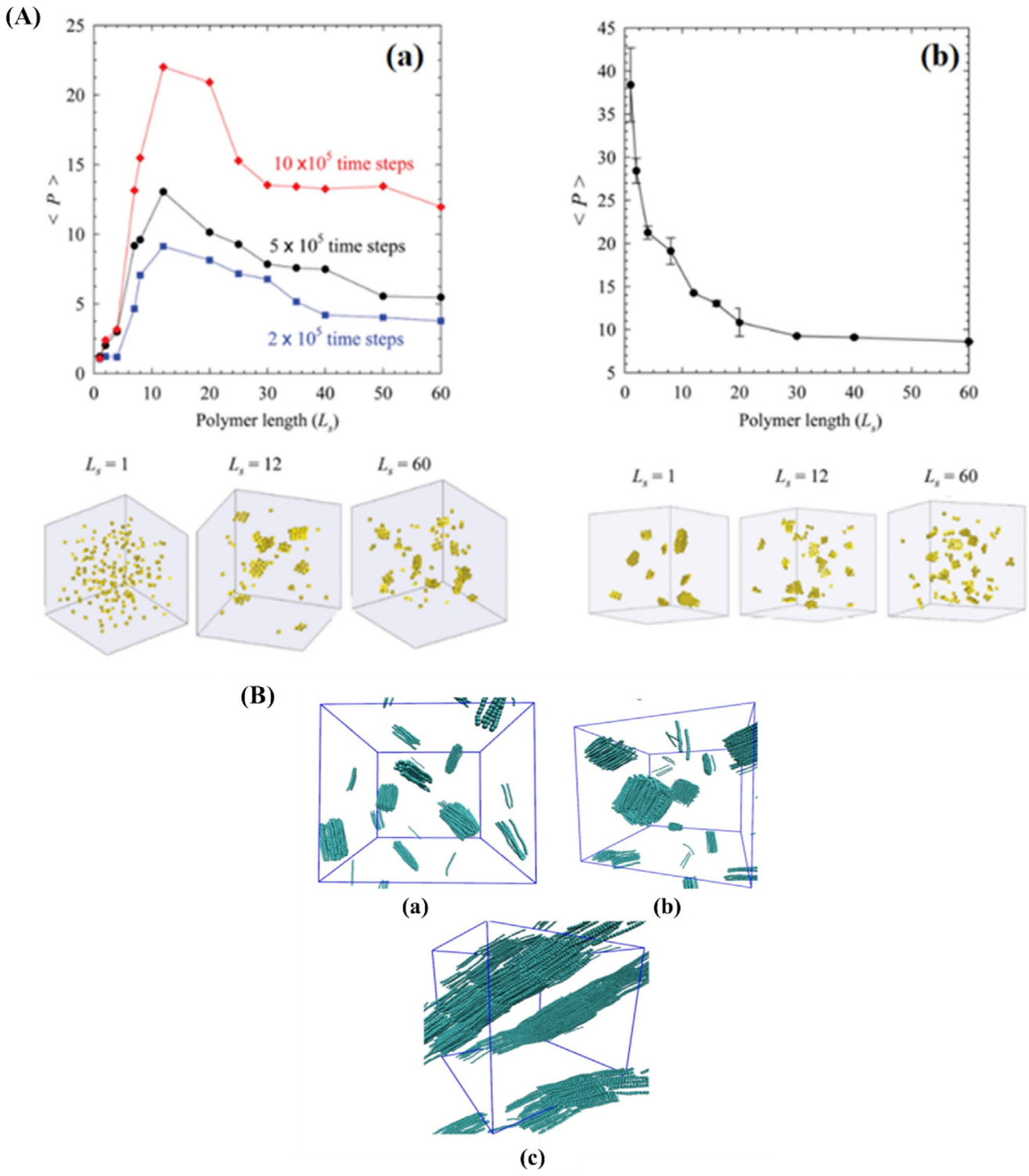

FIGURE 24 | (A) Variation of mean aggregation number with polymer chain length at different time steps: (Left) organophilic nanocubes, (Right) organophobic nanocubes. Bottom: Aggregation snapshots for polymer lengths—Left: Organophilic (1.2×10^6 time steps), Right: Organophilic (4×10^5 time steps) [365]. Reproduced with the permission of the American Chemical Society, Copyright 2023. (B) (Snapshot of an equilibrated 2% mixture showing nanotube bundles (polymer omitted for clarity). Right Panel: Snapshot of an equilibrated 5% mixture. Bottom Panel: Snapshot of an equilibrated 10% mixture showing nanotube percolation network formation (polymer omitted for clarity) [366]. Reproduced with the permission of the American Chemical Society, Copyright 2023.

Chakraborty et al. [366] performed DPD simulations on polycarbonate-CNT composite systems with varying nanotube concentrations to study the equilibrium morphology of nanotubes and their dynamics within the composite matrix. They studied the 2%, 5%, and 10% mixtures (total number of CNT beads in the simulation box/total number of beads in the simulation box) of CNT-polycarbonate and prepared polymer chains much longer than the nanotube. They observed the formation of

nanotube bundles in all three mixtures (2%, 5%, and 10%), with the bundle size in the equilibrium systems varying according to the nanotube concentration (see Figure 24B). By investigating the morphology in the mixtures with different nanotube concentrations, they observed the percolation pathway formed by nanotubes only in the mixture with 10% nanotubes. They concluded that a nanotube concentration of 10% was close to the threshold required to create a percolating pathway in the polycarbonate matrix without the need for external perturbations. Gavlirov et al. [367] performed a comprehensive DPD simulation to investigate structural changes in unfilled and filled elastomers under uniaxial deformation. The study set out to understand how filler reinforcement works in rubber nanocomposites. It found different groups of subchains within the matrix, each behaving in unique ways. Subchains that were not connected to the filler particles showed little deformation, while those attached to the filler particles experienced much more significant deformation.

Yan et al. [368] performed DPD simulation that could predict the self-assembly of Janus nanoparticles with two chemically different compartments (see Figure 25A) at the interface of block copolymers. This approach demonstrates that external fields can be used to control the scaffold of block copolymers, facilitating the formation of oriented structures or superstructures on a macroscopic scale. Achieving this level of control is difficult through self-assembly of particles in solutions. The study demonstrated that Janus nanoparticles with varying architectures induce polymer chain deformation, highlighting their role in interfacial stabilization and the kinetic pathways of structural evolution in nanocomposites (see Figure 25A). The research also explored the self-assembly mechanism of Janus nanoparticles within block copolymer lamellae. It was found that incorporating Janus nanoparticles into block copolymers offers a unique strategy for creating polymer nanocomposites with tunable and enhanced processing properties. Additionally, the study proposed the concept of associated self-assembly between two or more amphiphilic building blocks, offering new insights into complex self-assemblies in nature.

Wang et al. [364] employed DPD simulations to investigate the phase behavior, functionalization degree, and chain length effects in polyethylene-carbon nanotube (PE-CNT) composites across different CNT volume fractions. Their study focused on how functionalization levels influence CNT dispersion and aggregation within the polymer matrix. To simulate varying degrees of functionalization, the researchers systematically adjusted the repulsive interaction parameter between CNTs and the polymer chains. Their findings revealed that when the CNT volume fraction exceeded 50%, the functionalization degree had little impact on dispersion, as the high CNT concentration inherently limited structural rearrangements. However, at lower CNT concentrations, the effects of functionalization were more pronounced. Increasing the repulsive interaction parameter beyond a critical threshold led to CNT aggregation, as stronger repulsion caused phase separation within the system. Conversely, reducing the repulsive interaction parameter facilitated better CNT dispersion within the PE matrix, improving uniformity. Additionally, the study demonstrated that structural modifications in the composite were more easily controlled at lower CNT volume fractions, particularly when tuning functionalization levels. These insights provide a deeper understanding of CNT-polymer interactions, offering practical guidance for optimizing composite properties in nanocomposite materials, conductive films, and mechanical reinforcement applications, where CNT dispersion plays a critical role in performance.

Khani et al. [369] investigated the mechanisms and factors that define the final morphology and self-assembly of nanorods (NRs) in polymeric matrices using DPD simulations. Dispersion of NRs proved more complex than spherical nanoparticles due to their higher aspect ratio, which caused aggregation even in miscible matrices, driven by entropic depletion forces. To address this, NRs were grafted with polymer brushes matching the matrix's chemical identity, aiding their dispersion [370–372]. The researchers examined how enthalpic and entropic interactions influenced the phase behavior of rigid, one-dimensional NRs. By incorporating different enthalpic interactions, they found that aggregation was entropically favored, and the extent of this effect depended on grafting density and brush length. They constructed a pioneering three-dimensional phase diagram considering enthalpy, brush length, and grafting density (see Figure 25B). The results highlighted that strong attractive interactions between the matrix and polymer brushes significantly enhanced the dispersion range. The study found that a high grafting density and longer polymer brushes were essential for achieving the best dispersion, which led to a distinct NR arrangement in a heterogeneous network with parallel rod-like alignment.

Summary:

A concise overview of the potential applications of polymer (nano)composites modeling can be presented as follows:

1. DPD modeling is a useful tool for studying the interfacial interactions between the polymer matrix and fillers in polymer (nano)composites. By simulating the dynamics of the system at the mesoscale, DPD can provide insights into the behavior of the composite materials, which are difficult to obtain experimentally.
2. DPD simulations allow us to track how fillers are oriented in the polymer matrix. This helps us understand how the shape of the filler affects the properties of the composite and enables us to design materials with specific characteristics for different applications.
3. By analyzing the internal structure and mechanical properties of the composite, we can better understand its performance. This includes looking at how the concentration, size, and shape of the filler affect the properties, along with how the matrix influences the overall behavior of the composite.
4. DPD simulations give us a closer look at the microstructure of polymeric composites, allowing us to study how the fillers are arranged and distributed within the matrix. With this understanding, we can refine the manufacturing process and create composites with the specific properties needed.
5. By using the insights from DPD simulations, we can fine-tune the composite's properties, such as filler

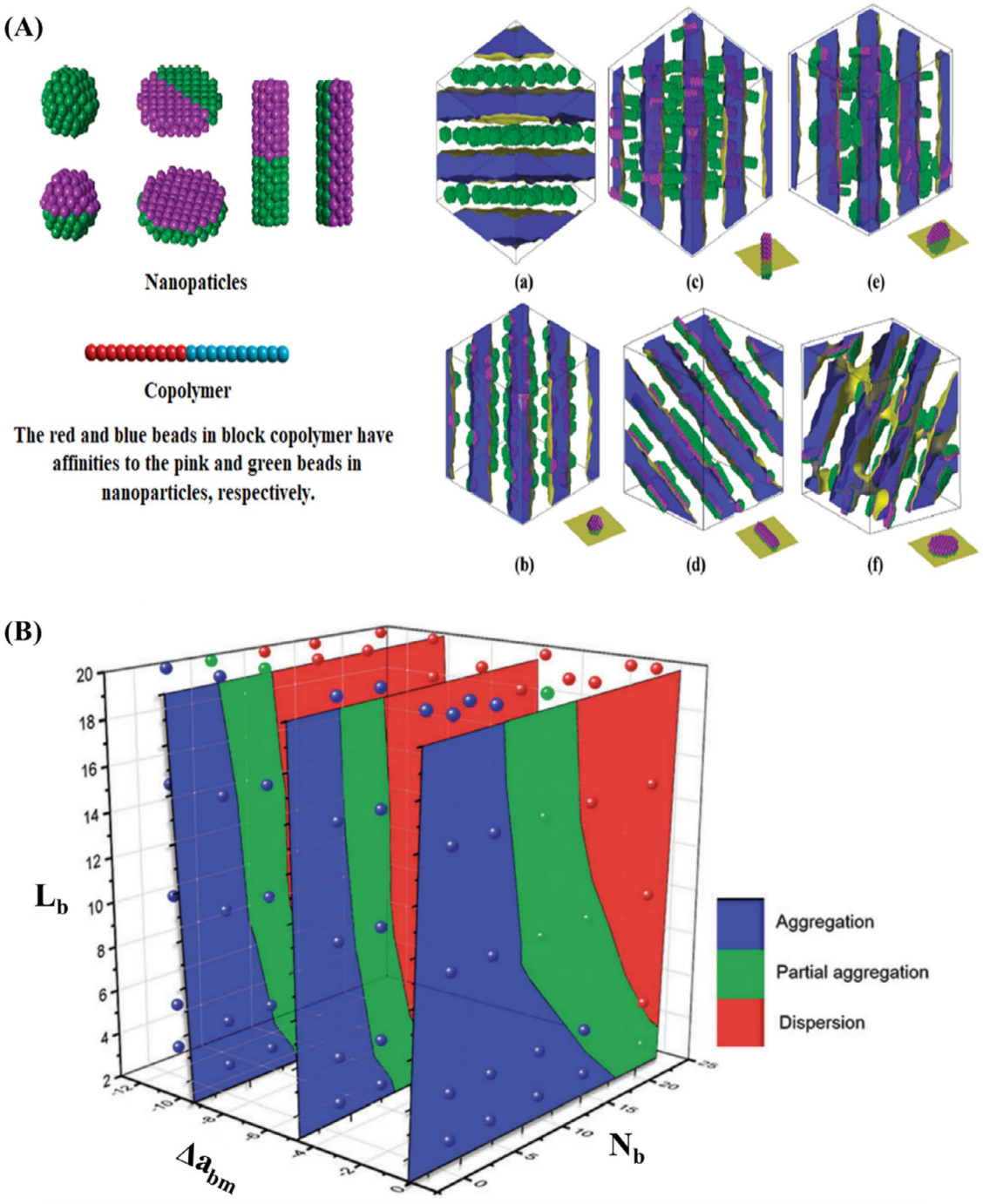

FIGURE 25 | (A) Left Panel: Model building blocks studied. Right Panel: Equilibrium self-assemblies of nanoparticles in symmetric diblock copolymers. Yellow marks the interface between phases A (blue) and B (transparent). Schematic diagrams at the bottom right of images b–f show the orientation of Janus nanoparticles relative to the interface [368]. Reproduced with the permission of the American Chemical Society, Copyright 2023. (B) Three-dimensional phase diagram showing the effects of enthalpy (Δa_{bm}), brush length (L_b), and grafting density (N_b). Dispersion, partial aggregation, and aggregation are represented by red, green, and blue balls, respectively. Contour maps for three planes are included for clarity [369]. Reproduced with the permission of the Royal Society of Chemistry, Copyright 2023.

concentration, size, and shape, along with modifying the properties of the polymer matrix itself to meet the needs of various applications. This allows us to tailor the composite to meet specific performance requirements, such as improved mechanical strength or enhanced electrical conductivity.

11 | Other Reviews

In this review, we have explored key advancements in our understanding of polymeric systems through the use of DPD modeling. We cover the background and development of DPD theory, along with its applications in polymer science and engineering. Notably,

while there are already valuable review papers focusing on specific applications of DPD simulations in polymeric systems (see Table 2), some concentrate on theory with an application-oriented focus, and others emphasize applications, including both polymer systems and other fluids, we assert that our review offers a more comprehensive analysis. Our review explores the latest research on DPD simulations and the recent advancements in the methodology. We delve into the core theory behind DPD and examine its wide range of applications in polymeric materials, covering various topics. What makes this review unique is its comprehensive approach, offering a perspective that extends beyond the typical scope in the field. We believe this review will be a valuable resource for anyone interested in gaining a deeper understanding of the field. By highlighting the potential of DPD modeling, we hope to encourage computational researchers to explore and adopt this technique in their own studies.

12 | DPD Limitations

Despite the numerous functionalities and applications of DPD discussed earlier, this section aims to consolidate its key limitations, which have been previously mentioned throughout the text, and explore possible solutions. While DPD is a powerful mesoscopic simulation technique, several inherent limitations affect its accuracy and applicability. One major challenge is the trade-off between computational efficiency and resolution. In DPD simulations, a higher resolution typically means more particles and, therefore, a higher computational load. Increasing the level of coarse-graining enhances efficiency but at the cost of losing essential molecular details, such as hydrogen bonding. Moreover, parameterization in DPD is often empirical, leading to limited transferability across different systems. Adaptive resolution techniques, which dynamically adjust resolution based on local molecular environments, could help balance accuracy and efficiency.

Another significant limitation is the absence of a standardized force field. DPD interaction parameters are typically system-specific, requiring careful calibration, which restricts their generalizability. Machine learning-based parameterization approaches could improve the consistency and transferability of DPD force fields.

Additionally, DPD does not inherently capture directional interactions such as hydrogen bonding, π-π stacking, or dipole–dipole interactions. While existing solutions, including Morse potentials, enhance accuracy, they also increase computational complexity. A promising alternative is the development of hybrid DPD models that incorporate anisotropic potentials.

Furthermore, DPD lacks explicit treatment of electrostatic interactions, which are crucial for accurately modeling charged systems, including polyelectrolytes and ionic liquids. One promising approach to overcoming this limitation involves incorporating Ewald summation techniques into the DPD framework, which enables a more accurate treatment of long-range Coulombic forces while preserving the mesoscopic nature of the simulation. This method provides a significant improvement in modeling charged systems, making DPD more suitable for applications involving polyelectrolytes, ionic liquids, and self-assembling charged materials.

Another challenge arises from DPD's soft potential, which can lead to the misrepresentation of long polymer relaxation times and dynamic properties. To enhance accuracy, multi-resolution approaches that couple DPD with MD or continuum-scale models could be explored. By overcoming these limitations, DPD can be enhanced for greater accuracy and broader applications in biomolecular, polymeric, and self-assembling systems.

13 | Enhancing the Reliability of DPD Simulations Through Experimental Validation and Calibration

The accuracy and predictive power of DPD simulations can be significantly improved by integrating experimental data, which plays a crucial role in validation, parameter calibration, and model refinement. Experimental validation is essential in computational modeling as it provides a benchmark against which simulation results can be assessed. By comparing key simulation outputs—such as transport properties, structural conformations, and dynamic behavior—with corresponding experimental measurements, discrepancies can be identified and addressed, leading to more reliable and physically meaningful models [18, 387].

Beyond validation, experimental data assists in calibrating key DPD interaction parameters, ensuring that coarse-grained models retain accurate representations of real-world systems. Properties such as diffusion coefficients, viscosity, and interfacial tension obtained from experimental studies can be used to optimize conservative force parameters in DPD models. Empirical calibration of these parameters enhances the transferability and predictive accuracy of DPD simulations, making them applicable to a broader range of soft matter and biological systems [374, 388].

Additionally, experimental data can reveal physical interactions that are not fully captured by the initial simulation framework. Techniques such as small-angle x-ray scattering (SAXS), neutron scattering, dynamic light scattering (DLS), and rheometry provide critical insights into mesoscale self-assembly, phase behavior, and viscoelastic properties. These methods help refine coarse-graining strategies, ensuring that simulated structures and dynamics align more closely with experimental observations [20, 49].

Finally, a well-validated DPD model expands the practical applications of simulations, particularly in scenarios where direct experimentation is expensive, time-consuming, or technically challenging. This is particularly relevant in fields such as materials design, biophysics, and drug delivery, where simulations can be used to explore conditions beyond the scope of conventional experiments [374].

14 | Machine Learning Advancements in Polymer DPD Simulations

With the increasing demand for machine learning (ML) in computational sciences, its integration into DPD simulations has led to significant advancements in accuracy, efficiency, and

TABLE 2 | Summary of the published review papers on the theory and applications of DPD.

Title	Target applications	Simulation method included	DPD type	Authors	Publishing year
Multiscale modeling and simulation of polymer nanocomposites	Polymer composites	MD, MC, Brownian dynamics (BD), DPD, lattice Boltzmann (LB), time-dependent Ginzburg–Lanau method, dynamic density functional theory (DFT), micromechanics, equivalent-continuum and self-similar approaches, finite element method (FEM)	Traditional DPD	Zeng et al. [373]	2008
Dissipative particle dynamics: Introductions, methodology, and complex fluid applications—A review	Complex fluids	DPD	Traditional DPD	Moeendarbary et al. [374]	2009
Dissipative particle dynamics in soft matter and polymeric applications—A review	Rheological properties of polymers, Block copolymers and mesophase separation, Membrane morphology and formation of lipid bilayer, Grafted polymer brush, Surfactant and Amphiphile Systems, Self-assembling systems of surfactants and amphiphiles, Polymers and surfactants in solution	DPD	Traditional DPD	Moeendarbary et al. [375]	2010
Dissipative Particle Dynamics (DPD): An Overview and Recent Developments		DPD	Traditional DPD	Liu et al. [376]	2015
Modeling of Polymer Structure and Conformations in Polymer Nanocomposites from Atomistic to Mesoscale: A Review	Homopolymers structure and dimensions in nanocomposites containing bare or grafted spherical or rod nanoparticles	MD, MC, DPD	Traditional DPD	Karatrantos et al. [13]	2016
Self-assembly and co-assembly of block polyelectrolytes in aqueous solutions. Dissipative particle dynamics with explicit electrostatics	Self-assembly and co-assembly of block polyelectrolytes in aqueous solutions	DPD	Traditional DPD	Procházka et al. [377]	2016
Simulating Transport of Soft Matter in Micro/Nano Channel Flows with Dissipative Particle Dynamics	Micro/Nano Channel Flows	DPD	Traditional DPD	Xu et al. [378]	2018

(Continues)

TABLE 2 | (Continued)

Title	Target applications	Simulation method included	DPD type	Authors	Publishing year
A Comparative Review of Smoothed Particle Hydrodynamics, Dissipative Particle Dynamics and Smoothed Dissipative Particle Dynamics	Simple fluid flows: self-diffusion of quiescent flow, time-dependent Couette flow, time-dependent Poiseuille flow, and lid-driven cavity flow	Smoothed particle hydrodynamics (SPH), dissipative particle dynamics (DPD) and smoothed dissipative particle dynamics (SDPD)	Smoothed particle hydrodynamics (SPH), Traditional DPD and smoothed dissipative particle dynamics (SDPD)	Ye et al. [379]	2018
Multiscale modeling and simulations of responsive polymers	Stimuli-responsive polymers	All-atom molecular dynamics (AAMD), coarse-grained molecular dynamics (CGMD), DPD, MC and theoretical methods	Traditional DPD	Hen et al. [380]	2019
Dissipative Particle Dynamics Aided Design of Drug Delivery Systems: A Review	Drug delivery systems	DPD	Traditional DPD	Feng et al. [381]	2020
Dissipative Particle Dynamics Simulation: A Review on Investigating Mesoscale Properties of Polymer Systems	Microchannel flow, electrospinning, free-radical polymerization, polymer self-assembly processes, polymer electrolyte fuel cells, and biomedical materials.	DPD	Traditional DPD	Wang et al. [382]	2021
Dissipative particle dynamics simulations in colloid and Interface science: a review	Thermodynamic, morphological, and transport properties of various colloidal and interfacial systems	DPD	Traditional DPD, mDPD, sDPD, Fluid particle model (fPM), eDPD, reactive DPD	Santo et al. [383]	2021
A review of many-body dissipative particle dynamics (mDPD): Theoretical models and its applications	Droplet and microbubble dynamics, evolution of liquid bridges, capillary wetting, polymer solutions, and phase change	DPD	mDPD	Zhao et al. [384]	2021
Comprehensive review of the interfacial behavior of water/oil/surfactant systems using dissipative particle dynamics simulation	Colloids and interface systems, especially surfactant/water/oil mixtures	DPD	Traditional DPD	Ahmadi et al. [385]	2022
Advances in self-assembling of pH-sensitive polymers: A mini review on dissipative particle dynamics	Self-assembly process of pH-sensitive polymers under neutral conditions	DPD	Traditional DPD	Guo et al. [386]	2022

TABLE 3 | Recent ML breakthroughs in polymer DPD simulations with applications, implications, and approaches.

Breakthrough	ML approach	Application in DPD	Potential implications	References
Data-Driven coarse-graining	Graph neural networks, autoencoders	Automated mapping from atomistic to DPD models	Improves accuracy, enhances transferability across polymer systems	[389]
Neural network-based coarse-graining	Neural networks	Utilizing neural networks to develop coarse-grained models that accurately represent polymer behavior	Enhances the accuracy and efficiency of coarse-grained models, leading to more reliable DPD simulations	[390]
Optimized DPD force fields	Bayesian optimization, neural networks	Predicting conservative and dissipative parameters	Eliminates manual fitting, improves interaction parameter selection	[391, 392]
Trajectory matching for coarse-grained model development	Supervised learning	Applying machine learning to match atomistic simulation trajectories, facilitating the creation of accurate CG models	Ensures that coarse-grained models retain essential polymer properties, enhancing the fidelity of DPD simulations	[16]

predictive capability. ML has revolutionized DPD simulations by automating complex tasks such as coarse-grained model development, force-field optimization, and phase behavior predictions, enabling the study of polymer self-assembly, miscibility, and large-scale morphologies with greater precision.

While DPD effectively models long-time-scale polymer behavior, it faces challenges related to parameter selection, coarse-graining fidelity, and the accurate representation of molecular interactions. ML-based methods enhance these aspects by learning optimal interaction parameters to improve coarse-grained representations and accelerate sampling strategies, leading to more reliable and computationally efficient simulations.

The application of ML in DPD has facilitated data-driven coarse-graining, refining how atomistic representations are mapped onto mesoscopic DPD beads. Automated force-field parameterization has reduced empirical fitting errors. Trajectory optimization allows for more efficient exploration of polymer phase space. Table 3 highlights key ML breakthroughs in DPD-based polymer simulations, summarizing their applications and potential implications for polymer modeling.

15 | Influence of Simulation Methods on Modeled Polymer Properties

The accuracy of modeled polymer properties is profoundly influenced by the choice of simulation method, as different computational approaches vary in their spatial resolution, time scale coverage, and force field approximations. Since this review covers a broad range of polymeric phenomena—including self-assembly, blends, solutions, interfacial behavior, and composites—it is essential to understand how different simulation techniques contribute to these representations.

Molecular simulation techniques are broadly classified based on the level of detail they retain, ranging from fully atomistic descriptions to coarse-grained and mesoscale models. The three primary computational methods employed for polymer simulations are MD, DPD, and Monte Carlo (MC) simulations, each of which offers distinct advantages and limitations. MD provides high-resolution atomistic details but is computationally intensive. Coarse-grained MD reduces computational cost while retaining key polymer characteristics. DPD is efficient for mesoscale modeling, enabling long time-scale simulations but with limited accuracy in capturing specific polymer properties such as chain entanglements. MC simulations are highly effective for predicting equilibrium phase behavior but lack dynamic information. These methods and their respective strengths and limitations are summarized in Table 4.

Selecting an appropriate simulation technique depends on the specific polymer property being modeled. Certain properties, such as molecular self-assembly, phase separation, rheology, and interfacial behavior, require distinct computational approaches to achieve accurate predictions. Table 5 outlines the most suitable simulation methods for capturing these polymer properties, considering the balance between accuracy and computational efficiency.

16 | Conclusions and Outlooks

The Dissipative Particle Dynamics (DPD) method is a mesoscopic simulation technique that has emerged as a powerful tool for the study of complex systems. It offers unique capabilities that are beyond what is currently feasible with other similar scale methods. In this review, we have discussed the basic principles of DPD and its applications in polymer science and engineering. We have highlighted the broad applicability of DPD to describe polymer self-assembly, blending, chemical reaction, and rheological processes for different polymer solutions, charged polymeric systems, interfaces, polymeric membranes, and nanocomposites.

- Challenges and opportunities

Despite the enormous potential of DPD, there are several issues that need to be addressed to make it more versatile and applicable. One of the critical challenges is the development

TABLE 4 | Comparative analysis of simulation methods for polymer modeling.

Simulation method	Resolution	Strengths	Limitations	Applications in this review	References
MD	High (atomistic level)	Captures intramolecular interactions, chain conformations, and hydrogen bonding	Computationally expensive; limited time and length scales	Polymer solutions, charged polymeric systems, polymerization	[393, 394]
Coarse-Grained MD (CG-MD)	Medium (bead-based representation)	Extends time and length scales while retaining key molecular interactions	Loses atomic detail; requires parameterization	Self-assembly of copolymers, polymer membranes, polymer blends	[395, 396]
DPD	Low (mesoscale, soft repulsions)	Efficient for large-scale polymer systems, phase separation, and diffusion studies	Limited in capturing entanglements, directional interactions	Self-assembly, polymer blends, interfaces, rheology, composites	[18, 132, 313, 397]
Monte Carlo (MC)	Variable (discrete or continuous)	Fast for predicting equilibrium properties and phase behavior	Does not capture polymer dynamics	Polymer phase separation, Flory-Huggins mapping, confined space polymerization	[398, 399]

TABLE 5 | Suitability of simulation methods for modeling polymer properties.

Polymer property	Most suitable simulation methods	Key considerations	References
Molecular self-assembly	CG-MD, DPD, MC	CG-MD and DPD capture morphology formation, MC predicts thermodynamic stability	[18, 395, 398]
Polymer solutions and blends	DPD, MD	DPD models solvent-polymer interactions, MD predicts local conformations	[18, 393]
Charged polymeric systems	DPD, MD	DPD with Ewald summation techniques models electrostatic interactions, MD resolves ion condensation	[313, 397]
Polymer rheology and interfaces	DPD, MD	DPD captures diffusion and interfacial tension, MD describes chain entanglements	[18, 48, 394]
Polymeric composites and membranes	CG-MD, DPD, MD	CG-MD/DPD model nanocomposite dispersion, MD studies interfacial adhesion	[395, 397]

of appropriate DPD algorithms and parameters capable of handling multiphase problems, complex heat transfer studies, and simulations of biological membranes or macromolecules subject to different flows and geometries. The improvement of atomistic force fields can inspire and be useful to refine DPD parameters. However, this will come with an additional computational cost. The huge computational costs associated with DPD simulations require fast time-evolution algorithms for the speed-up of the simulations. There are vast opportunities for particle methods to decrease computational costs.

- Future research directions

To further improve the accuracy, efficiency, and applicability of DPD modeling, several key advancements must be pursued. These advancements will not only refine DPD's computational capabilities but also expand its applicability beyond traditional polymer systems.

- One major challenge in DPD is the development of more accurate force fields. Current DPD force fields struggle to accurately describe heterogeneous and highly functionalized materials, limiting their predictive power in complex polymer and biomolecular systems. Future efforts should focus on refining force field parameters through data-driven

optimization and systematic coarse-graining approaches. These improvements will enhance the ability of DPD to model diverse soft matter systems with greater accuracy and realism.

- Another promising direction is the integration of DPD with multiscale modeling approaches. While DPD is computationally efficient for large-scale simulations, it lacks the molecular resolution needed to capture finer-scale interactions. Combining DPD with Molecular Dynamics (MD), Monte Carlo (MC) simulations, or hybrid multiscale techniques would allow researchers to bridge length and time scales, making it possible to study nanoscale processes while maintaining computational efficiency.
- The incorporation of machine learning (ML) in DPD simulations also presents an exciting opportunity. ML techniques can aid in force field parameterization, reducing computational costs while increasing accuracy. By training ML models on atomistic simulations and experimental data, researchers could develop adaptive interaction potentials, allowing for improved transferability across different material systems.
- As DPD is increasingly applied to larger and more complex systems, improvements in computational efficiency are essential. Optimizing parallel computing techniques, adaptive resolution methods, and scalable integration algorithms will enable DPD to handle high-dimensional, multicomponent systems with greater efficiency, making it more suitable for modeling highly branched polymers, multifunctional networks, and biopolymer assemblies.

These developments will enable the study of more complex polymer systems, such as highly branched polymers, polymers with multiple functional groups, and biopolymer systems. Overall, the future development and refinement of DPD modeling will allow for a deeper understanding of complex polymer systems and facilitate the design of novel materials with specific properties for various applications. Thus far, DPD has been successfully applied to determine elastic and plastic properties and deformation regimes for polymeric systems, nanocomposites, and many other molecular systems as reviewed herein; however, it is expected that DPD would also be useful to study the properties and mechanical behavior of metallic systems, shape memory alloys, high entropy alloys, etc. In summary, DPD has become a popular method in the study of complex systems due to its ability to address certain features beyond what is currently feasible with other similar scale methods. There is still potential to improve DPD algorithms and parametrization to allow the modeling of complex and even unknown systems.

Author Contributions

Sousa Javan Nikkhah: conceptualization (lead), data curation (lead), funding acquisition (equal), investigation (lead), methodology (lead), visualization (lead), writing – original draft (lead), writing – review and editing (lead). **Matthias Vandichel:** funding acquisition (equal), resources (lead), writing – review and editing (supporting).

Acknowledgments

S.J.N. thanks Enterprise Ireland and the European Union's Horizon 2020 research and innovation programme under the Marie Skłodowska-Curie grant agreement 847402 (ID: MF20210297). M.V. acknowledges funding from Research Ireland (MEM-E-TECH, 23/FFP-A/12221).

Conflicts of Interest

The authors declare no conflicts of interest.

Data Availability Statement

Data sharing is not applicable to this article as no new data were created or analyzed in this study.

Related WIREs Articles

The power of coarse graining in biomolecular simulations

References

1. R. G. Larson and P. S. Desai, "Modeling the Rheology of Polymer Melts and Solutions," *Annual Review of Fluid Mechanics* 47 (2015): 47–65.

2. O. E. Agwu, J. U. Akpabio, M. E. Ekpenyong, et al., "A Critical Review of Drilling Mud Rheological Models," *Journal of Petroleum Science and Engineering* 203 (2021): 108659.

3. T. E. Gartner and A. Jayaraman, "Modeling and Simulations of Polymers: A Roadmap," *Macromolecules* 52, no. 3 (2019): 755–786, https://doi.org/10.1021/acs.macromol.8b01836.

4. J. Shen, X. Li, L. Zhang, et al., "Mechanical and Viscoelastic Properties of Polymer-Grafted Nanorod Composites from Molecular Dynamics Simulation," *Macromolecules* 51 (2018): 2641–2652.

5. M. A. F. Afzal, A. R. Browning, A. Goldberg, et al., "High-Throughput Molecular Dynamics Simulations and Validation of Thermophysical Properties of Polymers for Various Applications," *ACS Applied Polymer Materials* 3, no. 2 (2021): 620–630, https://doi.org/10.1021/acsapm.0c00524.

6. A. F. Behbahani, A. Rissanou, G. Kritikos, et al., "Conformations and Dynamics of Polymer Chains in Cis and Trans Polybutadiene/Silica Nanocomposites Through Atomistic Simulations: From the Unentangled to the Entangled Regime," *Macromolecules* 53 (2020): 6173–6189.

7. F. D. Tsourtou, L. D. Peristeras, R. Apostolov, and V. G. Mavrantzas, "Molecular Dynamics Simulation of Amorphous Poly(3-Hexylthiophene)," *Macromolecules* 53 (2020): 7810–7824.

8. T. Onodera, J. Nunoshige, K. Kawasaki, K. Adachi, K. Kurihara, and M. Kubo, "Structure and Function of Transfer Film Formed From PTFE/PEEK Polymer Blend," *Journal of Physical Chemistry C* 121 (2017): 14589–14596.

9. P. J. Hoogerbrugge and J. M. V. A. Koelman, "Simulating Microscopic Hydrodynamic Phenomena With Dissipative Particle Dynamics," *EPL* 19 (1992): 155–160.

10. A. F. Voter, F. Montalenti, and T. C. Germann, "Extending the Time Scale in Atomistic Simulation of Materials," *Annual Review of Materials Research* 32 (2002): 321–346.

11. N. Moreno, S. Nunes, and V. M. Calo, "Restrictions in Model Reduction for Polymer Chain Models in Dissipative Particle Dynamics," *Procedia Computer Science* 29 (2014): 728–739.

12. S. C. Glotzer and W. Paul, "Molecular and Mesoscale Simulation Methods for Polymer Materials," *Annual Review of Materials Research* 32 (2002): 401–436.

13. A. Karatrantos, N. Clarke, and M. Kröger, "Modeling of Polymer Structure and Conformations in Polymer Nanocomposites From Atomistic to Mesoscale: A Review," *Polymer Reviews* 56 (2016): 385–428.

14. S. Kmiecik, D. Gront, M. Kolinski, L. Wieteska, A. E. Dawid, and A. Kolinski, "Coarse-Grained Protein Models and Their Applications," *Chemical Reviews* 116 (2016): 7898–7936.

15. G. Kacar, E. A. J. F. Peters, and G. de With, "Structure of a Thermoset Polymer Near an Alumina Substrate as Studied by Dissipative Particle Dynamics," *Journal of Physical Chemistry C* 117 (2013): 19038–19047.

16. K. Kempfer, J. Devémy, A. Dequidt, M. Couty, and P. Malfreyt, "Development of Coarse-Grained Models for Polymers by Trajectory Matching," *ACS Omega* 4 (2019): 5955–5967.

17. H. Wang, Y.-T. Liu, H.-J. Qian, and Z.-Y. Lu, "Dissipative Particle Dynamics Simulation Study on Complex Structure Transitions of Vesicles Formed by Comb-Like Block Copolymers," *Polymer* 52 (2011): 2094–2101.

18. R. D. Groot and P. B. Warren, "Dissipative Particle Dynamics: Bridging the Gap Between Atomistic and Mesoscopic Simulation," *Journal of Chemical Physics* 107 (1997): 4423–4435.

19. R. Miwatani, K. Z. Takahashi, and N. Arai, "Performance of Coarse Graining in Estimating Polymer Properties: Comparison With the Atomistic Model," *Polymers* 12 (2020): 382.

20. F. Müller-Plathe, "Coarse-Graining in Polymer Simulation: From the Atomistic to the Mesoscopic Scale and Back," *ChemPhysChem* 3 (2002): 754–769.

21. R. D. Groot and K. L. Rabone, "Mesoscopic Simulation of Cell Membrane Damage, Morphology Change and Rupture by Nonionic Surfactants," *Biophysical Journal* 81 (2001): 725–736.

22. C. Peter and K. Kremer, "Multiscale Simulation of Soft Matter Systems – From the Atomistic to the Coarse-Grained Level and Back," *Soft Matter* 5 (2009): 4357–4366.

23. H. Goel, P. R. Chandran, K. Mitra, S. Majumdar, and P. Ray, "Estimation of Interfacial Tension for Immiscible and Partially Miscible Liquid Systems by Dissipative Particle Dynamics," *Chemical Physics Letters* 600 (2014): 62–67.

24. C. J. Van Oss, M. K. Chaudhury, and R. J. Good, "Interfacial Lifshitz-Van der Waals and Polar Interactions in Macroscopic Systems," *Chemical Reviews* 88 (1988): 927–941.

25. T. Casalini, V. Limongelli, M. Schmutz, et al., "Molecular Modeling for Nanomaterial–Biology Interactions: Opportunities, Challenges, and Perspectives," *Frontiers in Bioengineering and Biotechnology* 7 (2019): 268, https://doi.org/10.3389/fbioe.2019.00268.

26. M. H. Nafar Sefiddashti, M. Boudaghi-Khajehnobar, B. J. Edwards, and B. Khomami, "High-Fidelity Scaling Relationships for Determining Dissipative Particle Dynamics Parameters From Atomistic Molecular Dynamics Simulations of Polymeric Liquids," *Scientific Reports* 10 (2020): 4458.

27. M. Yamanoi, O. Pozo, and J. M. Maia, "Linear and Non-linear Dynamics of Entangled Linear Polymer Melts by Modified Tunable Coarse-Grained Level Dissipative Particle Dynamics," *Journal of Chemical Physics* 135 (2011): 044904.

28. Z. Jarin, J. Newhouse, and G. A. Voth, "Coarse-Grained Force Fields From the Perspective of Statistical Mechanics: Better Understanding of the Origins of a MARTINI Hangover," *Journal of Chemical Theory and Computation* 17 (2021): 1170–1180.

29. J. Barnoud and L. Monticelli, "Coarse-Grained Force Fields for Molecular Simulations," *Methods in Molecular Biology* 1215 (2015): 125–149.

30. P. Depa, C. Chen, and J. K. Maranas, "Why Are Coarse-Grained Force Fields Too Fast? A Look at Dynamics of Four Coarse-Grained Polymers," *Journal of Chemical Physics* 134 (2011): 014903.

31. R. E. Rudd and J. Q. Broughton, "Coarse-Grained Molecular Dynamics and the Atomic Limit of Finite Elements," *Physical Review B* 58 (1998): R5893–R5896.

32. V. A. Harmandaris, D. Reith, N. F. A. van der Vegt, and K. Kremer, "Comparison Between Coarse-Graining Models for Polymer Systems: Two Mapping Schemes for Polystyrene," *Macromolecular Chemistry and Physics* 208 (2007): 2109–2120.

33. T. Lemos, C. Abreu, and J. C. Pinto, "DPD Simulations of Homopolymer–Copolymer–Homopolymer Mixtures: Effects of Copolymer Structure and Concentration," *Macromolecular Theory and Simulations* 29 (2020): 2000014.

34. U. Frisch, B. Hasslacher, and Y. Pomeau, "Lattice-Gas Automata for the Navier-Stokes Equation," *Physical Review Letters* 56 (1986): 1505–1508.

35. L.-S. Luo, "The Future of Lattice-Gas and Lattice Boltzmann Methods," in *Computational Aerosciences in the 21st Century*, ed. M. D. Salas and W. K. Anderson (Springer, 2000), 165–187, https://doi.org/10.1007/978-94-010-0948-5_9.

36. D. D'humières and P. Lallemand, "Lattice Gas Automata for Fluid Mechanics," *Physica A: Statistical Mechanics and Its Applications* 140, no. 1-2 (1986): 326–335, https://doi.org/10.1016/0378-4371(86)90239-6.

37. J.-P. Boon, *Correlations and Connectivity: Geometric Aspects of Physics, Chemistry and Biology*, ed. H. E. Stanley and N. Ostrowsky (Springer, 1990), 56–65.

38. P. B. Warren, "Dissipative Particle Dynamics," *Current Opinion in Colloid & Interface Science* 3 (1998): 620–624.

39. M. O. Steinhauser and S. Hiermaier, "A Review of Computational Methods in Materials Science: Examples From Shock-Wave and Polymer Physics," *International Journal of Molecular Sciences* 10 (2009): 5135–5216.

40. A. J. C. Ladd, M. E. Colvin, and D. Frenkel, "Application of Lattice-Gas Cellular Automata to the Brownian Motion of Solids in Suspension," *Physical Review Letters* 60 (1988): 975–978.

41. J. M. V. A. Koelman, *Numerical Methods for the Simulation of Multi-Phase and Complex Flow* (Springer, 1992), 146–153.

42. U. Frisch, D. d'Humieres, B. Hasslacher, P. Lallemand, Y. Pomeau, and J. P. Rivet, *Lattice gas hydrodynamics in two and three dimensions*. Los Alamos National Lab. (LANL), Los Alamos, NM (United States); Observatoire de Nice, 06 (France); Ecole Normale Superieure, 75 - Paris (France), 1986.

43. D. C. Rapaport and E. Clementi, "Eddy Formation in Obstructed Fluid Flow: A Molecular-Dynamics Study," *Physical Review Letters* 57 (1986): 695–698.

44. X. Fan, N. Phan-Thien, S. Chen, X. Wu, and T. Yong Ng, "Simulating Flow of DNA Suspension Using Dissipative Particle Dynamics," *Physics of Fluids* 18 (2006): 063102.

45. S. Litvinov, M. Ellero, X. Hu, and N. A. Adams, "Smoothed Dissipative Particle Dynamics Model for Polymer Molecules in Suspension," *Physical Review. E, Statistical, Nonlinear, and Soft Matter Physics* 77 (2008): 066703.

46. V. Symeonidis, G. Em Karniadakis, and B. Caswell, "Dissipative Particle Dynamics Simulations of Polymer Chains: Scaling Laws and Shearing Response Compared to DNA Experiments," *Physical Review Letters* 95 (2005): 076001.

47. D. A. Fedosov, B. Caswell, S. Suresh, and G. E. Karniadakis, "Quantifying the Biophysical Characteristics of Plasmodium-Falciparum-Parasitized Red Blood Cells in Microcirculation," *PNAS* 108 (2011): 35–39.

48. D. A. Fedosov, B. Caswell, and G. E. Karniadakis, "A Multiscale Red Blood Cell Model With Accurate Mechanics, Rheology, and Dynamics," *Biophysical Journal* 98 (2010): 2215–2225.

49. Z. Li, G.-H. Hu, Z.-L. Wang, Y.-B. Ma, and Z.-W. Zhou, "Three Dimensional Flow Structures in a Moving Droplet on Substrate: A Dissipative Particle Dynamics Study," *Physics of Fluids* 25 (2013): 072103.

50. Z. Li, Y.-H. Tang, H. Lei, B. Caswell, and G. E. Karniadakis, "Energy-Conserving Dissipative Particle Dynamics With Temperature-Dependent Properties," *Journal of Computational Physics* 265 (2014): 113–127.

51. P. Lallemand and L.-S. Luo, "Theory of the Lattice Boltzmann Method: Dispersion, Dissipation, Isotropy, Galilean Invariance, and Stability," *Physical Review E* 61 (2000): 6546–6562.

52. A. G. Baydin, *Dissipative Particle Dynamics and Coarse-Graining: Review of Existing Techniques, Trials with Evolutionary Computation*, Master's Thesis (Department of Applied Physics, Chalmers University of Technology, 2008).

53. X. Shi and F. Tian, "Multiscale Modeling and Simulation of Nano-Carriers Delivery Through Biological Barriers—A Review," *Advanced Theory and Simulations* 2 (2019): 1800105.

54. V. V. Ginzburg, K. Chang, P. K. Jog, A. B. Argenton, and L. Rakesh, "Modeling the Interfacial Tension in Oil–Water–Nonionic Surfactant Mixtures Using Dissipative Particle Dynamics and Self-Consistent Field Theory," *Journal of Physical Chemistry. B* 115 (2011): 4654–4661.

55. F. Goujon, P. Malfreyt, and D. J. Tildesley, "Mesoscopic Simulation of Entanglements Using Dissipative Particle Dynamics: Application to Polymer Brushes," *Journal of Chemical Physics* 129 (2008): 034902.

56. T. W. Sirk, Y. R. Slizoberg, J. K. Brennan, M. Lisal, and J. W. Andzelm, "An Enhanced Entangled Polymer Model for Dissipative Particle Dynamics," *Journal of Chemical Physics* 136 (2012): 134903.

57. A. Karatrantos, N. Clarke, R. J. Composto, and K. I. Winey, "Topological Entanglement Length in Polymer Melts and Nanocomposites by a DPD Polymer Model," *Soft Matter* 9 (2013): 3877–3884.

58. X. Li, I. V. Pivkin, H. Liang, and G. E. Karniadakis, "Shape Transformations of Membrane Vesicles From Amphiphilic Triblock Copolymers: A Dissipative Particle Dynamics Simulation Study," *Macromolecules* 42 (2009): 3195–3200.

59. T. Yamamoto and Y. Tezuka, "Topological Polymer Chemistry: A Cyclic Approach Toward Novel Polymer Properties and Functions," *Polymer Chemistry* 2 (2011): 1930–1941.

60. J. C. Shillcock, "Spontaneous Vesicle Self-Assembly: A Mesoscopic View of Membrane Dynamics," *Langmuir* 28 (2012): 541–547.

61. R. D. Groot and T. J. Madden, "Dynamic Simulation of Diblock Copolymer Microphase Separation," *Journal of Chemical Physics* 108 (1998): 8713–8724.

62. B. Chen, K. Jerger, J. M. J. Fréchet, and F. C. Szoka, "The Influence of Polymer Topology on Pharmacokinetics: Differences Between Cyclic and Linear PEGylated Poly(Acrylic Acid) Comb Polymers," *Journal of Controlled Release* 140, no. 3 (2009): 203–209, https://doi.org/10.1016/j.jconrel.2009.05.021.

63. J.-B. Xu, H. Wu, D.-Y. Lu, X.-F. He, Y.-H. Zhao, and H. Wen, "Dissipative Particle Dynamics Simulation on the Meso-Scale Structure of Diblock Copolymer Under Cylindrical Confinement," *Molecular Simulation* 32 (2006): 357–362.

64. K. E. Novik and P. V. Coveney, "Using Dissipative Particle Dynamics to Model Binary Immiscible Fluids," *International Journal of Modern Physics C: Computational Physics and Physical Computation* 08 (1997): 909–918.

65. D. S. Marques, U. Vainio, N. M. Chaparro, et al., "Self-Assembly in Casting Solutions of Block Copolymer Membranes," *Soft Matter* 9 (2013): 5557–5564.

66. M. A. Horsch, Z. Zhang, C. R. Iacovella, and S. C. Glotzer, "Hydrodynamics and Microphase Ordering in Block Copolymers: Are Hydrodynamics Required for Ordered Phases With Periodicity in More Than One Dimension?," *Journal of Chemical Physics* 121 (2004): 11455–11462.

67. W. Jiang, J. Huang, Y. Wang, and M. Laradji, "Hydrodynamic Interaction in Polymer Solutions Simulated With Dissipative Particle Dynamics," *Journal of Chemical Physics* 126 (2007): 044901.

68. Y. Kong, C. W. Manke, W. G. Madden, and A. G. Schlijper, "Modeling the Rheology of Polymer Solutions by Dissipative Particle Dynamics," *Tribology Letters* 3 (1997): 133–138.

69. T. Zhao and X. Wang, "Solvent Effect on Phase Transition of Lyotropic Rigid-Chain Liquid Crystal Polymer Studied by Dissipative Particle Dynamics," *Journal of Chemical Physics* 138 (2013): 024910.

70. P. Espanol, *Handbook of Materials Modeling: Methods*, ed. S. Yip (Springer Netherlands, 2005), 2503–2512.

71. S.-F. Zhang, L. Sun, J.-B. Xu, H. Wu, and H. Wen, "Aggregate Structure in Heavy Crude Oil: Using a Dissipative Particle Dynamics Based Mesoscale Platform," *Energy & Fuels* 24, no. 8 (2010): 4312–4326, https://doi.org/10.1021/ef1003446.

72. P. Español and P. Warren, "Statistical Mechanics of Dissipative Particle Dynamics," *EPL* 30 (1995): 191–196.

73. R. D. Groot, "Mesoscopic Simulation of Polymer–Surfactant Aggregation," *Langmuir* 16 (2000): 7493–7502.

74. R. D. Groot, "Electrostatic Interactions in Dissipative Particle Dynamics—Simulation of Polyelectrolytes and Anionic Surfactants," *Journal of Chemical Physics* 118 (2003): 11265–11277.

75. J. M. V. A. Koelman and P. J. Hoogerbrugge, "Dynamic Simulations of Hard-Sphere Suspensions Under Steady Shear," *EPL* 21 (1993): 363–368.

76. Y. Jin, D. Guo, B. Li, et al., "Synthesis and Self-Assembly Behavior of Polyhedral Oligomeric Silsesquioxane-Based Triblock Copolymers in Selective Solvents by Dissipative Particle Dynamics Simulation," *Physical Chemistry Chemical Physics* 20 (2018): 4074–4082.

77. B. Zhou, W. Luo, J. Yang, et al., "Simulation of Dispersion and Alignment of Carbon Nanotubes in Polymer Flow Using Dissipative Particle Dynamics," *Computational Materials Science* 126 (2017): 35–42.

78. P. Meakin and Z. Xu, "Dissipative Particle Dynamics and Other Particle Methods for Multiphase Fluid Flow in Fractured and Porous Media," *Progress in Computational Fluid Dynamics* 9 (2009): 399–408.

79. V. Symeonidis, G. E. Karniadakis, and B. Caswell, "Schmidt Number Effects in Dissipative Particle Dynamics Simulation of Polymers," *Journal of Chemical Physics* 125 (2006): 184902.

80. H. Droghetti, I. Pagonabarraga, P. Carbone, P. Asinari, and D. Marchisio, "Dissipative Particle Dynamics Simulations of Tri-Block Co-Polymer and Water: Phase Diagram Validation and Microstructure Identification," *Journal of Chemical Physics* 149 (2018): 184903.

81. M. Doi, S. F. Edwards, and S. F. Edwards, *The Theory of Polymer Dynamics* (Clarendon Press, 1988).

82. C. Soto-Figueroa, L. Vicente, J.-M. Martínez-Magadán, and M.-R. Rodríguez-Hidalgo, "Self-Organization Process of Ordered Structures in Linear and Star Poly(Styrene)–Poly(Isoprene) Block Copolymers: Gaussian Models and Mesoscopic Parameters of Polymeric Systems," *Journal of Physical Chemistry. B* 111 (2007): 11756–11764.

83. G. R. Strobl, *The Physics of Polymers: Concepts for Understanding Their Structures and Behavior*, 3rd ed. (Springer-Verlag, 2007).

84. S. B. Kukadiya, P. K. Chan, and M. Mehrvar, "The Ludwig-Soret Effect on the Thermally Induced Phase Separation Process in Polymer Solutions: A Computational Study," *Macromolecular Theory and Simulations* 18 (2009): 97–107.

85. K.-W. D. Lee, P. K. Chan, and X. Feng, "A Computational Study Into Thermally Induced Phase Separation in Polymer Solutions Under a Temperature Gradient," *Macromolecular Theory and Simulations* 11 (2002): 996–1005.

86. W. Yave, A. Car, S. S. Funari, S. P. Nunes, and K.-V. Peinemann, "CO_2-Philic Polymer Membrane With Extremely High Separation Performance," *Macromolecules* 43 (2010): 326–333.

87. M. J. Ko, S. H. Kim, and W. H. Jo, "The Effects of Copolymer Architecture on Phase Separation Dynamics of Immiscible Homopolymer Blends in the Presence of Copolymer: A Monte Carlo Simulation," *Polymer* 41 (2000): 6387–6394.

88. A. Boromand, S. Jamali, and J. M. Maia, "Viscosity Measurement Techniques in Dissipative Particle Dynamics," *Computer Physics Communications* 196 (2015): 149–160.

89. J. Cheng, A. Vishnyakov, and A. V. Neimark, "Morphological Transformations in Polymer Brushes in Binary Mixtures: DPD Study," *Langmuir* 30 (2014): 12932–12940.

90. M. Jehser, G. Zifferer, and C. N. Likos, "Scaling and Interactions of Linear and Ring Polymer Brushes via DPD Simulations," *Polymers* 11, no. 3 (2019): 541, https://doi.org/10.3390/polym11030541.

91. F. Alvarez, E. A. Flores, L. V. Castro, J. G. Hernández, A. López, and F. Vázquez, "Dissipative Particle Dynamics (DPD) Study of Crude Oil–Water Emulsions in the Presence of a Functionalized Co-Polymer," *Energy & Fuels* 25 (2011): 562–567.

92. K. Shi, C. Lian, Z. Bai, S. Zhao, and H. Liu, "Dissipative Particle Dynamics Study of the Water/Benzene/Caprolactam System in the Absence or Presence of Non-ionic Surfactants," *Chemical Engineering Science* 122 (2015): 185–196.

93. T. D. Nguyen and S. J. Plimpton, "Accelerating Dissipative Particle Dynamics Simulations for Soft Matter Systems," *Computational Materials Science* 100 (2015): 173–180.

94. D. Broseta, G. H. Fredrickson, E. Helfand, and L. Leibler, "Molecular Weight and Polydispersity Effects at Polymer-Polymer Interfaces," *Macromolecules* 23 (1990): 132–139.

95. P. Español, "Hydrodynamics From Dissipative Particle Dynamics," *Physical Review E* 52 (1995): 1734–1742.

96. X. Yong and L. T. Zhang, "Thermostats and Thermostat Strategies for Molecular Dynamics Simulations of Nanofluidics," *Journal of Chemical Physics* 138 (2013): 084503.

97. S. D. Stoyanov and R. D. Groot, "From Molecular Dynamics to Hydrodynamics: A Novel Galilean Invariant Thermostat," *Journal of Chemical Physics* 122 (2005): 114112.

98. T. Soddemann, B. Dünweg, and K. Kremer, "Dissipative Particle Dynamics: A Useful Thermostat for Equilibrium and Nonequilibrium Molecular Dynamics Simulations," *Physical Review E* 68 (2003): 046702.

99. P. Español, "Dissipative Particle Dynamics With Energy Conservation," *EPL* 40 (1997): 631–636.

100. M. Ripoll, P. Español, and M. H. Ernst, "Dissipative Particle Dynamics With Energy Conservation: Heat Conduction," *International Journal of Modern Physics C: Computational Physics and Physical Computation* 09 (1998): 1329–1338.

101. R. Qiao and P. He, "Simulation of Heat Conduction in Nanocomposite Using Energy-Conserving Dissipative Particle Dynamics," *Molecular Simulation* 33 (2007): 677–683.

102. E. Abu-Nada, "Natural Convection Heat Transfer Simulation Using Energy Conservative Dissipative Particle Dynamics," *Physical Review E* 81 (2010): 056704.

103. P. He and R. Qiao, "Self-Consistent Fluctuating Hydrodynamics Simulations of Thermal Transport in Nanoparticle Suspensions," *Journal of Applied Physics* 103 (2008): 094305.

104. A. D. Mackie, J. B. Avalos, and V. Navas, "Dissipative Particle Dynamics With Energy Conservation: Modelling of Heat Flow," *Physical Chemistry Chemical Physics* 1, no. 9 (1999): 2039–2049, https://doi.org/10.1039/a809502g.

105. Y.-D. He, Y.-H. Tang, and X.-L. Wang, "Dissipative Particle Dynamics Simulation on the Membrane Formation of Polymer–Diluent System via Thermally Induced Phase Separation," *Journal of Membrane Science* 368 (2011): 78–85.

106. P. J. Flory, *Principles of Polymer Chemistry* (Cornell University Press, 1953).

107. A. Vishnyakov and A. V. Neimark, "Self-Assembly in Nafion Membranes Upon Hydration: Water Mobility and Adsorption Isotherms," *Journal of Physical Chemistry. B* 118 (2014): 11353–11364.

108. J. Yang, R. Wang, and D. Xie, "Aqueous Self-Assembly of Amphiphilic Cyclic Brush Block Copolymers as Asymmetry-Tunable Building Blocks," *Macromolecules* 52 (2019): 7042–7051.

109. L. Hao, L. Lin, and J. Zhou, "pH-Responsive Zwitterionic Copolymer DHA-PBLG-PCB for Targeted Drug Delivery: A Computer Simulation Study," *Langmuir* 35 (2019): 1944–1953.

110. H. Chen and E. Ruckenstein, "Formation of Complex Colloidal Particles: Morphologies and Mechanisms," *Soft Matter* 8 (2012): 8911–8916.

111. X. Cao, G. Xu, Y. Li, and Z. Zhang, "Aggregation of Poly(Ethylene Oxide)-poly(Propylene Oxide) Block Copolymers in Aqueous Solution: DPD Simulation Study," *Journal of Physical Chemistry. A* 109 (2005): 10418–10423.

112. K. P. Travis, M. Bankhead, K. Good, and S. L. Owens, "New Parametrization Method for Dissipative Particle Dynamics," *Journal of Chemical Physics* 127 (2007): 014109.

113. P. Nikunen, I. Vattulainen, and M. Karttunen, "Reptational Dynamics in Dissipative Particle Dynamics Simulations of Polymer Melts," *Physical Review E* 75 (2007): 036713.

114. I. V. Pivkin and G. E. Karniadakis, "Accurate Coarse-Grained Modeling of Red Blood Cells," *Physical Review Letters* 101 (2008): 118105.

115. G. Kacar and G. de With, "Hydrogen Bonding in DPD: Application to Low Molecular Weight Alcohol–Water Mixtures," *Physical Chemistry Chemical Physics* 18 (2016): 9554–9560.

116. G. Kacar and G. de With, "Parametrizing Hydrogen Bond Interactions in Dissipative Particle Dynamics Simulations: The Case of Water, Methanol and Their Binary Mixtures," *Journal of Molecular Liquids* 302 (2020): 112581.

117. G. Kacar, "Characterizing the Structure and Properties of Dry and Wet Polyethylene Glycol Using Multi-Scale Simulations," *Physical Chemistry Chemical Physics* 20 (2018): 12303–12311.

118. A. Vishnyakov, D. S. Talaga, and A. V. Neimark, "DPD Simulation of Protein Conformations: From α-Helices to β-Structures," *Journal of Physical Chemistry Letters* 3 (2012): 3081–3087.

119. G. Kacar, "Molecular Understanding of Interactions, Structure, and Drug Encapsulation Efficiency of Pluronic Micelles From Dissipative Particle Dynamics Simulations," *Colloid & Polymer Science* 297 (2019): 1037–1051.

120. J. C. Shillcock and R. Lipowsky, "Equilibrium Structure and Lateral Stress Distribution of Amphiphilic Bilayers From Dissipative Particle Dynamics Simulations," *Journal of Chemical Physics* 117 (2002): 5048–5061.

121. J. R. Spaeth, T. Dale, I. G. Kevrekidis, and A. Z. Panagiotopoulos, "Coarse-Graining of Chain Models in Dissipative Particle Dynamics Simulations," *Industrial and Engineering Chemistry Research* 50 (2011): 69–77.

122. A. G. Schlijper, P. J. Hoogerbrugge, and C. W. Manke, "Computer Simulation of Dilute Polymer Solutions With the Dissipative Particle Dynamics Method," *Journal of Rheology* 39 (1995): 567–579.

123. M. Langeloth, Y. Masubuchi, M. C. Böhm, and F. Müller-Plathe, "Recovering the Reptation Dynamics of Polymer Melts in Dissipative

Particle Dynamics Simulations via Slip-Springs," *Journal of Chemical Physics* 138 (2013): 104907.

124. Y. R. Sliozberg, J. L. Gair, and A. J. Hsieh, "Dissipative Particle Dynamics Simulation of Microphase Separation in Polyurethane Urea Nanocomposites," *Polymer* 193 (2020): 122339, https://doi.org/10.1016/j.polymer.2020.122339.

125. Y. R. Sliozberg, J. W. Andzelm, J. K. Brennan, M. R. Vanlandingham, V. Pryamitsyn, and V. Ganesan, "Modeling Viscoelastic Properties of Triblock Copolymers: A DPD Simulation Study," *Journal of Polymer Science, Part B: Polymer Physics* 48, no. 1 (2010): 15–25, https://doi.org/10.1002/polb.21839.

126. A. A. Gavrilov, Y. V. Kudryavtsev, P. G. Khalatur, and A. V. Chertovich, "Microphase Separation in Regular and Random copolymer Melts by DPD Simulations," *Chemical Physics Letters* 503 (2011): 277–282.

127. D.-W. Li, X. Y. Liu, and Y. P. Feng, "Bond-Angle-Potential-Dependent Dissipative Particle Dynamics Simulation and Lipid Inverted Phase," *Journal of Physical Chemistry. B* 108 (2004): 11206–11213.

128. S. Chakraborty and S. Roy, "Structure of Nanorod Assembly in the Gyroid Phase of Diblock Copolymer," *Journal of Physical Chemistry. B* 119 (2015): 6803–6812.

129. H.-J. Qian, L.-J. Chen, Z.-Y. Lu, Z.-S. Li, and C.-C. Sun, "The Dependence of Nanostructures on the Molecule Rigidity of A2 (B4) 2-Type Miktoarm Block Copolymer," *Journal of Chemical Physics* 124 (2006): 014903.

130. C. Chen, L. Zhuang, X. Li, J. Dong, and J. Lu, "A Many-Body Dissipative Particle Dynamics Study of Forced Water-Oil Displacement in Capillary," *Langmuir* 28 (2012): 1330–1336.

131. P. B. Warren, "Vapor-Liquid Coexistence in Many-Body Dissipative Particle Dynamics," *Physical Review E* 68 (2003): 066702.

132. I. Pagonabarraga and D. Frenkel, "Dissipative Particle Dynamics for Interacting Systems," *Journal of Chemical Physics* 115 (2001): 5015–5026.

133. S. Y. Trofimov, E. L. F. Nies, and M. A. J. Michels, "Thermodynamic Consistency in Dissipative Particle Dynamics Simulations of Strongly Nonideal Liquids and Liquid Mixtures," *Journal of Chemical Physics* 117 (2002): 9383–9394.

134. G. M. Whitesides and B. Grzybowski, "Self-Assembly at All Scales," *Science* 295 (2002): 2418–2421.

135. S. Zhang, "Fabrication of Novel Biomaterials Through Molecular Self-Assembly," *Nature Biotechnology* 21 (2003): 1171–1178.

136. V. Percec, D. A. Wilson, P. Leowanawat, et al., "Self-Assembly of Janus Dendrimers Into Uniform Dendrimersomes and Other Complex Architectures," *Science* 328 (2010): 1009–1014.

137. R. F. Service, "How Far Can We Push Chemical Self-Assembly?," *Science* 309, no. 95 (2005): 5731, https://doi.org/10.1126/science.309.5731.95.

138. D. J. Pochan, Z. Chen, H. Cui, K. Hales, K. Qi, and K. L. Wooley, "Toroidal Triblock Copolymer Assemblies," *Science* 306 (2004): 94–97.

139. Y.-Y. Won, H. T. Davis, and F. S. Bates, "Giant Wormlike Rubber Micelles," *Science* 283 (1999): 960–963.

140. S. Kubowicz, J.-F. Baussard, J.-F. Lutz, A. F. Thünemann, H. von Berlepsch, and A. Laschewsky, "Multicompartment Micelles Formed by Self-Assembly of Linear ABC Triblock Copolymers in Aqueous Medium," *Angewandte Chemie International Edition* 44 (2005): 5262–5265.

141. S. Javan Nikkhah, E. Turunen, A. Lepo, T. Ala-Nissila, and M. Sammalkorpi, "Multicore Assemblies from Three-Component Linear Homo-Copolymer Systems: A Coarse-Grained Modeling Study," *Polymers* 13 (2021): 2193.

142. S. Javan Nikkhah and M. Sammalkorpi, "Single Core and Multicore Aggregates From a Polymer Mixture: A Dissipative Particle Dynamics Study," *Journal of Colloid and Interface Science* 635 (2023): 231–241.

143. H. Engelkamp, S. Middelbeek, and R. J. M. Nolte, "Self-Assembly of Disk-Shaped Molecules to Coiled-Coil Aggregates With Tunable Helicity," *Science* 284, no. 5415 (1999): 785–788, https://doi.org/10.1126/science.284.5415.785.

144. M. D. Hollingsworth, "Crystal Engineering: From Structure to Function," *Science* 295 (2002): 2410–2413.

145. T. Scheibel, R. Parthasarathy, G. Sawicki, X.-M. Lin, H. Jaeger, and S. L. Lindquist, "Conducting Nanowires Built by Controlled Self-Assembly of Amyloid Fibers and Selective Metal Deposition," *PNAS* 100 (2003): 4527–4532.

146. S. I. Stupp, V. LeBonheur, K. Walker, et al., "Supramolecular Materials: Self-Organized Nanostructures," *Science* 276 (1997): 384–389.

147. S. A. Jenekhe and X. L. Chen, "Self-Assembly of Ordered Microporous Materials From Rod-Coil Block Copolymers," *Science* 283 (1999): 372–375.

148. R. Oda, I. Huc, M. Schmutz, S. J. Candau, and F. C. MacKintosh, "Tuning Bilayer Twist Using Chiral Counterions," *Nature* 399 (1999): 566–569.

149. G. C. L. Wong, J. X. Tang, A. Lin, Y. Li, P. A. Janmey, and C. R. Safinya, "Hierarchical Self-Assembly of F-Actin and Cationic Lipid Complexes: Stacked Three-Layer Tubule Networks," *Science* 288 (2000): 2035–2039.

150. W. J. Blau and A. J. Fleming, "Designer Nanotubes by Molecular Self-Assembly," *Science* 304 (2004): 1457–1458.

151. L. Zhang and A. Eisenberg, "Multiple Morphologies of 'Crew-Cut' Aggregates of Polystyrene-b-Poly(Acrylic Acid) Block Copolymers," *Science* 268 (1995): 1728–1731.

152. B. M. Discher, Y.-Y. Won, D. S. Ege, et al., "Polymersomes: Tough Vesicles Made From Diblock Copolymers," *Science* 284 (1999): 1143–1146.

153. D. E. Discher and A. Eisenberg, "Polymer Vesicles," *Science* 297 (2002): 967–973.

154. A. L. Harmat, S. Javan Nikkhah, and M. Sammalkorpi, "Dissipative Particle Dynamics Simulations of H-Shaped Diblock Copolymer Self-Assembly in Solvent," *Polymer* 233 (2021): 124198.

155. K. Ariga, M. Nishikawa, T. Mori, J. Takeya, L. K. Shrestha, and J. P. Hill, "Self-Assembly as a Key Player for Materials Nanoarchitectonics," *Science and Technology of Advanced Materials* 20 (2019): 51–95.

156. D. Chen, H. K. Y. Wu, S. Naderi-Gohar, Y. Wu, Y. Huang, and H.-Y. Nie, "An Extremely Rapid Dip-Coating Method for Self-Assembly of Octadecylphosphonic Acid and Its Thermal Stability on an Aluminum Film," *Journal of Materials Chemistry C* 2, no. 46 (2014): 9941–9948, https://doi.org/10.1039/C4TC02017K.

157. J. K. Lee, J. M. Link, J. C. Y. Hu, and K. A. Athanasiou, "The Self-Assembling Process and Applications in Tissue Engineering," *Cold Spring Harbor Perspectives in Medicine* 7, no. 11 (2017): a025668, https://doi.org/10.1101/cshperspect.a025668.

158. K. Jakab, F. Marga, C. Norotte, K. Murphy, G. Vunjak-Novakovic, and G. Forgacs, "Tissue Engineering by Self-Assembly and Bio-Printing of Living Cells," *Biofabrication* 2, no. 2 (2010): 022001, https://doi.org/10.1088/1758-5082/2/2/022001.

159. S. Yadav, A. K. Sharma, and P. Kumar, "Nanoscale Self-Assembly for Therapeutic Delivery," *Frontiers in Bioengineering and Biotechnology* 8 (2020): 127, https://doi.org/10.3389/fbioe.2020.00127.

160. S. Javan Nikkhah and D. Thompson, "Molecular Modelling Guided Modulation of Molecular Shape and Charge for Design of Smart Self-Assembled Polymeric Drug Transporters," *Pharmaceutics* 13 (2021): 141.

161. S. Javan Nikkhah and M. Vandichel, "Modeling Polyzwitterion-Based Drug Delivery Platforms: A Perspective of the Current State-of-the-Art and Beyond," *ACS Engineering Au* 2, no. 4 (2022): 274–294, https://doi.org/10.1021/acsengineeringau.2c00008.

162. S. Javan Nikkhah and D. Thompson, "Copolyelectrolyte-Based Nanocapsules for Oral Monoclonal Antibody Therapy: A Mesoscale Modeling Survey," *Biomacromolecules* 23 (2022): 3875–3886.

163. H. Tan, W. Wang, C. Yu, Y. Zhou, Z. Lu, and D. Yan, "Dissipative Particle Dynamics Simulation Study on Self-Assembly of Amphiphilic Hyperbranched Multiarm Copolymers With Different Degrees of Branching," *Soft Matter* 11 (2015): 8460–8470.

164. M. Singh, N. Kaur, and E. Comini, "The Role of Self-Assembled Monolayers in Electronic Devices," *Journal of Materials Chemistry C* 8 (2020): 3938–3955.

165. Q. Li, W. Yao, X. Yu, B. Zhang, J. Dong, and Y. Jin, "Drug-Loaded pH-Responsive Polymeric Micelles: Simulations and Experiments of Micelle Formation, Drug Loading and Drug Release," *Colloids and Surfaces B: Biointerfaces* 158 (2017): 709–716.

166. L. Wang, R. Xu, Z. Wang, and X. He, "Kinetics of Multicompartment Micelle Formation by Self-Assembly of ABC Miktoarm Star Terpolymer in Dilute Solution," *Soft Matter* 8 (2012): 11462–11470.

167. A. L. Z. Lee, S. Venkataraman, S. B. M. Sirat, S. Gao, J. L. Hedrick, and Y. Y. Yang, "The Use of Cholesterol-Containing Biodegradable Block Copolymers to Exploit Hydrophobic Interactions for the Delivery of Anticancer Drugs," *Biomaterials* 33 (2012): 1921–1928.

168. A. J. Sawdon and C.-A. Peng, "Polymeric Micelles for Acyclovir Drug Delivery," *Colloids and Surfaces B: Biointerfaces* 122 (2014): 738–745.

169. Y. Wang, D. D. Zhu, J. Zhou, et al., "Mesoscopic Simulation Studies on the Formation Mechanism of Drug Loaded Polymeric Micelles," *Colloids and Surfaces B: Biointerfaces* 136 (2015): 536–544.

170. J. Yu, X. Li, Y. Luo, W. Lu, J. Huang, and S. Liu, "Poly(Ethylene Glycol) Shell-Sheddable Magnetic Nanomicelle as the Carrier of Doxorubicin With Enhanced Cellular Uptake," *Colloids and Surfaces B: Biointerfaces* 107 (2013): 213–219.

171. H. Zhang, K. Wang, P. Zhang, W. He, A. Song, and Y. Luan, "Redox-Sensitive Micelles Assembled From Amphiphilic mPEG-PCL-SS-DTX Conjugates for the Delivery of Docetaxel," *Colloids and Surfaces B: Biointerfaces* 142 (2016): 89–97.

172. M. Huo, Y. Liu, L. Wang, et al., "Redox-Sensitive Micelles Based onO,N-Hydroxyethyl Chitosan–Octylamine Conjugates for Triggered Intracellular Delivery of Paclitaxel," *Molecular Pharmaceutics* 13 (2016): 1750–1762.

173. Y. Huang, R. Dong, X. Zhu, and D. Yan, "Photo-Responsive Polymeric Micelles," *Soft Matter* 10 (2014): 6121–6138.

174. J. Akimoto, M. Nakayama, and T. Okano, "Temperature-Responsive Polymeric Micelles for Optimizing Drug Targeting to Solid Tumors," *Journal of Controlled Release* 193 (2014): 2–8.

175. S. Zheng, Z. Jin, J. Han, et al., "Preparation of HIFU-Triggered Tumor-Targeted Hyaluronic Acid Micelles for Controlled Drug Release and Enhanced Cellular Uptake," *Colloids and Surfaces B: Biointerfaces* 143 (2016): 27–36.

176. X. Chen, L. Tai, J. Gao, et al., "A Stapled Peptide Antagonist of MDM2 Carried by Polymeric Micelles Sensitizes Glioblastoma to Temozolomide Treatment Through p53 Activation," *Journal of Controlled Release* 218 (2015): 29–35.

177. Z. M. Wu, X. D. Guo, L. J. Zhang, et al., "Solvent Mediated Microstructures and Release Behavior of Insulin From pH-Sensitive Nanoparticles," *Colloids and Surfaces B: Biointerfaces* 94 (2012): 206–212.

178. X. D. Guo, J. P. K. Tan, S. H. Kim, et al., "Computational Studies on Self-Assembled Paclitaxel Structures: Templates for Hierarchical Block Copolymer Assemblies and Sustained Drug Release," *Biomaterials* 30, no. 33 (2009): 6556–6563, https://doi.org/10.1016/j.biomaterials.2009.08.022.

179. L. He, L. Zhang, and H. Liang, "The Effects of Nanoparticles on the Lamellar Phase Separation of Diblock Copolymers," *Journal of Physical Chemistry. B* 112 (2008): 4194–4203.

180. Y. Nie, H. Gao, M. Yu, Z. Hu, G. Reiter, and W. Hu, "Competition of Crystal Nucleation to Fabricate the Oriented Semi-Crystalline Polymers," *Polymer* 54 (2013): 3402–3407.

181. K. Šindelka, Z. Limpouchová, M. Lísal, and K. Procházka, "Dissipative Particle Dynamics Study of Electrostatic Self-Assembly in Aqueous Mixtures of Copolymers Containing One Neutral Water-Soluble Block and One Either Positively or Negatively Charged Polyelectrolyte Block," *Macromolecules* 47 (2014): 6121–6134.

182. S. Y. Nie, Y. Sun, W. J. Lin, et al., "Dissipative Particle Dynamics Studies of Doxorubicin-Loaded Micelles Assembled From Four-Arm Star Triblock Polymers 4AS-PCL-b-PDEAEMA-b-PPEGMA and Their pH-Release Mechanism," *Journal of Physical Chemistry. B* 117 (2013): 13688–13697.

183. Z. Chen, X. Wang, L. Zhang, and L. He, "Vesicles From the Self-Assembly of Coil–Rod–Coil Triblock Copolymers in Selective Solvents," *Polymer* 55 (2014): 2921–2927.

184. Y. Liu, Y. Li, J. He, K. J. Duelge, Z. Lu, and Z. Nie, "Entropy-Driven Pattern Formation of Hybrid Vesicular Assemblies Made From Molecular and Nanoparticle Amphiphiles," *Journal of the American Chemical Society* 136 (2014): 2602–2610.

185. D. Liu and C. Zhong, "Multicompartment Micelles Formed From Star-Dendritic Triblock Copolymers in Selective Solvents: A Dissipative Particle Dynamics Study," *Polymer* 49 (2008): 1407–1413.

186. S. Javan Nikkhah, P. A. Cazade, J. J. McManus, and D. Thompson, "Design Rules for Antibody Delivery by Self-Assembled Block-Copolyelectrolyte Nanocapsules," *Macromolecules* 55, no. 7 (2022): 2383–2397, https://doi.org/10.1021/acs.macromol.2c00118.

187. G. Riess, "Micellization of Block Copolymers," *Progress in Polymer Science* 28 (2003): 1107–1170.

188. Z. Li and E. E. Dormidontova, "Kinetics of Diblock Copolymer Micellization by Dissipative Particle Dynamics," *Macromolecules* 43 (2010): 3521–3531.

189. S. Tao, Y. Chu, Z. Wang, X. Xu, and Q. Tan, "Morphological Transition of Amphiphilic Block Copolymer/PEGylated Phospholipid Complexes Induced by the Dynamic Subtle Balance Interactions in the Self-Assembled Aggregates," *E-Polymers* 20, no. 1 (2020): 242–253, https://doi.org/10.1515/epoly-2020-0018.

190. A. Maiti and S. McGrother, "Bead-Bead Interaction Parameters in Dissipative Particle Dynamics: Relation to Bead-Size, Solubility Parameter, and Surface Tension," *Journal of Chemical Physics* 120 (2004): 1594–1601.

191. W. Min, D. Zhao, X. Quan, D. Sun, L. Li, and J. Zhou, "Computer Simulations on the pH-Sensitive Tri-Block Copolymer Containing Zwitterionic Sulfobetaine as a Novel Anti-Cancer Drug Carrier," *Colloids and Surfaces B: Biointerfaces* 152 (2017): 260–268.

192. Z. Luo, Y. Li, B. Wang, and J. Jiang, "pH-Sensitive Vesicles Formed by Amphiphilic Grafted Copolymers With Tunable Membrane Permeability for Drug Loading/Release: A Multiscale Simulation Study," *Macromolecules* 49 (2016): 6084–6094.

193. X. D. Guo, J. P. K. Tan, L. J. Zhang, et al., "Phase Behavior Study of Paclitaxel Loaded Amphiphilic Copolymer in Two Solvents by Dissipative Particle Dynamics Simulations," *Chemical Physics Letters* 473 (2009): 336–342.

194. Z. Luo and J. Jiang, "pH-Sensitive Drug Loading/Releasing in Amphiphilic Copolymer PAE-PEG: Integrating Molecular Dynamics and Dissipative Particle Dynamics Simulations," *Journal of Controlled Release* 162 (2012): 185–193.

195. X. Wang, J. Gao, Z. Wang, et al., "Dissipative Particle Dynamics Simulation on the Self-Assembly and Disassembly of pH-Sensitive Polymeric Micelle With Coating Repair Agent," *Chemical Physics Letters* 685 (2017): 328–337.

196. Y. Mai and A. Eisenberg, "Self-Assembly of Block Copolymers," *Chemical Society Reviews* 41 (2012): 5969–5985.

197. X. Huang and B. Voit, "Progress on Multi-Compartment Polymeric Capsules," *Polymer Chemistry* 4 (2013): 435–443.

198. A. O. Moughton, M. A. Hillmyer, and T. P. Lodge, "Multicompartment Block Polymer Micelles," *Macromolecules* 45 (2012): 2–19.

199. Z. Wang, J. Gao, V. Ustach, et al., "Tunable Permeability of Cross-Linked Microcapsules From pH-Responsive Amphiphilic Diblock Copolymers: A Dissipative Particle Dynamics Study," *Langmuir* 33 (2017): 7288–7297.

200. Y. Li, M. Leng, M. Cai, L. Huang, Y. Chen, and X. Luo, "pH Responsive Micelles Based on Copolymers mPEG-PCL-PDEA: The Relationship Between Composition and Properties," *Colloids and Surfaces B: Biointerfaces* 154 (2017): 397–407.

201. Y. Zhao, L.-Y. You, Z.-Y. Lu, and C.-C. Sun, "Dissipative Particle Dynamics Study on the Multicompartment Micelles Self-Assembled From the Mixture of Diblock Copolymer Poly(Ethyl Ethylene)-block-Poly(Ethylene Oxide) and Homopolymer Poly(Propylene Oxide) in Aqueous Solution," *Polymer* 50 (2009): 5333–5340.

202. M. del Rodríguez-Hidalgo, C. Soto-Figueroa, and L. Vicente, "Identification of Micellar Stability Zones and Structural Inversion Process of Thermoresponsive Polymeric Micelles by Dissipative Particle Dynamics Simulations," *Molecular Physics* 114 (2016): 608–617.

203. S. Ma, M. Xiao, and R. Wang, "Formation and Structural Characteristics of Thermosensitive Multiblock Copolymer Vesicles," *Langmuir* 29 (2013): 16010–16017.

204. M. Chen, M. Sun, and X. Liu, "Core-Corona Micelles Formed by Self-Assembly of Random Copolymer and Homopolymer Mixtures: Dissipative Particle Dynamics Simulations," *Journal of Dispersion Science and Technology* 37 (2016): 625–632.

205. M. Chen, M. Sun, and X. Liu, "Dissipative Particle Dynamics Simulations on the Self-Assembly of New Segmented Random-Block Copolymers in Selective Solvents," *Journal of Dispersion Science and Technology* 37 (2016): 900–907.

206. S. Li, Q. Xu, K. Li, Y. Wang, C. Yu, and Y. Zhou, "Multigeometry Nanoparticles From the Orthogonal Self-Assembly of Block Alternating Copolymers via Simulation," *Journal of Physical Chemistry. B* 123 (2019): 8333–8340.

207. M. Liao, H. Liu, H. Guo, and J. Zhou, "Mesoscopic Structures of Poly(Carboxybetaine) Block Copolymer and Poly(Ethylene Glycol) Block Copolymer in Solutions," *Langmuir* 33 (2017): 7575–7582.

208. Z. Wang, S. Sun, C. Li, S. Hu, and R. Faller, "Controllable Multicompartment Morphologies From Cooperative Self-Assembly of Copolymer–Copolymer Blends," *Soft Matter* 13 (2017): 5877–5887.

209. N. Arai, K. Yasuoka, and X. C. Zeng, "Self-Assembly of Janus Oligomers Into Onion-Like Vesicles With Layer-By-Layer Water Discharging Capability: A Minimalist Model," *ACS Nano* 10 (2016): 8026–8037.

210. M. Wang, S. Pei, T. Fang, Y. Yan, J. Xu, and J. Zhang, "Dissipative Particle Dynamics Simulation on Vesicles Self-Assembly Controlled by Terminal Groups," *Journal of Physical Chemistry. B* 122 (2018): 10607–10614.

211. P. M. Vlahovska, T. Podgorski, and C. Misbah, "Vesicles and Red Blood Cells in Flow: From Individual Dynamics to Rheology," *Comptes Rendus Physique* 10 (2009): 775–789.

212. K. Tsubota, S. Wada, and H. Liu, "Elastic Behavior of a Red Blood Cell With the membrane's Nonuniform Natural State: Equilibrium Shape, Motion Transition Under Shear Flow, and Elongation During Tank-Treading Motion," *Biomechanics and Modeling in Mechanobiology* 13 (2014): 735–746.

213. J. Mai, D. Sun, L. Li, and J. Zhou, "Phase Behavior of an Amphiphilic Block Copolymer in Ionic Liquid: A Dissipative Particle Dynamics Study," *Journal of Chemical & Engineering Data* 61 (2016): 3998–4005.

214. L. Meli and T. P. Lodge, "Equilibrium vs Metastability: High-Temperature Annealing of Spherical Block Copolymer Micelles in an Ionic Liquid," *Macromolecules* 42 (2009): 580–583.

215. A. C. Miller, A. Bershteyn, W. Tan, P. T. Hammond, R. E. Cohen, and D. J. Irvine, "Block Copolymer Micelles as Nanocontainers for Controlled Release of Proteins From Biocompatible Oil Phases," *Biomacromolecules* 10 (2009): 732–741.

216. Y. He and T. P. Lodge, "The Micellar Shuttle: Thermoreversible, Intact Transfer of Block Copolymer Micelles Between an Ionic Liquid and Water," *Journal of the American Chemical Society* 128 (2006): 12666–12667.

217. C. Soto-Figueroa, M. d. R. Rodríguez-Hidalgo, and L. Vicente, "Dissipative Particle Dynamics Simulation of the Micellization–Demicellization Process and Micellar Shuttle of a Diblock Copolymer in a Biphasic System (Water/Ionic-Liquid)," *Soft Matter* 8, no. 6 (2012): 1871–1877, https://doi.org/10.1039/C1SM07037A.

218. W. Wu, P. Yi, J. Zhang, et al., "4/6-Herto-Arm and 4/6-Mikto-Arm Star-Shaped Block Polymeric Drug-Loaded Micelles and Their pH-Responsive Controlled Release Properties: A Dissipative Particle Dynamics Simulation," *Physical Chemistry Chemical Physics* 21 (2019): 15222–15232.

219. H. Chen and E. Ruckenstein, "Formation and Degradation of Multicomponent Multicore Micelles: Insights From Dissipative Particle Dynamics Simulations," *Langmuir* 29 (2013): 5428–5434.

220. J. Xin, D. Liu, and C. Zhong, "Multicompartment Micelles From Star and Linear Triblock Copolymer Blends," *Journal of Physical Chemistry. B* 111 (2007): 13675–13682.

221. Y.-J. Sheng, C.-H. Nung, and H.-K. Tsao, "Morphologies of Star-Block Copolymers in Dilute Solutions," *Journal of Physical Chemistry. B* 110 (2006): 21643–21650.

222. J. J. K. Kirkensgaard, "Systematic Progressions of Core-Shell Polygon Containing Tiling Patterns in Melts of 2nd Generation Dendritic Miktoarm Star Copolymers," *Soft Matter* 7 (2011): 10756–10762.

223. Y. Wang, B. Li, H. Jin, Y. Zhou, Z. Lu, and D. Yan, "Dissipative Particle Dynamics Simulation Study on Vesicles Self-Assembled From Amphiphilic Hyperbranched Multiarm Copolymers," *Chemistry – An Asian Journal* 9, no. 8 (2014): 2281–2288, https://doi.org/10.1002/asia.201402146.

224. H. Tan, C. Yu, Z. Lu, Y. Zhou, and D. Yan, "A Dissipative Particle Dynamics Simulation Study on Phase Diagrams for the Self-Assembly of Amphiphilic Hyperbranched Multiarm Copolymers in Various Solvents," *Soft Matter* 13 (2017): 6178–6188.

225. Y. Wang, B. Li, Y. Zhou, Z. Lu, and D. Yan, "Dissipative Particle Dynamics Simulation Study on the Mechanisms of Self-Assembly of Large Multimolecular Micelles From Amphiphilic Dendritic Multiarm Copolymers," *Soft Matter* 9 (2013): 3293–3304.

226. C. Yu, L. Ma, K. Li, et al., "Computer Simulation Studies on the pH-Responsive Self-Assembly of Amphiphilic Carboxy-Terminated Polyester Dendrimers in Aqueous Solution," *Langmuir* 33 (2017): 388–399.

227. S. Y. Nie, W. J. Lin, N. Yao, X. D. Guo, and L. J. Zhang, "Drug Release From pH-Sensitive Polymeric Micelles With Different Drug Distributions: Insight From Coarse-Grained Simulations," *ACS Applied Materials & Interfaces* 6, no. 20 (2014): 17668–17678, https://doi.org/10.1021/am503920m.

228. Y.-L. Lin, H.-Y. Chang, Y.-J. Sheng, and H.-K. Tsao, "Photoresponsive Polymersomes Formed by Amphiphilic Linear–Dendritic Block Copolymers: Generation-Dependent Aggregation Behavior," *Macromolecules* 45 (2012): 7143–7156.

229. Y.-T. Liu, Y.-R. Li, and X. Wang, "Dynamic Evolution of a Vesicle Formed by Comb-Like Block Copolymer-Tethered Nanoparticles: A Dissipative Particle Dynamics Simulation Study," *Physical Chemistry Chemical Physics* 19 (2017): 27313–27319.

230. H.-Y. Chang, Y.-L. Lin, Y.-J. Sheng, and H.-K. Tsao, "Multilayered Polymersome Formed by Amphiphilic Asymmetric Macromolecular Brushes," *Macromolecules* 45 (2012): 4778–4789.

231. H.-J. Qian, Z.-Y. Lu, L.-J. Chen, Z.-S. Li, and C.-C. Sun, "Computer Simulation of Cyclic Block Copolymer Microphase Separation," *Macromolecules* 38 (2005): 1395–1401.

232. Y. Xu, J. Feng, H. Liu, and Y. H, "Microphase Separation of Graft-Diblock Copolymer by Dissipative Particle Dynamics Simulation," *Molecular Simulation* 34, no. 5 (2008): 559–565, https://doi.org/10.1080/08927020801930570.

233. A. Prhashanna and E. E. Dormidontova, "Micelle Self-Assembly and Chain Exchange Kinetics of Tadpole Block Copolymers With a Cyclic Corona Block," *Macromolecules* 53 (2020): 982–991.

234. S. Zhang, X. Cheng, J. Wang, Z. Zhang, W. Zhang, and X. Zhu, "Synthesis of a Cyclic-Brush Polymer With a High Grafting Density Using Activated Ester Chemistryviathe "Grafting Onto" Approach," *Polymer Chemistry* 9 (2018): 5155–5163.

235. X.-Y. Tu, C. Meng, Y.-F. Wang, et al., "Fabrication of Thermosensitive Cyclic Brush Copolymer with Enhanced Therapeutic Efficacy for Anticancer Drug Delivery," *Macromolecular Rapid Communications* 39 (2018): 1700744.

236. M. Romio, L. Trachsel, G. Morgese, S. N. Ramakrishna, N. D. Spencer, and E. M. Benetti, "Topological Polymer Chemistry Enters Materials Science: Expanding the Applicability of Cyclic Polymers," *ACS Macro Letters* 9 (2020): 1024–1033.

237. B. Golba, E. M. Benetti, and B. G. De Geest, "Biomaterials Applications of Cyclic Polymers," *Biomaterials* 267 (2021): 120468.

238. C. Tschierske, "Liquid Crystal Engineering – New Complex Mesophase Structures and Their Relations to Polymer Morphologies, Nanoscale Patterning and Crystal Engineering," *Chemical Society Reviews* 36 (2007): 1930–1970.

239. V. J. Haaren and D. J. Broer, "In Search of the Perfect Image," *Chemistry and Industry* 24 (1998): 1017–1021.

240. N. Mohieddin Abukhdeir and A. D. Rey, "Edge Dislocation Core Structure in Lamellar Smectic-A Liquid Crystals," *Soft Matter* 6 (2010): 1117–1120.

241. X. Liu, K. Yang, and H. Guo, "Dissipative Particle Dynamics Simulation of the Phase Behavior of T-Shaped Ternary Amphiphiles Possessing Rodlike Mesogens," *Journal of Physical Chemistry. B* 117 (2013): 9106–9120.

242. H. Chen and E. Ruckenstein, "Self-Assembly of π-Shaped Copolymers," *Soft Matter* 8 (2012): 1327–1333.

243. C. Wang, S. Ma, Y. Hu, and R. Wang, "Hierarchical Colloidal Polymeric Structure From Surfactant-Like Amphiphiles in Selective Solvents," *Langmuir* 33 (2017): 3427–3433.

244. S. Ma, Y. Hu, and R. Wang, "Self-Assembly of Polymer Tethered Molecular Nanoparticle Shape Amphiphiles in Selective Solvents," *Macromolecules* 48 (2015): 3112–3120.

245. X. Li, F. Huang, T. Jiang, X. He, S. Lin, and J. Lin, "Phase Behaviors of Side Chain Liquid Crystalline Block Copolymers," *RSC Advances* 5 (2014): 1514–1521.

246. M. Gong, Q. Yu, S. Ma, F. Luo, R. Wang, and D. Chen, "Self-Assembly Behavior of Triphenylene-Based Side-Chain Discotic Liquid Crystalline Polymers," *Macromolecules* 50 (2017): 5556–5564.

247. J. Huang and Y. Wang, "Control of Aggregation of Nanoparticles by Double-Hydrophilic Block Copolymers: A Dissipative Particle Dynamics Study," *Journal of Physical Chemistry. B* 111 (2007): 7735–7741.

248. B.-S. Kim and T. A. Taton, "Multicomponent Nanoparticles via Self-Assembly With Cross-Linked Block Copolymer Surfactants," *Langmuir* 23 (2007): 2198–2202.

249. E.-Q. Song, G.-P. Wang, H.-Y. Xie, et al., "Visual Recognition and Efficient Isolation of Apoptotic Cells With Fluorescent-Magnetic-Biotargeting Multifunctional Nanospheres," *Clinical Chemistry* 53 (2007): 2177–2185.

250. S. J. Rosenthal, I. Tomlinson, E. M. Adkins, et al., "Targeting Cell Surface Receptors With Ligand-Conjugated Nanocrystals," *Journal of the American Chemical Society* 124 (2002): 4586–4594.

251. J. O. Winter, T. Y. Liu, B. A. Korgel, and C. E. Schmidt, "Recognition Molecule Directed Interfacing Between Semiconductor Quantum Dots and Nerve Cells," *Advanced Materials* 13 (2001): 1673–1677.

252. Z. Liu, W. Cai, L. He, et al., "In Vivo Biodistribution and Highly Efficient Tumour Targeting of Carbon Nanotubes in Mice," *Nature Nanotechnology* 2 (2007): 47–52.

253. N. Nasongkla, E. Bey, J. Ren, et al., "Multifunctional Polymeric Micelles as Cancer-Targeted, MRI-Ultrasensitive Drug Delivery Systems," *Nano Letters* 6 (2006): 2427–2430.

254. P. Pi, D. Qin, J. Lan, et al., "Dissipative Particle Dynamics Simulation on the Nanocomposite Delivery System of Quantum Dots and Poly(Styrene-b-Ethylene Oxide) Copolymer," *Industrial and Engineering Chemistry Research* 54 (2015): 6123–6134.

255. K. Hpone Myint, J. R. Brown, A. R. Shim, B. E. Wyslouzil, and L. M. Hall, "Encapsulation of Nanoparticles During Polymer Micelle Formation: A Dissipative Particle Dynamics Study," *Journal of Physical Chemistry. B* 120 (2016): 11582–11594.

256. S. Ma, Y. Hu, and R. Wang, "Amphiphilic Block Copolymer Aided Design of Hybrid Assemblies of Nanoparticles: Nanowire, Nanoring, and Nanocluster," *Macromolecules* 49 (2016): 3535–3541.

257. N. Yan, Y. Zhu, and W. Jiang, "Self-Assembly of ABC Triblock Copolymers Under 3D Soft Confinement: A Monte Carlo Study," *Soft Matter* 12 (2016): 965–972.

258. H. H. Pham, I. Gourevich, J. K. Oh, J. E. N. Jonkman, and E. Kumacheva, "A Multidye Nanostructured Material for Optical Data Storage and Security Data Encryption," *Advanced Materials* 16 (2004): 516–520.

259. J. Y. Cheng, C. A. Ross, H. I. Smith, and E. L. Thomas, "Templated Self-Assembly of Block Copolymers: Top-Down Helps Bottom-Up," *Advanced Materials* 18 (2006): 2505–2521.

260. P. Petrus, M. Lísal, and J. K. Brennan, "Self-Assembly of Lamellar- and Cylinder-Forming Diblock Copolymers in Planar Slits: Insight From Dissipative Particle Dynamics Simulations," *Langmuir* 26 (2010): 14680–14693.

261. A. Nikoubashman, R. A. Register, and A. Z. Panagiotopoulos, "Self-Assembly of Cylinder-Forming Diblock Copolymer Thin Films," *Macromolecules* 46 (2013): 6651–6658.

262. J. Feng, H. Liu, and Y. Hu, "Micro-Phase Separation of Diblock Copolymer in a Nanosphere: Dissipative Particle Dynamics Approach," *Fluid Phase Equilibria* 261 (2007): 50–57.

263. C. Sanchez, H. Arribart, and M. M. Giraud Guille, "Biomimetism and Bioinspiration as Tools for the Design of Innovative Materials and Systems," *Nature Materials* 4 (2005): 277–288.

264. N. Zhang, S. Yang, L. Xiong, Y. Hong, and Y. Chen, "Nanoscale Toughening Mechanism of Nacre Tablet," *Journal of the Mechanical Behavior of Biomedical Materials* 53 (2016): 200–209.

265. D. J. Responte, R. M. Natoli, and K. A. Athanasiou, "Collagens of Articular Cartilage: Structure, Function, and Importance in Tissue Engineering," *Critical Reviews in Biomedical Engineering* 35, no. 5 (2007): 363–411, https://doi.org/10.1615/CritRevBiomedEng.v35.i5.20.

266. C. Sanchez, C. Boissière, D. Grosso, C. Laberty, and L. Nicole, "Design, Synthesis, and Properties of Inorganic and Hybrid Thin Films Having Periodically Organized Nanoporosity," *Chemistry of Materials* 20 (2008): 682–737.

267. Z. Ma, H. Yu, and W. Jiang, "Bump-Surface Multicompartment Micelles From a Linear ABC Triblock Copolymer: A Combination Study by Experiment and Computer Simulation," *Journal of Physical Chemistry. B* 113 (2009): 3333–3338.

268. C. Park, J. Yoon, and E. L. Thomas, "Enabling Nanotechnology With Self Assembled Block Copolymer Patterns," *Polymer* 44 (2003): 6725–6760.

269. N. Koneripalli, N. Singh, R. Levicky, F. S. Bates, P. D. Gallagher, and S. K. Satija, "Confined Block Copolymer Thin Films," *Macromolecules* 28 (1995): 2897–2904.

270. E. Huang, T. P. Russell, C. Harrison, et al., "Using Surface Active Random Copolymers to Control the Domain Orientation in Diblock Copolymer Thin Films," *Macromolecules* 31 (1998): 7641–7650.

271. T. P. Russell, A. Menelle, S. H. Anastasiadis, S. K. Satija, and C. F. Majkrzak, "Unconventional Morphologies of Symmetric, Diblock Copolymers due to Film Thickness Constraints," *Macromolecules* 24 (1991): 6263–6269.

272. X. Zhang, L. Wang, L. Zhang, J. Lin, and T. Jiang, "Controllable Hierarchical Microstructures Self-Assembled From Multiblock Copolymers Confined in Thin Films," *Langmuir* 31 (2015): 2533–2544.

273. S. Rasouli, M. R. Moghbeli, and S. J. Nikkhah, "A Comprehensive Molecular Dynamics Study of a Single Polystyrene Chain in a Good Solvent," *Current Applied Physics* 18 (2018): 68–78.

274. S. Rasouli, M. R. Moghbeli, and S. J. Nikkhah, "A Deep Insight Into the Polystyrene Chain in Cyclohexane at Theta Temperature: Molecular Dynamics Simulation and Quantum Chemical Calculations," *Journal of Molecular Modeling* 25 (2019): 195.

275. S. Rasouli, M. R. Moghbeli, and S. J. Nikkhah, "Molecular Dynamics Simulation of Polystyrene Copolymer With Octyl Short-Chain Branches in Toluene," *Journal of Molecular Modeling* 26 (2020): 80.

276. X. Yong, "Hydrodynamic Interactions and Entanglements of Polymer Solutions in Many-Body Dissipative Particle Dynamics," *Polymers* 8 (2016): 426.

277. R. Wang and Z.-G. Wang, "Theory of Polymer Chains in Poor Solvent: Single-Chain Structure, Solution Thermodynamics, and Θ Point," *Macromolecules* 47 (2014): 4094–4102.

278. *Introduction to Physical Polymer Science* (John Wiley & Sons, Ltd, 2005), 71–143.

279. "Polymer Solutions," https://www.wiley.com/en-us/Polymer+Solutions%3A+An+Introduction+to+Physical+Properties-p-9780471389293.

280. D. W. Schubert, "Novel Theoretical Self-Consistent Mean-Field Approach to Describe the Conductivity of Carbon Fiber-Filled Thermoplastics: Part III—Application of the Concept to Mechanical Properties of Composites and Polymer Solutions," *Advanced Engineering Materials* 22 (2020): 2000171.

281. T. Zhao and X. Wang, "Diffusion of Rigid Rodlike Polymer in Isotropic Solutions Studied by Dissipative Particle Dynamics Simulation," *Polymer* 54 (2013): 5241–5249.

282. I. L. Shulgin and E. Ruckenstein, "The Kirkwood–Buff Theory of Solutions and the Local Composition of Liquid Mixtures," *Journal of Physical Chemistry. B* 110 (2006): 12707–12713.

283. J. G. Kirkwood, "Theory of Liquids," https://www.abebooks.com/Theory-Liquids-Kirkwood-J-G-Routledge/30580877791/bd.

284. Y.-H. Wu, D.-M. Wang, and J.-Y. Lai, "Effects of Polymer Chain Length and Stiffness on Phase Separation Dynamics of Semidilute Polymer Solution," *Journal of Physical Chemistry. B* 112 (2008): 4604–4612.

285. M. Rubinstein and R. H. Colby, *Polymer Physics* (Oxford University Press, 2003).

286. Z. Dai and C. Wu, "Internal Motions of Linear Chains and Spherical Microgels in Θ and Poor Solvents," *Macromolecules* 43 (2010): 10064–10070.

287. Z. Dai, T. Ngai, and C. Wu, "Internal Motions of Linear Chains and Spherical Microgels in Dilute Solution," *Soft Matter* 7 (2011): 4111–4121.

288. Y. Liu, Y. Dai, and X. Xu, "Dynamic Feature of Incipient Polymer Collapse Below the Theta Point," *Journal of Physical Chemistry. B* 121 (2017): 9469–9475.

289. J.-J. Wang, Z.-Z. Li, X.-P. Gu, L.-F. Feng, C.-L. Zhang, and G.-H. Hu, "A Dissipative Particle Dynamics Study on the Compatibilizing Process of Immiscible Polymer Blends With Graft Copolymers," *Polymer* 53 (2012): 4448–4454.

290. I. Khan, M. Mansha, and M. A. J. Mazumder, *Functional Polymers*, ed. M. A. J. Mazumder, H. Sheardown, and A. Al-Ahmed (Springer International Publishing, 2019), 513–549.

291. J. Parameswaranpillai, S. Thomas, and Y. Grohens, *Characterization of Polymer Blends* (John Wiley & Sons, Ltd, 2014), 1–6.

292. D. R. Paul and L. H. Sperling, eds., *Multicomponent Polymer Materials*, vol. 211 (American Chemical Society, 1985).

293. T. Li, V. A. Topolkaraev, A. Hiltner, E. Baer, X. Z. Ji, and R. P. Quirk, "Block Copolymers as Compatibilizers for Blends of Linear Low Density Polyethylene and Polystyrene," *Journal of Polymer Science Part B: Polymer Physics* 33 (1995): 667–683.

294. H. Li, G.-H. Hu, and J. A. Sousa, "Morphology Development of Immiscible Polymer Blends During Melt Blending: Effects of Interfacial Agents on the Liquid-Solid Interfacial Heat Transfer," *Journal of Polymer Science Part B: Polymer Physics* 37 (1999): 3368–3384.

295. "Polymer-Polymer Miscibility—1st ed," https://www.elsevier.com/books/polymer-polymer-miscibility/olabis/978-0-12-525050-4.

296. Z. Bartczak and A. Galeski, *Polymer Blends Handbook*, ed. L. A. Utracki and C. A. Wilkie (Springer Netherlands, 2014), 1203–1297.

297. L. Dong, C. Xiong, T. Wang, D. Liu, S. Lu, and Y. Wang, "Preparation and Properties of Compatibilized PVC/SMA-g-PA6 Blends," *Journal of Applied Polymer Science* 94 (2004): 432–439.

298. S. Chuayjuljit, S. Moolsin, and P. Potiyaraj, "Use of Natural Rubber-g-Polystyrene as a Compatibilizer in Casting Natural Rubber/Polystyrene Blend Films," *Journal of Applied Polymer Science* 95 (2005): 826–831.

299. H. K. Jeon, B. J. Feist, S. B. Koh, K. Chang, C. W. Macosko, and R. P. Dion, "Reactively Formed Block and Graft Copolymers as Compatibilizers for Polyamide 66/PS Blends," *Polymer* 45 (2004): 197–206.

300. J. Kwak, P. Lacroix-Desmazes, J. J. Robin, B. Boutevin, and N. Torres, "Synthesis of Mono Functional Carboxylic Acid Poly(Methyl Methacrylate) in Aqueous Medium Using Sur-Iniferter. Application to the Synthesis of Graft Copolymers Polyethylene-g-Poly(Methyl

Methacrylate) and the Compatibilization of LDPE/PVDF Blends," *Polymer* 44 (2003): 5119–5130.

301. C.-L. Zhang, L.-F. Feng, J. Zhao, H. Huang, S. Hoppe, and G.-H. Hu, "Efficiency of Graft Copolymers at Stabilizing Co-Continuous Polymer Blends During Quiescent Annealing," *Polymer* 49 (2008): 3462–3469.

302. A. Gooneie and C. Holzer, "Reinforced Local Heterogeneities in Interfacial Tension Distribution in Polymer Blends by Incorporating Carbon Nanotubes," *Polymer* 125 (2017): 90–101.

303. F. Bates and G. Fredrickson, "Block Copolymer Thermodynamics: Theory and Experiment," *Annual Review of Physical Chemistry* 41, no. 1 (1990): 525–557, https://doi.org/10.1146/annurev.pc.41.100190.002521.

304. I. W. Hamley, *The Physics of Block Copolymers* (Oxford University Press, 1998).

305. L. Leibler, "Theory of Microphase Separation in Block Copolymers," *Macromolecules* 13 (1980): 1602–1617.

306. M. W. Matsen and F. S. Bates, "Unifying Weak- and Strong-Segregation Block Copolymer Theories," *Macromolecules* 29 (1996): 1091–1098.

307. G. H. Fredrickson and E. Helfand, "Fluctuation Effects in the Theory of Microphase Separation in Block Copolymers," *Journal of Chemical Physics* 87 (1987): 697–705.

308. S. A. Brazovskiĭ, *World Scientific Series in 20th Century Physics*, vol. 11 (World Scientific, 1996), 109–113.

309. K. Almdal, K. A. Koppi, F. S. Bates, and K. Mortensen, "Multiple Ordered Phases in a Block Copolymer Melt," *Macromolecules* 25 (1992): 1743–1751.

310. S. Sakurai, H. Kawada, T. Hashimoto, and L. J. Fetters, "Thermoreversible Morphology Transition Between Spherical and Cylindrical Microdomains of Block Copolymers," *Macromolecules* 26 (1993): 5796–5802.

311. C. Soto-Figueroa, M.-R. Rodríguez-Hidalgo, J.-M. Martínez-Magadán, and L. Vicente, "Dissipative Particle Dynamics Study of Order−Order Phase Transition of BCC, HPC, OBDD, and LAM Structures of the Poly(Styrene)−Poly(Isoprene) Diblock Copolymer," *Macromolecules* 41 (2008): 3297–3304.

312. J. V. L. Beckers, C. P. Lowe, and S. W. D. Leeuw, "An Iterative PPPM Method for Simulating Coulombic Systems on Distributed Memory Parallel Computers," *Molecular Simulation* 20, no. 6 (1998): 369–383, https://doi.org/10.1080/08927029808022044.

313. M. González-Melchor, E. Mayoral, M. E. Velázquez, and J. Alejandre, "Electrostatic Interactions in Dissipative Particle Dynamics Using the Ewald Sums," *Journal of Chemical Physics* 125 (2006): 224107.

314. C. Zhai, H. Zhou, T. Gao, L. Zhao, and S. Lin, "Electrostatically Tuned Microdomain Morphology and Phase-Dependent Ion Transport Anisotropy in Single-Ion Conducting Block Copolyelectrolytes," *Macromolecules* 51 (2018): 4471–4483.

315. Z. Posel, Z. Limpouchová, K. Šindelka, M. Lísal, and K. Procházka, "Dissipative Particle Dynamics Study of the pH-Dependent Behavior of Poly(2-Vinylpyridine)-block-Poly(Ethylene Oxide) Diblock Copolymer in Aqueous Buffers," *Macromolecules* 47 (2014): 2503–2514.

316. M. Lísal, Z. Limpouchová, and K. Procházka, "The Self-Assembly of Copolymers With One Hydrophobic and One Polyelectrolyte Block in Aqueous Media: A Dissipative Particle Dynamics Study," *Physical Chemistry Chemical Physics* 18 (2016): 16127–16136.

317. K. Šindelka, Z. Limpouchová, M. Lísal, and K. Procházka, "The Electrostatic Co-Assembly in Non-stoichiometric Aqueous Mixtures of Copolymers Composed of One Neutral Water-Soluble and One Polyelectrolyte (Either Positively or Negatively Charged) Block: A Dissipative Particle Dynamics Study," *Physical Chemistry Chemical Physics* 18 (2016): 16137–16151.

318. S. Javan Nikkhah, M. R. Moghbeli, and S. M. Hashemianzadeh, "Investigation of the Interface Between Polyethylene and Functionalized Graphene: A Computer Simulation Study," *Current Applied Physics* 15 (2015): 1188–1199.

319. S. J. Nikkhah, M. R. Moghbeli, and S. M. Hashemianzadeh, "A Molecular Simulation Study on the Adhesion Behavior of a Functionalized Polyethylene-Functionalized Graphene Interface," *Physical Chemistry Chemical Physics* 17, no. 41 (2015): 27414–27427, https://doi.org/10.1039/C5CP04699H.

320. S. J. Nikkhah, M. R. Moghbeli, and S. M. Hashemianzadeh, "Dynamic Study of Deformation and Adhesion of an Amorphous Polyethylene/Graphene Interface: A Simulation Study," *Macromolecular Theory and Simulations* 25 (2016): 533–549.

321. S. J. Nikkhah, M. R. Moghbeli, and S. M. Hashemianzadeh, "Interfacial Adhesion Between Functionalized Polyethylene Surface and Graphene via Molecular Dynamic Simulation," *Journal of Molecular Modeling* 21 (2015): 121.

322. S. Javan Nikkhah, M. R. Moghbeli, and S. M. Hashemianzadeh, "A Quantitative Correlation Between Polyethylene/Graphene Interfacial Viscoelastic Dissipation and Deformation Parameters: A Molecular Simulation Study," *International Journal of Adhesion and Adhesives* 84 (2018): 54–62.

323. G. Raos and B. Zappone, "Polymer Adhesion: Seeking New Solutions for an Old Problem," *Macromolecules* 54 (2021): 10617–10644.

324. S. G. Falkovich, V. M. Nazarychev, S. V. Larin, J. M. Kenny, and S. V. Lyulin, "Mechanical Properties of a Polymer at the Interface Structurally Ordered by Graphene," *Journal of Physical Chemistry C* 120 (2016): 6771–6777.

325. X. Yao, Y. Wang, X. Lang, Y. Zhu, and Q. Jiang, "Raising Glass Transition Temperature of Polymer Nanofilms as a Function of Negative Interface Energy," *Physical Chemistry Chemical Physics* 21 (2019): 5224–5231.

326. J. Chen, J. Li, L. Xu, W. Hong, Y. Yang, and X. Chen, "The Glass-Transition Temperature of Supported PMMA Thin Films With Hydrogen Bond/Plasmonic Interface," *Polymers* 11 (2019): 601.

327. I. V. Pivkin and G. E. Karniadakis, "A New Method to Impose No-Slip Boundary Conditions in Dissipative Particle Dynamics," *Journal of Computational Physics* 207 (2005): 114–128.

328. D. A. Fedosov, I. V. Pivkin, and G. E. Karniadakis, "Velocity Limit in DPD Simulations of Wall-Bounded Flows," *Journal of Computational Physics* 227 (2008): 2540–2559.

329. A. G. Goicochea, "Adsorption and Disjoining Pressure Isotherms of Confined Polymers Using Dissipative Particle Dynamics," *Langmuir* 23 (2007): 11656–11663.

330. Y. Kong, C. W. Manke, W. G. Madden, and A. G. Schlijper, "Simulation of a Confined Polymer in Solution Using the Dissipative Particle Dynamics Method," *International Journal of Thermophysics* 15 (1994): 1093–1101.

331. B. Kong and X. Yang, "Dissipative Particle Dynamics Simulation of Contact Angle Hysteresis on a Patterned Solid/Air Composite Surface," *Langmuir* 22 (2006): 2065–2073.

332. G. Maurel, F. Goujon, B. Schnell, and P. Malfreyt, "Multiscale Modeling of the Polymer–Silica Surface Interaction: From Atomistic to Mesoscopic Simulations," *Journal of Physical Chemistry C* 119 (2015): 4817–4826.

333. A. V. Berezkin, F. Jung, D. Posselt, D. M. Smilgies, and C. M. Papadakis, "Vertical vs Lateral Macrophase Separation in Thin Films of Block Copolymer Mixtures: Computer Simulations and GISAXS Experiments," *ACS Applied Materials & Interfaces* 9, no. 37 (2017): 31291–31301, https://doi.org/10.1021/acsami.6b16563.

334. D. Ramírez-Gutiérrez, C. Nieto-Draghi, N. Pannacci, L. V. Castro, F. Álvarez-Ramírez, and B. Creton, "Surface Photografting of Acrylic

Acid on Poly(Dimethylsiloxane). Experimental and Dissipative Particle Dynamics Studies," *Langmuir* 31 (2015): 1400–1409.

335. A. Scacchi, K. Hasheminejad, S. Javan Nikkhah, and M. Sammalkorpi, "Controlling Self-Assembling Co-Polymer Coatings of Hydrophilic Polysaccharide Substrates via Co-Polymer Block Length Ratio," *Journal of Colloid and Interface Science* 640 (2023): 809–819.

336. K. Hasheminejad, A. Scacchi, S. Javan Nikkhah, and M. Sammalkorpi, "Cracking Polymer Coatings of Paper-Like Surfaces: Control via Block Co-Polymer Structure and System Composition," *Applied Surface Science* 640 (2023): 158324.

337. Y.-H. Weng, H.-K. Tsao, and Y.-J. Sheng, "Self-Healing and Dewetting Dynamics of a Polymer Nanofilm on a Smooth Substrate: Strategies for Dewetting Suppression," *Physical Chemistry Chemical Physics* 20 (2018): 20459–20467.

338. Y.-C. Li, H. Liu, X.-R. Huang, and C.-C. Sun, "Evaporation- and Surface-Induced Morphology of Symmetric Diblock Copolymer Thin Films: A Multibody Dissipative Particle Dynamics Study," *Molecular Simulation* 37 (2011): 875–883.

339. Y.-L. Yang, H.-K. Tsao, and Y.-J. Sheng, "Morphology and Wetting Stability of Nanofilms of ABC Miktoarm Star Terpolymers," *Macromolecules* 53 (2020): 594–601.

340. "Morphology and Wetting Stability of Nanofilms of ABC Miktoarm Star Terpolymers|Macromolecules," https://doi.org/10.1021/acs.macromol.9b02621.

341. A. Chatterjee, "Modification to Lees–Edwards Periodic Boundary Condition for Dissipative Particle Dynamics Simulation With High Dissipation Rates," *Molecular Simulation* 33 (2007): 1233–1236.

342. S. Jamali, A. Boromand, S. Khani, and J. Maia, "Gaussian-Inspired Auxiliary Non-equilibrium Thermostat (GIANT) for Dissipative Particle Dynamics Simulations," *Computer Physics Communications* 197 (2015): 27–34.

343. M. Darbandi, R. Zakeri, and G. E. Schneider, "American Society of Mechanical Engineers Digital Collection, 2011, 1035–1040".

344. C. Pastorino and A. G. Goicochea, *Selected Topics of Computational and Experimental Fluid Mechanics*, ed. J. Klapp, G. Ruíz Chavarría, A. Medina Ovando, A. López Villa, and L. D. G. Sigalotti (Springer International Publishing, 2015), 51–79.

345. L. Zhao, Z. Li, Z. Wang, B. Caswell, J. Ouyang, and G. E. Karniadakis, "Active- and Transfer-Learning Applied to Microscale-Macroscale Coupling to Simulate Viscoelastic Flows," *Journal of Computational Physics* 427 (2021): 110069.

346. S. Chen, N. Phan-Thien, X.-J. Fan, and B. C. Khoo, "Dissipative Particle Dynamics Simulation of Polymer Drops in a Periodic Shear Flow," *Journal of Non-Newtonian Fluid Mechanics* 118 (2004): 65–81.

347. S. Bashir, M. Hina, J. Iqbal, et al., "Fundamental Concepts of Hydrogels: Synthesis, Properties, and Their Applications," *Polymers* 12, no. 11 (2020): 2702, https://doi.org/10.3390/polym12112702.

348. M. Bahram, N. Mohseni, and M. Moghtader, *An Introduction to Hydrogels and Some Recent Applications* (IntechOpen, 2016).

349. Y. R. Sliozberg, R. A. Mrozek, J. D. Schieber, M. Kröger, J. L. Lenhart, and J. W. Andzelm, "Effect of Polymer Solvent on the Mechanical Properties of Entangled Polymer Gels: Coarse-Grained Molecular Simulation," *Polymer* 54 (2013): 2555–2564.

350. D. M. Heyes and H. Okumura, "Equation of State and Structural Properties of the Weeks-Chandler-Andersen Fluid," *Journal of Chemical Physics* 124 (2006): 164507.

351. J. Schneider, L. D. Süss, and F. Müller-Plathe, "The Influence of Entanglements on the Dynamics of Flash Nanoprecipitation: A Slip-Spring Dissipative-Particle-Dynamics Investigation," *Journal of Chemical & Engineering Data* 65 (2020): 1264–1272.

352. F. Zheng, F. Goujon, A. C. F. Mendonça, P. Malfreyt, and D. J. Tildesley, "Structure and Rheology of Star Polymers in Confined Geometries: A Mesoscopic Simulation Study," *Soft Matter* 11 (2015): 8590–8598.

353. X.-L. Wang, H.-J. Qian, L.-J. Chen, Z.-Y. Lu, and Z.-S. Li, "Dissipative Particle Dynamics Simulation on the Polymer Membrane Formation by Immersion Precipitation," *Journal of Membrane Science* 311 (2008): 251–258.

354. D. Wu, S. J. Paddison, J. A. Elliott, and S. J. Hamrock, "Mesoscale Modeling of Hydrated Morphologies of 3M Perfluorosulfonic Acid-Based Fuel Cell Electrolytes," *Langmuir* 26 (2010): 14308–14315.

355. X. Huang, W. Wang, Z. Zheng, et al., "Dissipative Particle Dynamics Study and Experimental Verification on the Pore Morphologies and Diffusivity of the Poly (4-Methyl-1-Pentene)-Diluent System via Thermally Induced Phase Separation: The Effect of Diluent and Polymer Concentration," *Journal of Membrane Science* 514 (2016): 487–500.

356. Y.-H. Tang, Y.-D. He, and X.-L. Wang, "Effect of Adding a Second Diluent on the Membrane Formation of Polymer/Diluent System via Thermally Induced Phase Separation: Dissipative Particle Dynamics Simulation and Its Experimental Verification," *Journal of Membrane Science* 409–410 (2012): 164–172.

357. A. J. Reuvers, J. W. A. van den Berg, and C. A. Smolders, "Formation of Membranes by Means of Immersion Precipitation," *Journal of Membrane Science* 34 (1987): 45–65.

358. H. Liu, H. Li, and Z.-Y. Lu, "Incorporating Chemical Reactions in Dissipative Particle Dynamics Simulations," *Procedia Computer Science* 4 (2011): 1021–1028.

359. H. Liu, M. Li, Z.-Y. Lu, Z.-G. Zhang, and C.-C. Sun, "Influence of Surface-Initiated Polymerization Rate and Initiator Density on the Properties of Polymer Brushes," *Macromolecules* 42 (2009): 2863–2872.

360. H. Liu, Y.-H. Xue, H.-J. Qian, Z.-Y. Lu, and C.-C. Sun, "A Practical Method to Avoid Bond Crossing in Two-Dimensional Dissipative Particle Dynamics Simulations," *Journal of Chemical Physics* 129 (2008): 024902.

361. J. Wang, J. Li, Q. Yao, X. Sun, Y. Yan, and J. Zhang, "One-Pot Production of Porous Assemblies by PISA of Star Architecture Copolymers: A Simulation Study," *Physical Chemistry Chemical Physics* 20 (2018): 10069–10076.

362. J. Jancar, J. F. Douglas, F. W. Starr, et al., "Current Issues in Research on Structure–Property Relationships in Polymer Nanocomposites," *Polymer* 51 (2010): 3321–3343.

363. S. Lu, Z. Wu, and A. Jayaraman, "Molecular Modeling and Simulation of Polymer Nanocomposites With Nanorod Fillers," *Journal of Physical Chemistry. B* 125 (2021): 2435–2449.

364. Y.-C. Wang, S.-P. Ju, H.-Z. Cheng, J.-M. Lu, and H.-H. Wang, "Modeling of Polyethylene and Functionalized CNT Composites: A Dissipative Particle Dynamics Study," *Journal of Physical Chemistry C* 114 (2010): 3376–3384.

365. S.-W. Hu, Y.-J. Sheng, and H.-K. Tsao, "Self-Assembly of Organophilic Nanoparticles in a Polymer Matrix: Depletion Interactions," *Journal of Physical Chemistry C* 116 (2012): 1789–1797.

366. S. Chakraborty, C. K. Choudhury, and S. Roy, "Morphology and Dynamics of Carbon Nanotube in Polycarbonate Carbon Nanotube Composite From Dissipative Particle Dynamics Simulation," *Macromolecules* 46 (2013): 3631–3638.

367. A. A. Gavrilov, A. V. Chertovich, P. G. Khalatur, and A. R. Khokhlov, "Study of the Mechanisms of Filler Reinforcement in Elastomer Nanocomposites," *Macromolecules* 47 (2014): 5400–5408.

368. L.-T. Yan, N. Popp, S.-K. Ghosh, and A. Böker, "Self-Assembly of Janus Nanoparticles in Diblock Copolymers," *ACS Nano* 4 (2010): 913–920.

369. S. Khani, S. Jamali, A. Boromand, M. J. A. Hore, and J. Maia, "Polymer-Mediated Nanorod Self-Assembly Predicted by Dissipative Particle Dynamics Simulations," *Soft Matter* 11 (2015): 6881–6892.

370. J. P. Koski, N. M. Krook, J. Ford, et al., "Phase Behavior of Grafted Polymer Nanocomposites From Field-Based Simulations," *Macromolecules* 52 (2019): 5110–5121.

371. S. K. Kumar, N. Jouault, B. Benicewicz, and T. Neely, "Nanocomposites With Polymer Grafted Nanoparticles," *Macromolecules* 46 (2013): 3199–3214.

372. D. Sunday, J. Ilavsky, and D. L. Green, "A Phase Diagram for Polymer-Grafted Nanoparticles in Homopolymer Matrices," *Macromolecules* 45 (2012): 4007–4011.

373. Q. H. Zeng, A. B. Yu, and G. Q. Lu, "Multiscale Modeling and Simulation of Polymer Nanocomposites," *Progress in Polymer Science* 33 (2008): 191–269.

374. E. Moeendarbary, T. Y. Ng, and M. Zangeneh, "Dissipative Particle Dynamics: Introduction, Methodology and Complex Fluid Applications — A Review," *International Journal of Applied Mechanics* 01 (2009): 737–763.

375. E. Moeendarbary, T. Y. Ng, and M. Zangeneh, "Dissipative Particle Dynamics in Soft Matter and Polymeric Applications — A Review," *International Journal of Applied Mechanics* 02 (2010): 161–190.

376. M. B. Liu, G. R. Liu, L. W. Zhou, and J. Z. Chang, "Dissipative Particle Dynamics (DPD): An Overview and Recent Developments," *Archives of Computational Methods in Engineering* 22 (2015): 529–556.

377. K. Procházka, K. Šindelka, X. Wang, Z. Limpouchová, and M. Lísal, "Self-Assembly and Co-Assembly of Block Polyelectrolytes in Aqueous Solutions. Dissipative Particle Dynamics With Explicit Electrostatics," *Molecular Physics* 114 (2016): 3077–3092.

378. Z. Xu, Y. Yang, G. Zhu, et al., "Simulating Transport of Soft Matter in Micro/Nano Channel Flows With Dissipative Particle Dynamics," *Advanced Theory and Simulations* 2 (2019): 1800160.

379. T. Ye and Y. Li, "A Comparative Review of Smoothed Particle Hydrodynamics, Dissipative Particle Dynamics and Smoothed Dissipative Particle Dynamics," *International Journal of Computational Methods* 15 (2018): 1850083.

380. Z. Chen, J. Huo, L. Hao, and J. Zhou, "Multiscale Modeling and Simulations of Responsive Polymers," *Current Opinion in Chemical Engineering* 23 (2019): 21–33.

381. Y. H. Feng, X. P. Zhang, Z. Q. Zhao, and X. D. Guo, "Dissipative Particle Dynamics Aided Design of Drug Delivery Systems: A Review," *Molecular Pharmaceutics* 17, no. 6 (2020): 1778–1799, https://doi.org/10.1021/acs.molpharmaceut.0c00175.

382. J. Wang, Y. Han, Z. Xu, X. Yang, S. Ramakrishna, and Y. Liu, "Dissipative Particle Dynamics Simulation: A Review on Investigating Mesoscale Properties of Polymer Systems," *Macromolecular Materials and Engineering* 306 (2021): 2000724.

383. K. P. Santo and A. V. Neimark, "Dissipative Particle Dynamics Simulations in Colloid and Interface Science: A Review," *Advances in Colloid and Interface Science* 298 (2021): 102545.

384. J. Zhao, S. Chen, K. Zhang, and Y. Liu, "A Review of Many-Body Dissipative Particle Dynamics (MDPD): Theoretical Models and Its Applications," *Physics of Fluids* 33 (2021): 112002.

385. M. Ahmadi, E. Aliabadian, B. Liu, et al., "Comprehensive Review of the Interfacial Behavior of Water/Oil/Surfactant Systems Using Dissipative Particle Dynamics Simulation," *Advances in Colloid and Interface Science* 309 (2022): 102774.

386. W. X. Guo, L. F. Hu, Y. H. Feng, B. Z. Chen, and X. D. Guo, "Advances in Self-Assembling of pH-Sensitive Polymers: A Mini Review on Dissipative Particle Dynamics," *Colloids and Surfaces B: Biointerfaces* 210 (2022): 112202.

387. J. T. Padding and A. A. Louis, "Hydrodynamic Interactions and Brownian Forces in Colloidal Suspensions: Coarse-Graining Over Time and Length Scales," *Physical Review E* 74 (2006): 031402.

388. P. Español and P. B. Warren, "Perspective: Dissipative Particle Dynamics," *Journal of Chemical Physics* 146 (2017): 150901.

389. W. Wang and R. Gómez-Bombarelli, "Coarse-Graining Auto-Encoders for Molecular Dynamics," *npj Computational Materials* 5, no. 1 (2019): 125, https://doi.org/10.1038/s41524-019-0261-5.

390. D. Nguyen, L. Tao, and Y. Li, "Integration of Machine Learning and Coarse-Grained Molecular Simulations for Polymer Materials: Physical Understandings and Molecular Design," *Frontiers in Chemistry* 9 (2022): 820417, https://doi.org/10.3389/fchem.2021.820417.

391. K. Hagita, T. Aoyagi, Y. Abe, S. Genda, and T. Honda, "Deep Learning-Based Estimation of Flory–Huggins Parameter of A–B Block Copolymers From Cross-Sectional Images of Phase-Separated Structures," *Scientific Reports* 11 (2021): 12322.

392. H. Doi, S. Matsuoka, K. Okuwaki, et al., "Machine Learning to Improve Efficiency of Non-empirical Interaction Parameter for Dissipative Particle Dynamics (DPD) Simulation," *Japanese Journal of Applied Physics* 62 (2023): 070901.

393. D. Frenkel and B. Smit, *Understanding Molecular Simulation: From Algorithms to Applications* (Elsevier, 2023).

394. K. Kremer and G. S. Grest, "Dynamics of Entangled Linear Polymer Melts: A Molecular-Dynamics Simulation," *Journal of Chemical Physics* 92 (1990): 5057–5086.

395. S. J. Marrink, A. H. de Vries, and A. E. Mark, "Coarse Grained Model for Semiquantitative Lipid Simulations," *Journal of Physical Chemistry. B* 108 (2004): 750–760.

396. G. Milano and T. Kawakatsu, "Hybrid Particle-Field Molecular Dynamics Simulations for Dense Polymer Systems," *Journal of Chemical Physics* 130 (2009): 214106.

397. I. Pagonabarraga, M. H. J. Hagen, and D. Frenkel, "Self-Consistent Dissipative Particle Dynamics Algorithm," *EPL* 42 (1998): 377–382.

398. K. Binder and D. W. Heermann, *Monte Carlo Simulation in Statistical Physics: An Introduction* (Springer International Publishing, 2019).

399. M. Mueller and K. Binder, "Computer Simulation of Asymmetric Polymer Mixtures," *Macromolecules* 28 (1995): 1825–1834.